OROBIX

TOOLS WITH A MIND

L’utilizzo delle immagini TC per il trauma cranico: le tecniche di deep learning

Luca Antiga, Lisa Lozza, Sara Zanchi, Daniele Cortinovis
Orobix, Bergamo

ALPHA GO

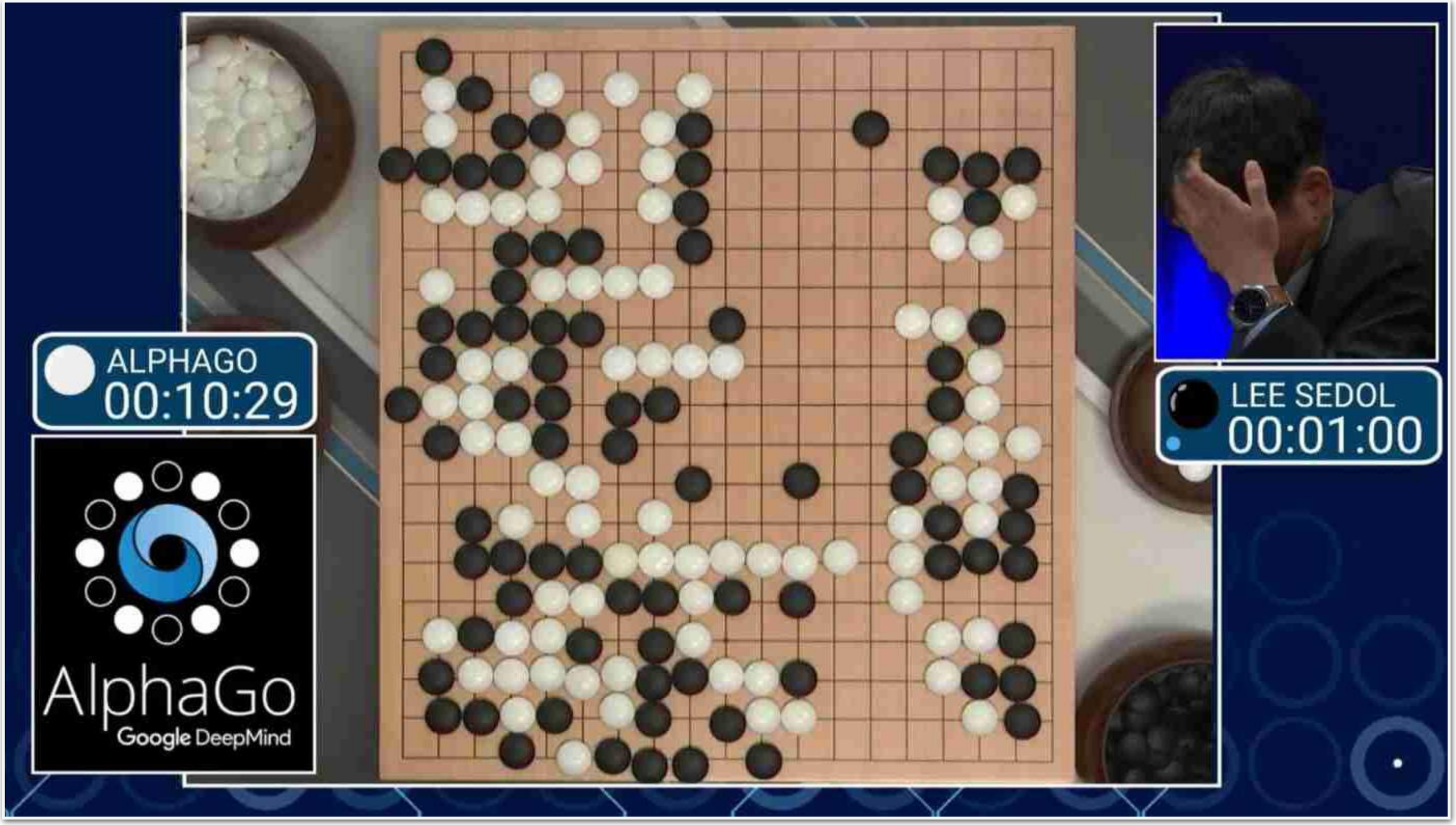

VIDEO CAPTIONING

train on the tracks. trees are green. front of the train is yellow. grass is green. green trees in the background. photo taken during the day. red train car.

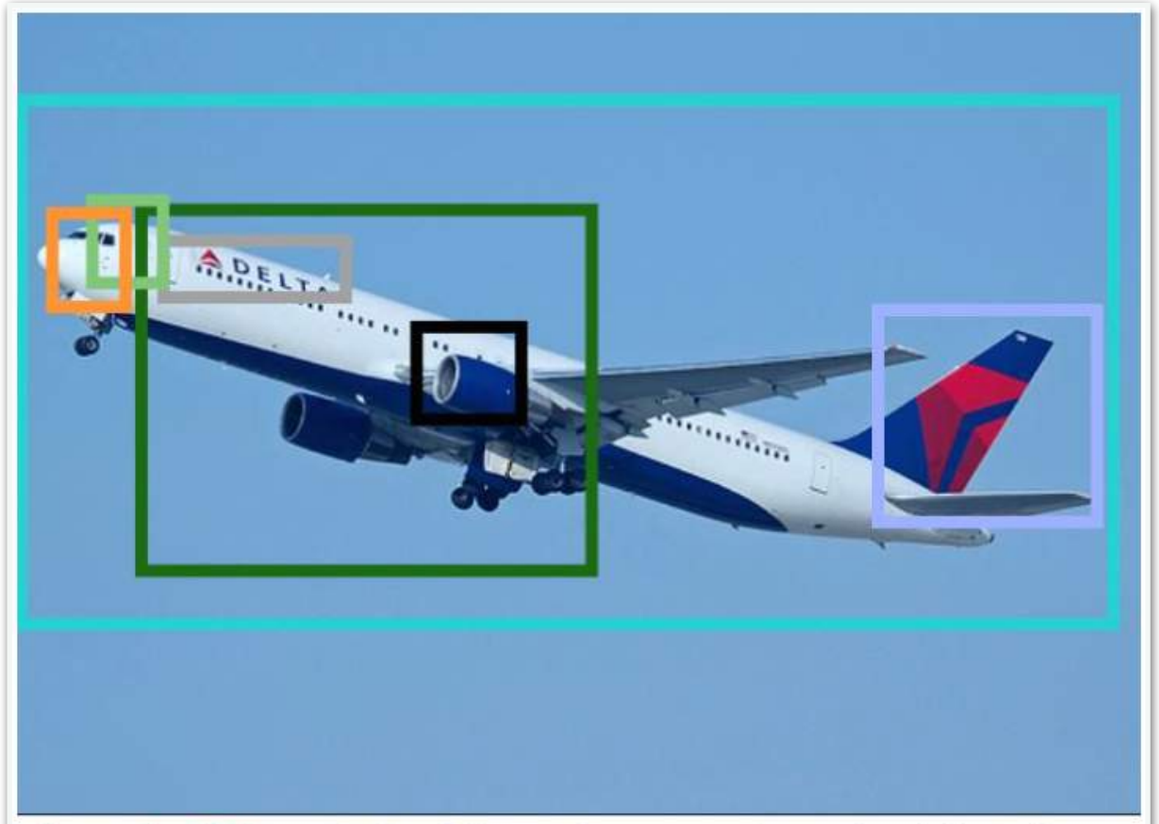

plane is flying. tail of the plane. red and white plane. plane is white. engine on the plane. windows on the plane. nose of the plane.

MACHINE TRANSLATION

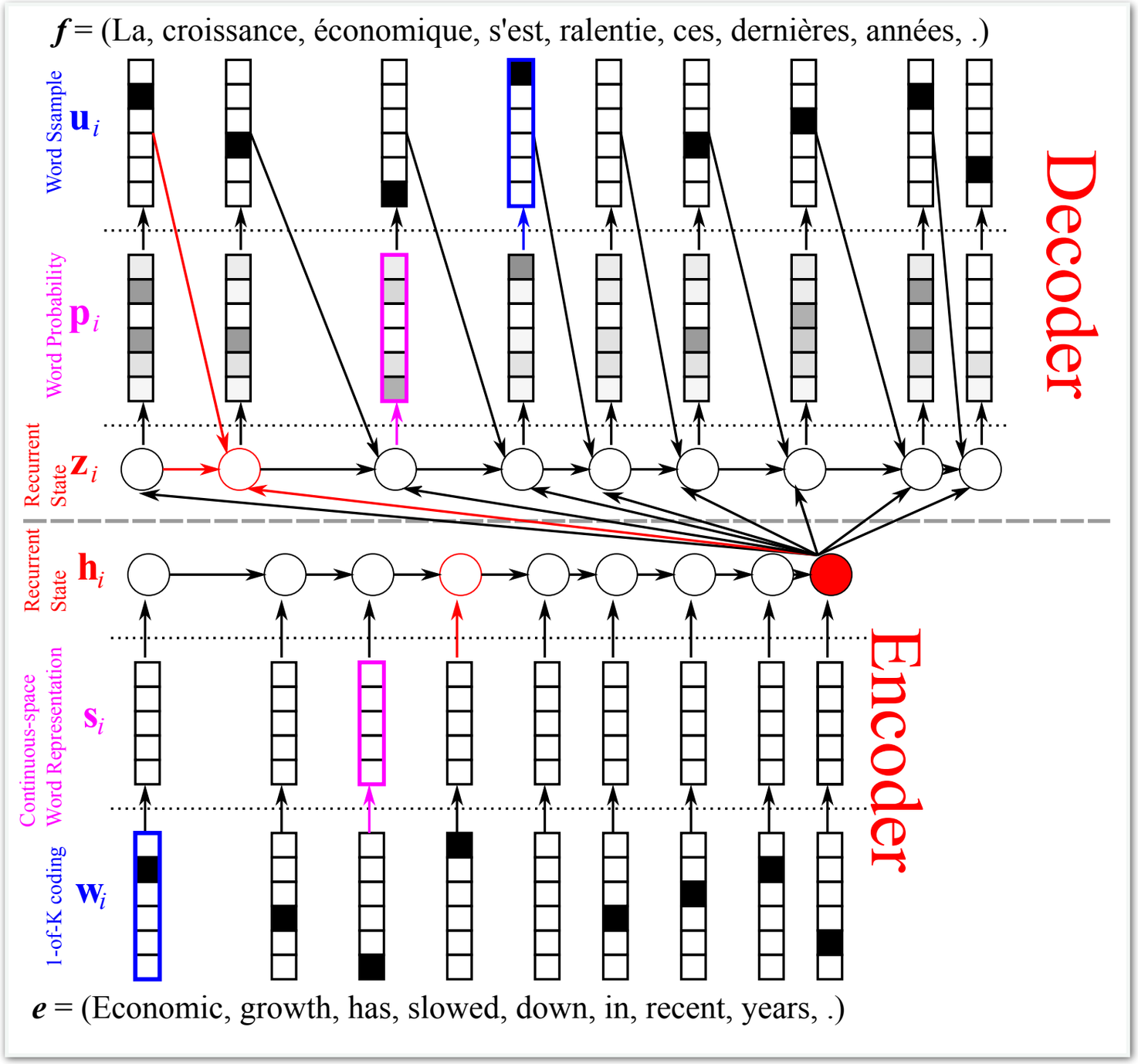

From Sequence Modeling to Translation, Kyunghyun Cho, https://t.co/sDjI2k4cS8

THE A.I. SPECTRUM

fuzzy boundaries

rule-based decision making

if condition fulfilled *then*
activity 1
else
activity 2

boolean data
(yes or no)

Examples:

- phone notification
- time- or threshold-based alarms
- simple pattern matching

statistical reasoning

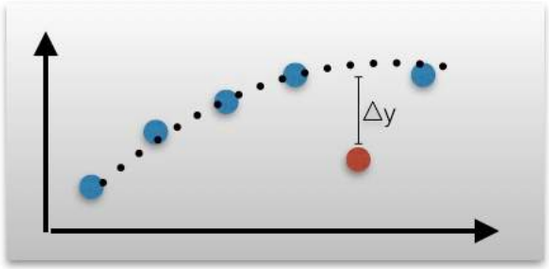

simple regression

numerical data
allowing for curve fitting

Examples:

- extra- and interpolation
- outlier detection
- predictive maintenance

machine learning

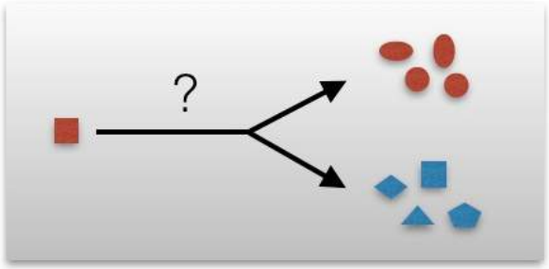

classification tasks

arbitrary data
that needs to be abstracted into numbers

Examples:

- identification of relevant features from large input datasets
- quality control using various metrics

artificial intelligence

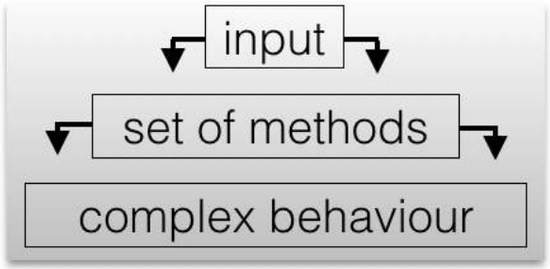

dynamic adaptation to novelty

autonomous selection of best methodology when presented with **arbitrary data**

Examples:

- autonomous vehicles
- human-like conversational skills
- intelligent digital assistant

SYMBOLYSM VS CONNECTIONISM

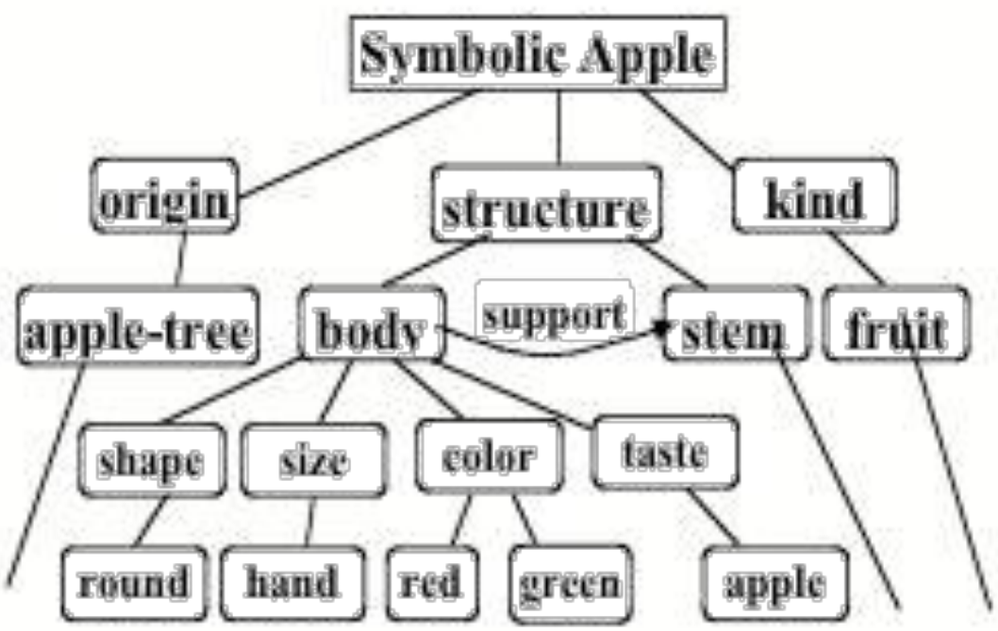

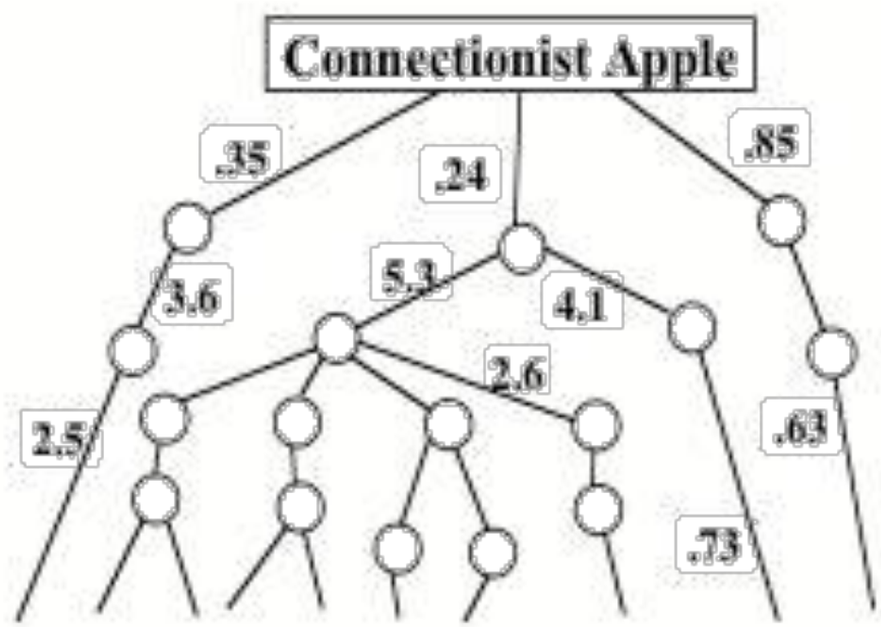

http://web.media.mit.edu/~minsky/papers/SymbolicVs.Connectionist.html

THE DEEP LEARNING REVOLUTION

End-to-end learning (no feature engineering), chained cascade of non-linear transforms.

Deep neural networks learn hierarchical feature representations

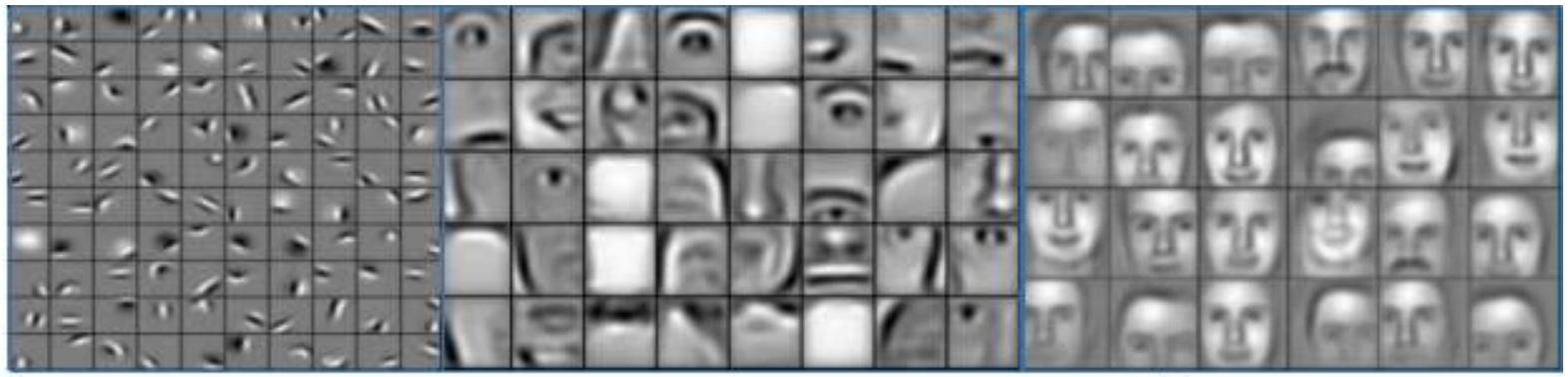

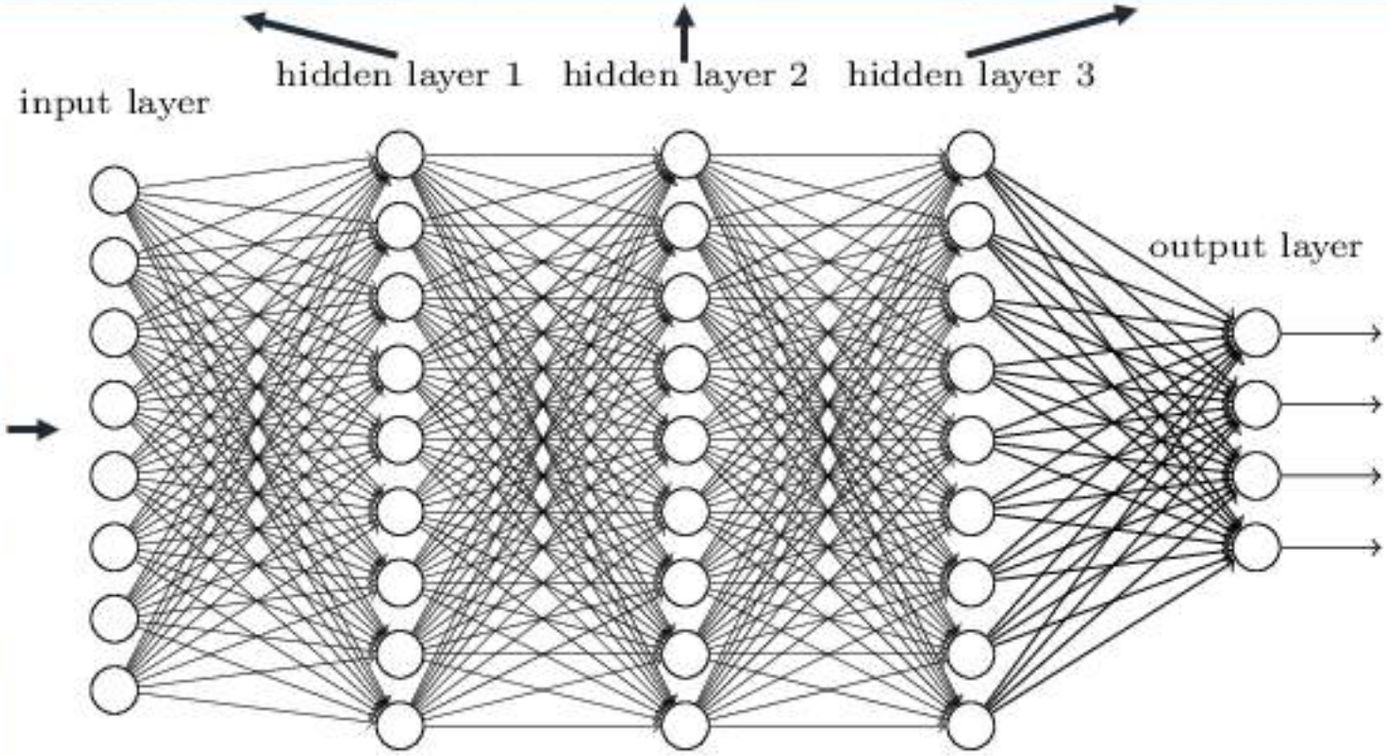

NEURAL NETWORKS

$$f(x, y, a, b, c) = \sigma(ax + by + c)$$

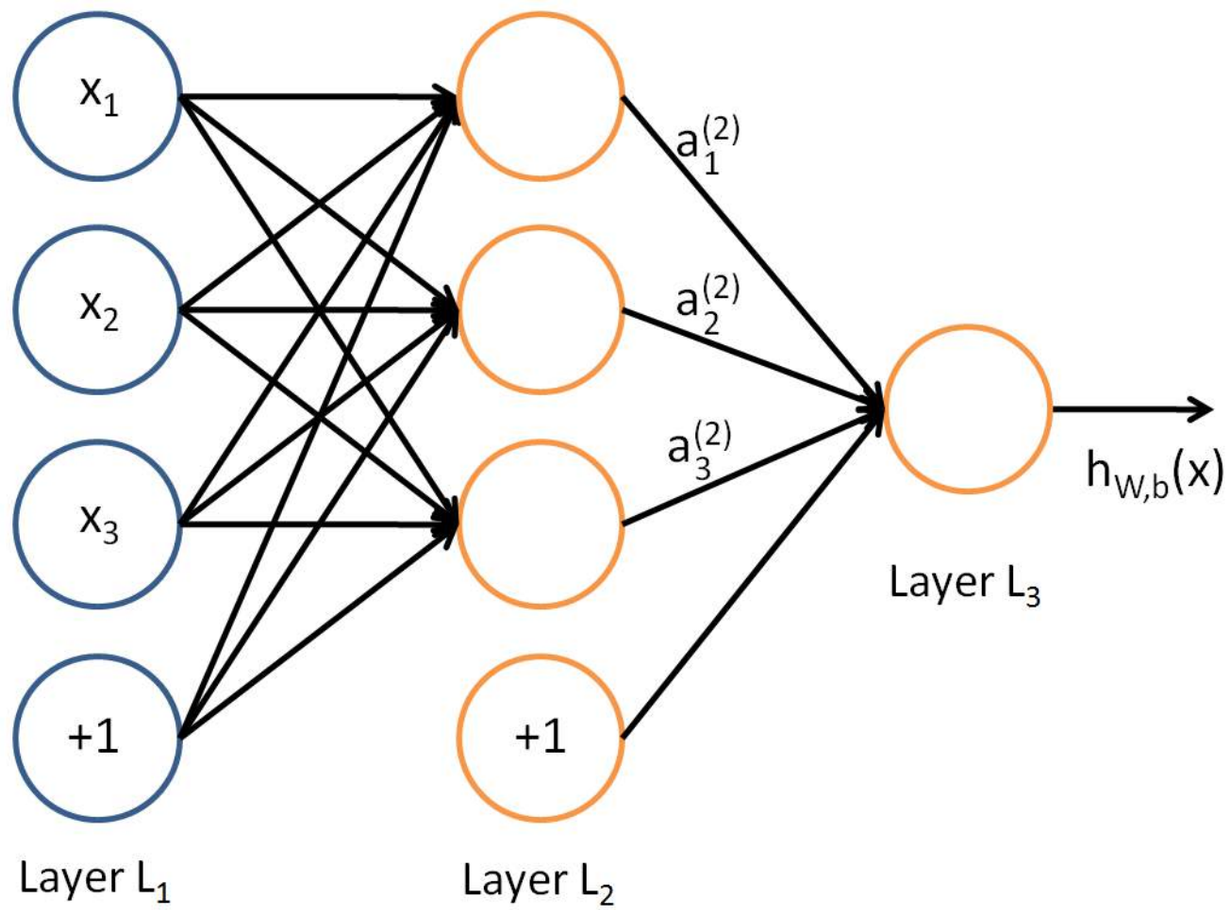

http://ufldl.stanford.edu/tutorial/supervised/MultiLayerNeuralNetworks

BACK-PROPAGATION

$$W_{ij}^{(l)} = W_{ij}^{(l)} - \alpha \frac{\partial}{\partial W_{ij}^{(l)}} J(W, b)$$

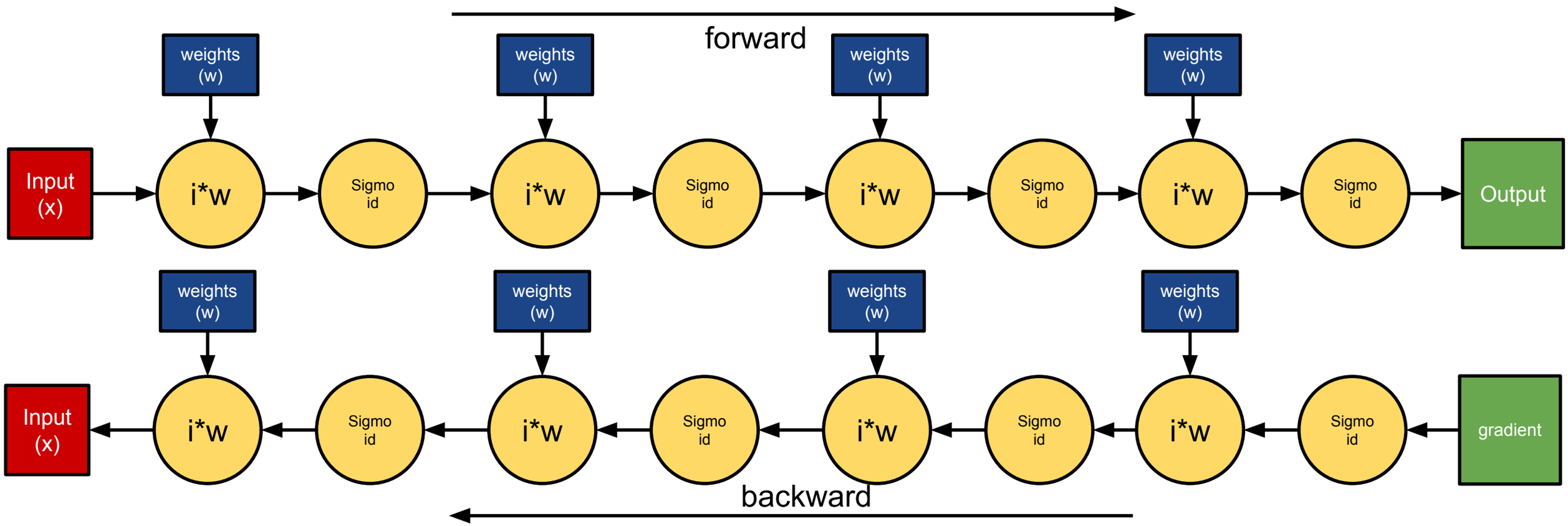

The Deep Learning Revolution: Rethinking Machine Learning Pipelines. Soumith Chintala

CONVOLUTIONAL NETWORKS

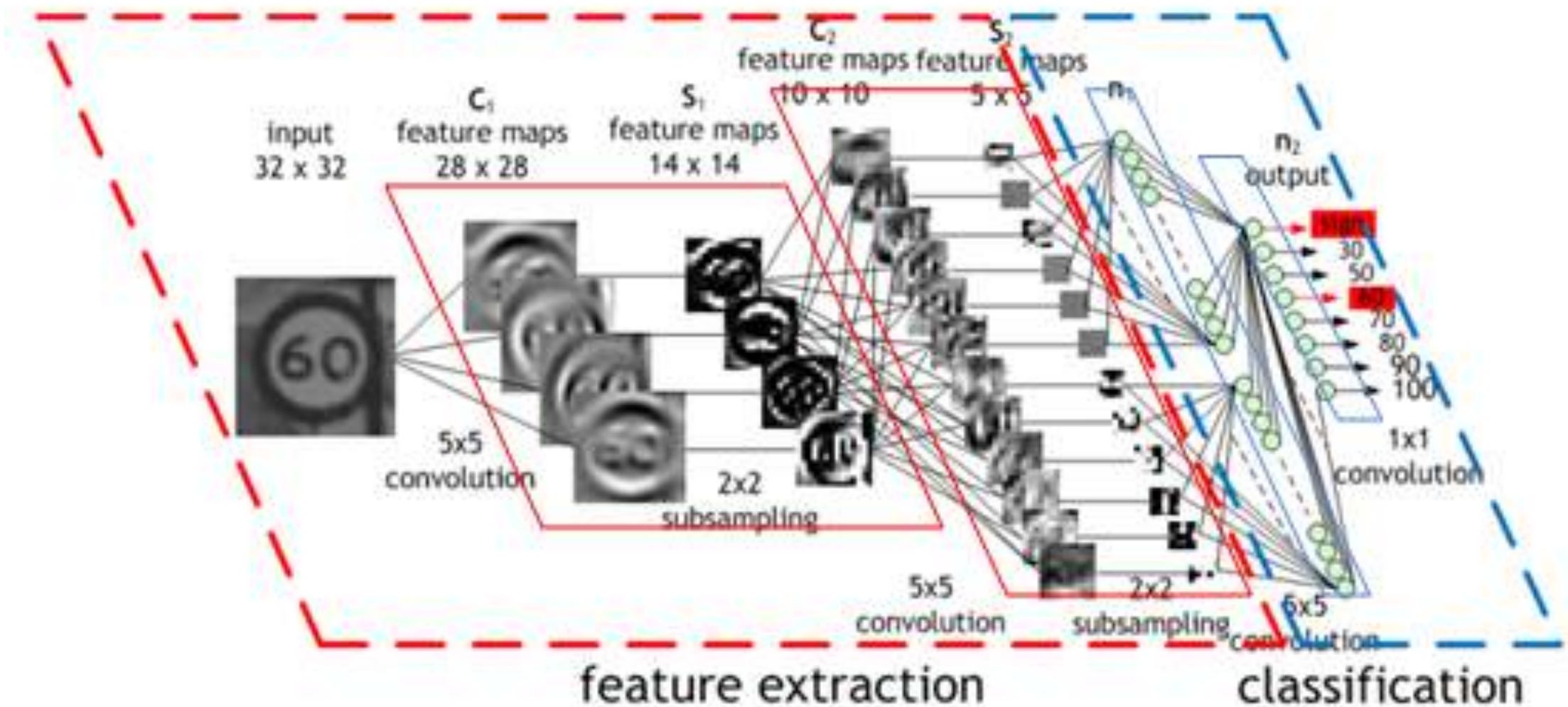

https://devblogs.nvidia.com/parallelforall/deep-learning-nutshell-core-concepts/

DEEP LEARNING AND MEDICAL IMAGING

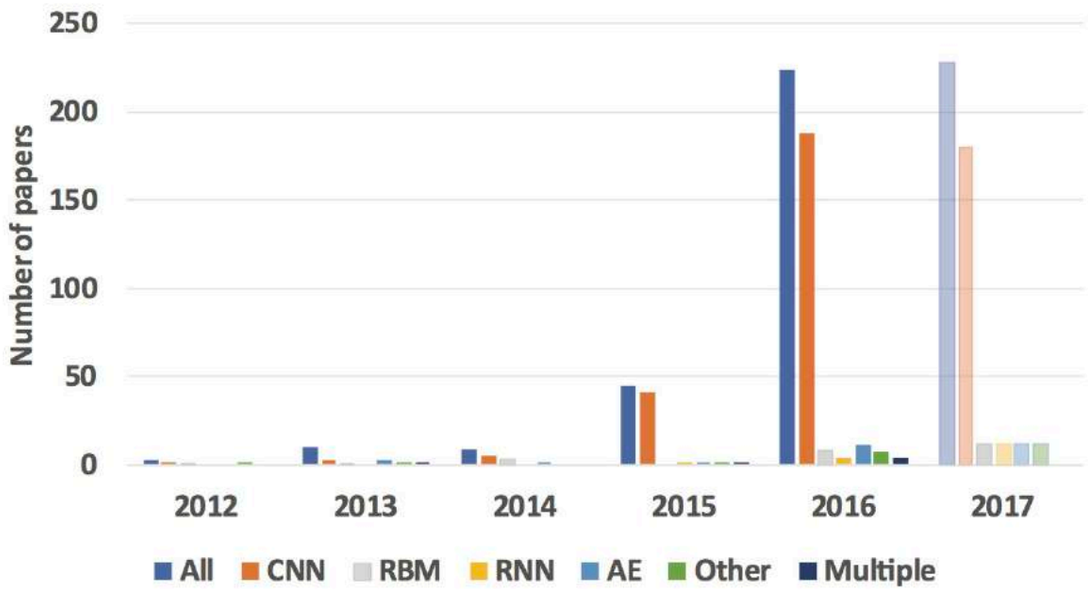

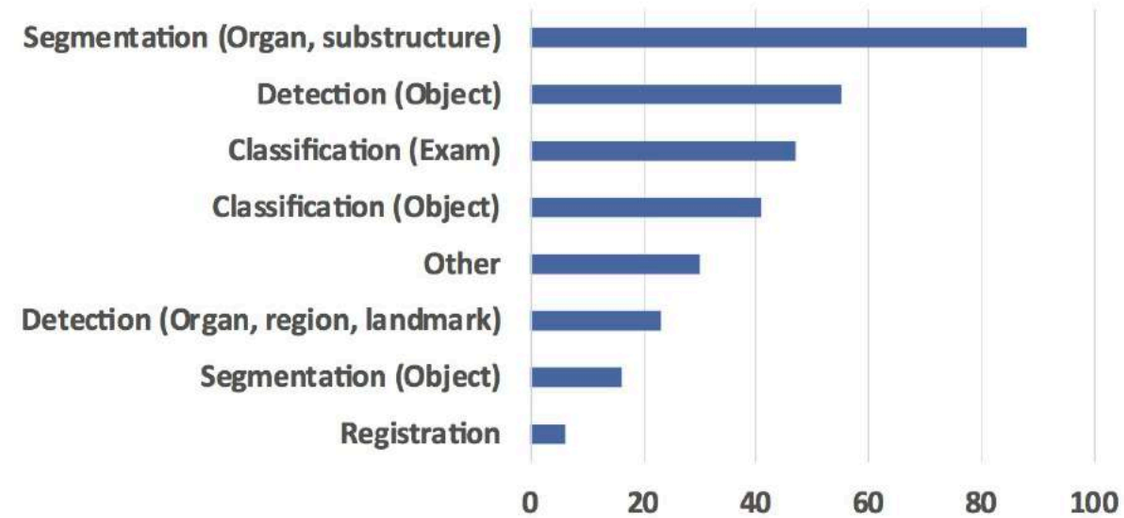

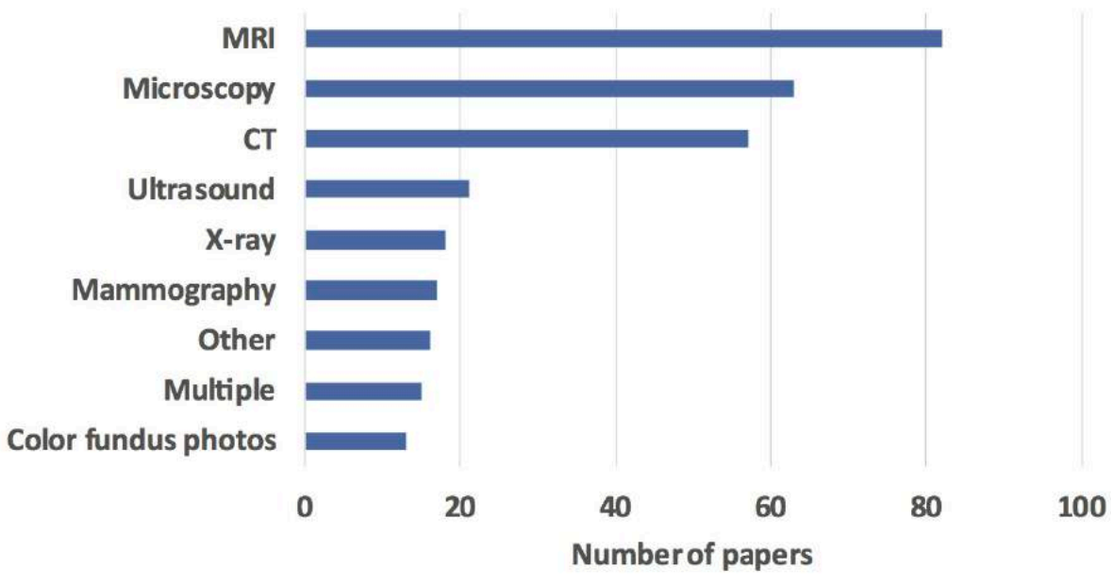

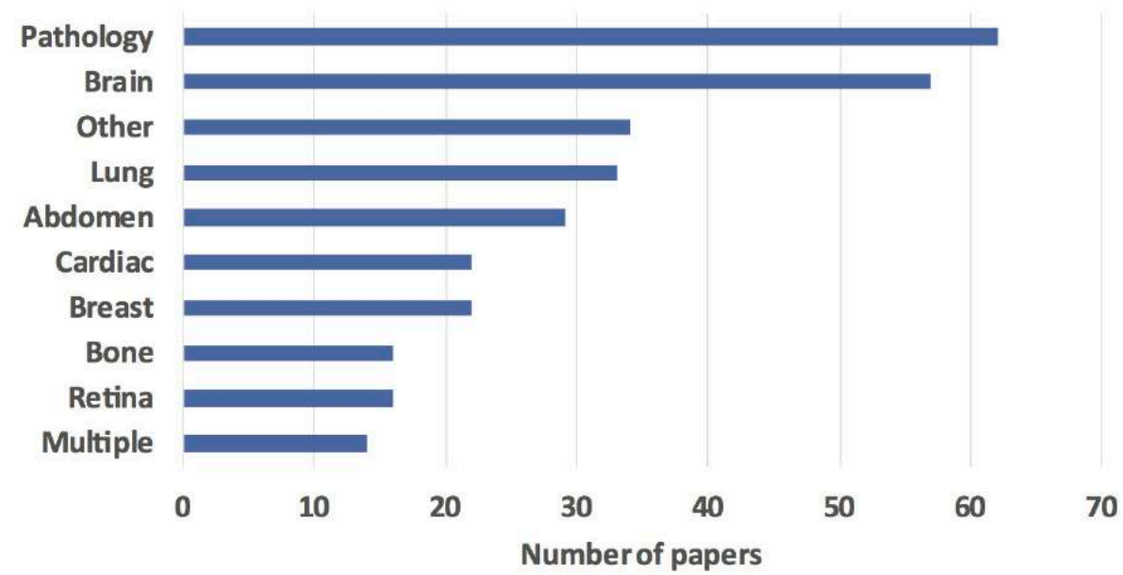

Litjiens et al. A survey on deep learning in medical image analysis. arXiv:1702.05747 2017

OROBIX

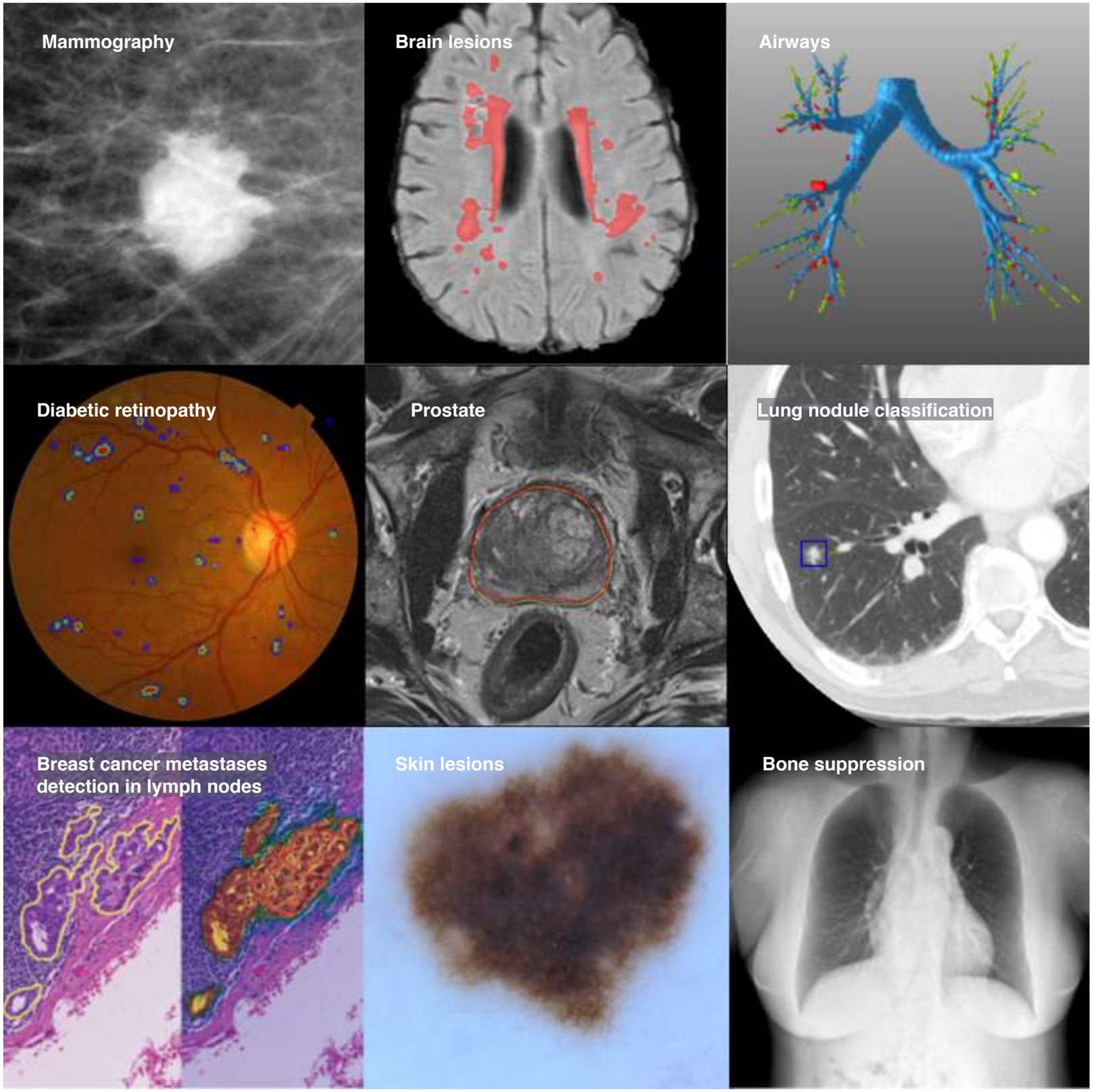

Litjiens et al. A survey on deep learning in medical image analysis. arXiv:1702.05747 2017

OROBIX

Arterys Receives FDA Clearance For The First Zero-Footprint Medical Imaging Analytics Cloud Software With Deep Learning For Cardiac MRI

ARTERYS

NEWS PROVIDED BY
Arterys →
Jan 09, 2017, 12:51 ET

SHARE THIS ARTICLE

SAN FRANCISCO, Jan. 9, 2017 /PRNewswire/ -- Arterys, a pioneer in cloud-based medical imaging software, has received 510(k) clearance from the U.S. Food and Drug Administration (FDA) to market its Arterys Cardio DL™ application. Arterys Cardio DL™ is the first technology to be cleared by the FDA that leverages cloud computing and deep learning in a clinical setting. Arterys Cardio DL™ provides automated, editable ventricle segmentations based on conventional cardiac MRI images that are as accurate as segmentations performed manually by experienced physicians. The U.S. clearance complements the CE Mark received in late December for commercialization of the Arterys Cardio DL™ product in Europe.

"Arterys is committed to broadly accelerate the transformation of data-driven medicine through advanced cloud medical imaging analytics applications while always protecting patient data privacy," said Fabien Beckers, Arterys CEO. "Today's approval signifies a major regulatory milestone. This application demonstrates the power of deep learning combined with cloud supercomputation to aid physicians in interpreting medical images - eliminating tedious manual tasks carried out on a workstation by accurately automating those processes."

http://www.prnewswire.com/news-releases/arterys-receives-fda-clearance-for-the-first-zero-footprint-medical-imaging-analytics-cloud-software-with-deep-learning-for-cardiac-mri-300387880.html

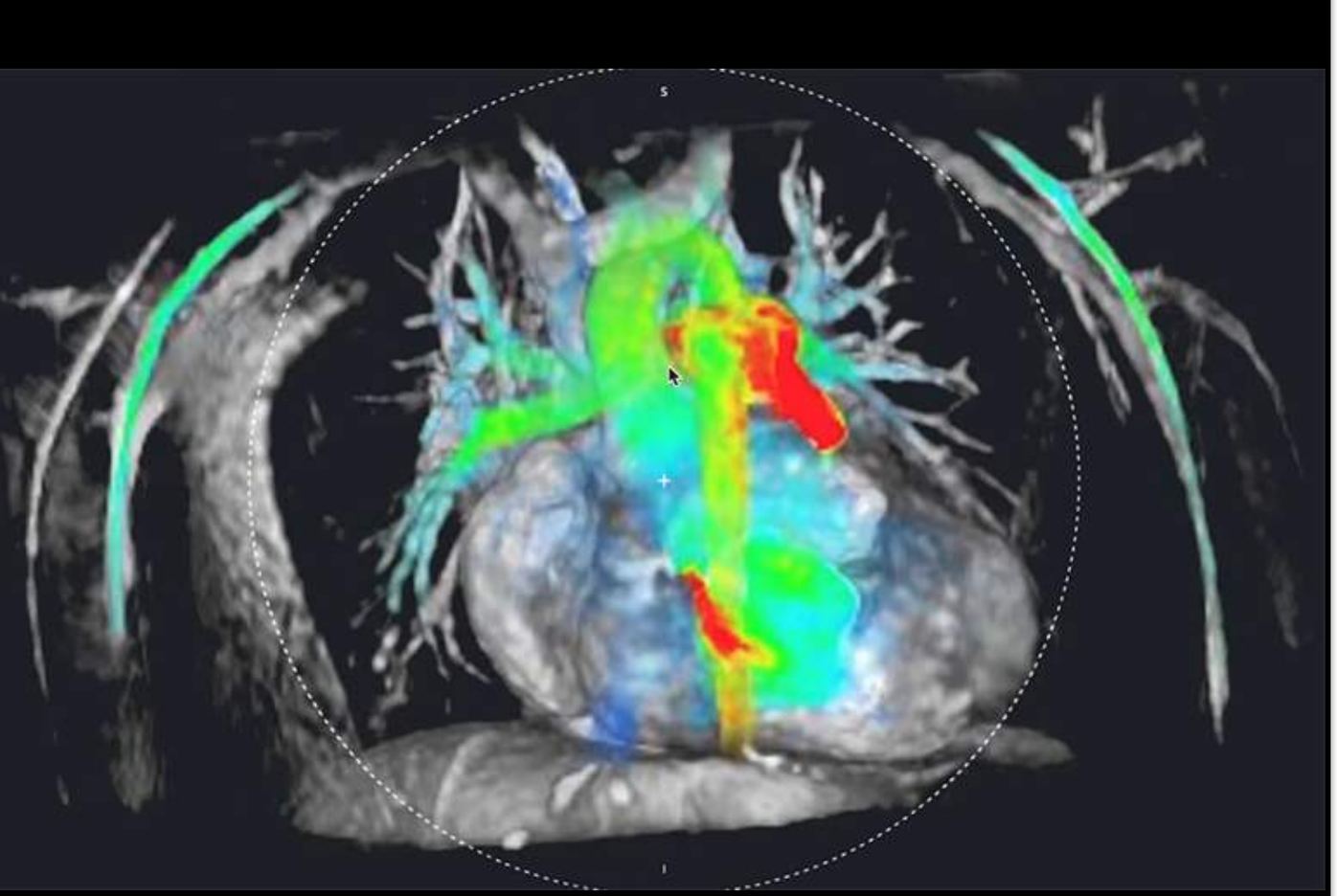

OROBIX

FDA approval Nov 2016
4D Flow

both 510(k)
(equivalence to predicate device)

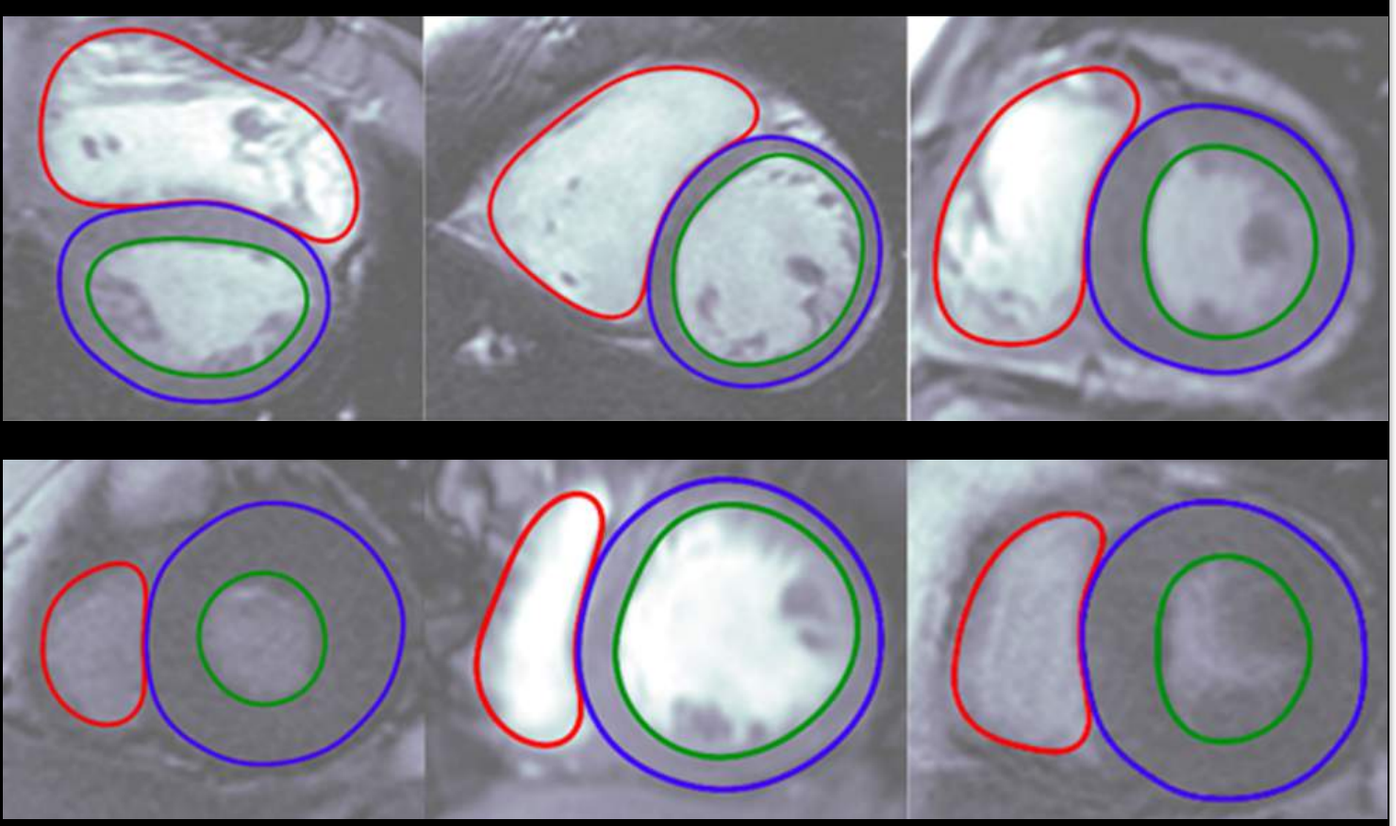

FDA approval Feb 2017
Arterys Cardio DL

ARTERYS

Deep learning algorithms for detection of critical findings in head CT scans: a retrospective study

Sasank Chilamkurthy, Rohit Ghosh, Swetha Tanamala, Mustafa Biviji, Norbert G Campeau, Vasantha Kumar Venugopal, Vidur Mahajan, Pooja Rao, Prashant Warier

Summary

Background Non-contrast head CT scan is the current standard for initial imaging of patients with head trauma or stroke symptoms. We aimed to develop and validate a set of deep learning algorithms for automated detection of the following key findings from these scans: intracranial haemorrhage and its types (ie, intraparenchymal, intraventricular, subdural, extradural, and subarachnoid); calvarial fractures; midline shift; and mass effect.

Methods We retrospectively collected a dataset containing 313 318 head CT scans together with their clinical reports from around 20 centres in India between Jan 1, 2011, and June 1, 2017. A randomly selected part of this dataset (Qure25k dataset) was used for validation and the rest was used to develop algorithms. An additional validation dataset (CQ500 dataset) was collected in two batches from centres that were different from those used for the development and Qure25k datasets. We excluded postoperative scans and scans of patients younger than 7 years. The original clinical radiology report and consensus of three independent radiologists were considered as gold standard for the Qure25k and CQ500 datasets, respectively. Areas under the receiver operating characteristic curves (AUCs) were primarily used to assess the algorithms.

Findings The Qure25k dataset contained 21 095 scans (mean age 43 years; 9030 [43%] female patients), and the CQ500 dataset consisted of 214 scans in the first batch (mean age 43 years; 94 [44%] female patients) and 277 scans in the second batch (mean age 52 years; 84 [30%] female patients). On the Qure25k dataset, the algorithms achieved an AUC of 0·92 (95% CI 0·91–0·93) for detecting intracranial haemorrhage (0·90 [0·89–0·91] for intraparenchymal, 0·96 [0·94–0·97] for intraventricular, 0·92 [0·90–0·93] for subdural, 0·93 [0·91–0·95] for extradural, and 0·90 [0·89–0·92] for subarachnoid). On the CQ500 dataset, AUC was 0·94 (0·92–0·97) for intracranial haemorrhage (0·95 [0·93–0·98], 0·93 [0·87–1·00], 0·95 [0·91–0·99], 0·97 [0·91–1·00], and 0·96 [0·92–0·99], respectively). AUCs on the Qure25k dataset were 0·92 (0·91–0·94) for calvarial fractures, 0·93 (0·91–0·94) for midline shift, and 0·86 (0·85–0·87) for mass effect, while AUCs on the CQ500 dataset were 0·96 (0·92–1·00), 0·97 (0·94–1·00), and 0·92 (0·89–0·95), respectively.

Interpretation Our results show that deep learning algorithms can accurately identify head CT scan abnormalities requiring urgent attention, opening up the possibility to use these algorithms to automate the triage process.

Funding Qure.ai.

Copyright © 2018 Elsevier Ltd. All rights reserved.

Published Online
October 11, 2018
http://dx.doi.org/10.1016/S0140-6736(18)31645-3

See Online/Comment
http://dx.doi.org/10.1016/S0140-6736(18)31925-1

Qure.ai, Goregaon East, Mumbai, India (S Chilamkurthy BTech, R Ghosh BTech, S Tanamala MTech, P Rao PhD, P Warier PhD); **CT & MRI Center, Dhantoli, Nagpur, India** (M Biviji DNB); **Department of Radiology, Mayo Clinic, Rochester, MN, USA** (N G Campeau MD); **and Centre for Advanced Research in Imaging, Neurosciences and Genomics, New Delhi, India** (V K Venugopal MD, V Mahajan MBA)

Correspondence to: Mr Sasank Chilamkurthy, Qure.ai, Goregaon East, Mumbai 400063, India
sasank.chilamkurthy@qure.ai

	AUC (95% CI)	High sensitivity operating point		High specificity operating point	
		Sensitivity (95% CI)	Specificity (95% CI)	Sensitivity (95% CI)	Specificity (95% CI)
Qure25k dataset					
Intracranial haemorrhage	0·9194 (0·9119–0·9269)	0·9006 (0·8882–0·9121)	0·7295 (0·7230–0·7358)	0·8349 (0·8197–0·8492)	0·9004 (0·8960–0·9047)
Intra-parenchymal	0·8977 (0·8884–0·9069)	0·9031 (0·8894–0·9157)	0·6046 (0·5976–0·6115)	0·7670 (0·7479–0·7853)	0·9046 (0·9003–0·9087)
Intraventricular	0·9559 (0·9424–0·9694)	0·9358 (0·9085–0·9569)	0·8343 (0·8291–0·8393)	0·9220 (0·8927–0·9454)	0·9267 (0·9231–0·9302)
Subdural	0·9161 (0·9001–0·9321)	0·9152 (0·8888–0·9370)	0·6542 (0·6476–0·6607)	0·7960 (0·7600–0·8288)	0·9041 (0·9000–0·9081)
Extradural	0·9288 (0·9083–0·9494)	0·9034 (0·8635–0·9349)	0·7936 (0·7880–0·7991)	0·8207 (0·7716–0·8631)	0·9068 (0·9027–0·9107)
Subarachnoid	0·9044 (0·8882–0·9205)	0·9100 (0·8844–0·9315)	0·6678 (0·6613–0·6742)	0·7758 (0·7406–0·8083)	0·9012 (0·8971–0·9053)
Calvarial fracture	0·9244 (0·9130–0·9359)	0·9002 (0·8798–0·9181)	0·7749 (0·7691–0·7807)	0·8115 (0·7857–0·8354)	0·9020 (0·8978–0·9061)
Midline shift	0·9276 (0·9139–0·9413)	0·9114 (0·8872–0·9319)	0·8373 (0·8322–0·8424)	0·8754 (0·8479–0·8995)	0·9006 (0·8964–0·9047)
Mass effect	0·8583 (0·8462–0·8703)	0·8622 (0·8439–0·8792)	0·6157 (0·6089–0·6226)	0·7086 (0·6851–0·7314)	0·9068 (0·9026–0·9108)
CQ500 dataset					
Intracranial haemorrhage	0·9419 (0·9187–0·9651)	0·9463 (0·9060–0·9729)	0·7098 (0·6535–0·7617)	0·8195 (0·7599–0·8696)	0·9021 (0·8616–0·9340)
Intra-parenchymal	0·9544 (0·9293–0·9795)	0·9478 (0·8953–0·9787)	0·8123 (0·7679–0·8515)	0·8433 (0·7705–0·9003)	0·9076 (0·8726–0·9355)
Intraventricular	0·9310 (0·8654–0·9965)	0·9286 (0·7650–0·9912)	0·6652 (0·6202–0·7081)	0·8929 (0·7177–0·9773)	0·9028 (0·8721–0·9282)
Subdural	0·9521 (0·9117–0·9925)	0·9434 (0·8434–0·9882)	0·7215 (0·6769–0·7630)	0·8868 (0·7697–0·9573)	0·9041 (0·8726–0·9300)
Extradural	0·9731 (0·9113–1·0000)	0·9231 (0·6397–0·9981)	0·8828 (0·8506–0·9103)	0·8462 (0·5455–0·9808)	0·9477 (0·9238–0·9659)
Subarachnoid	0·9574 (0·9214–0·9934)	0·9167 (0·8161–0·9724)	0·8654 (0·8295–0·8962)	0·8667 (0·7541–0·9406)	0·9049 (0·8732–0·9309)
Calvarial fracture	0·9624 (0·9204–1·0000)	0·9487 (0·8268–0·9937)	0·8606 (0·8252–0·8912)	0·8718 (0·7257–0·9570)	0·9027 (0·8715–0·9284)
Midline shift	0·9697 (0·9403–0·9991)	0·9385 (0·8499–0·9830)	0·8944 (0·8612–0·9219)	0·9077 (0·8098–0·9654)	0·9108 (0·8796–0·9361)
Mass effect	0·9216 (0·8883–0·9548)	0·9055 (0·8408–0·9502)	0·7335 (0·6849–0·7782)	0·8189 (0·7408–0·8816)	0·9038 (0·8688–0·9321)

Neither of the datasets was used during the training process. AUCs are shown for nine critical CT findings in both these datasets. Two operating points were chosen on the ROC curve for high sensitivity and high specificity, respectively. Absolute number used for calculation of sensitivity and specificity are in the appendix (p 7). AUC=area under the receiver operating characteristic curve. ROC=receiver operating characteristic.

Table 4: **Performance of the algorithms on the Qure25k and CQ500 datasets**

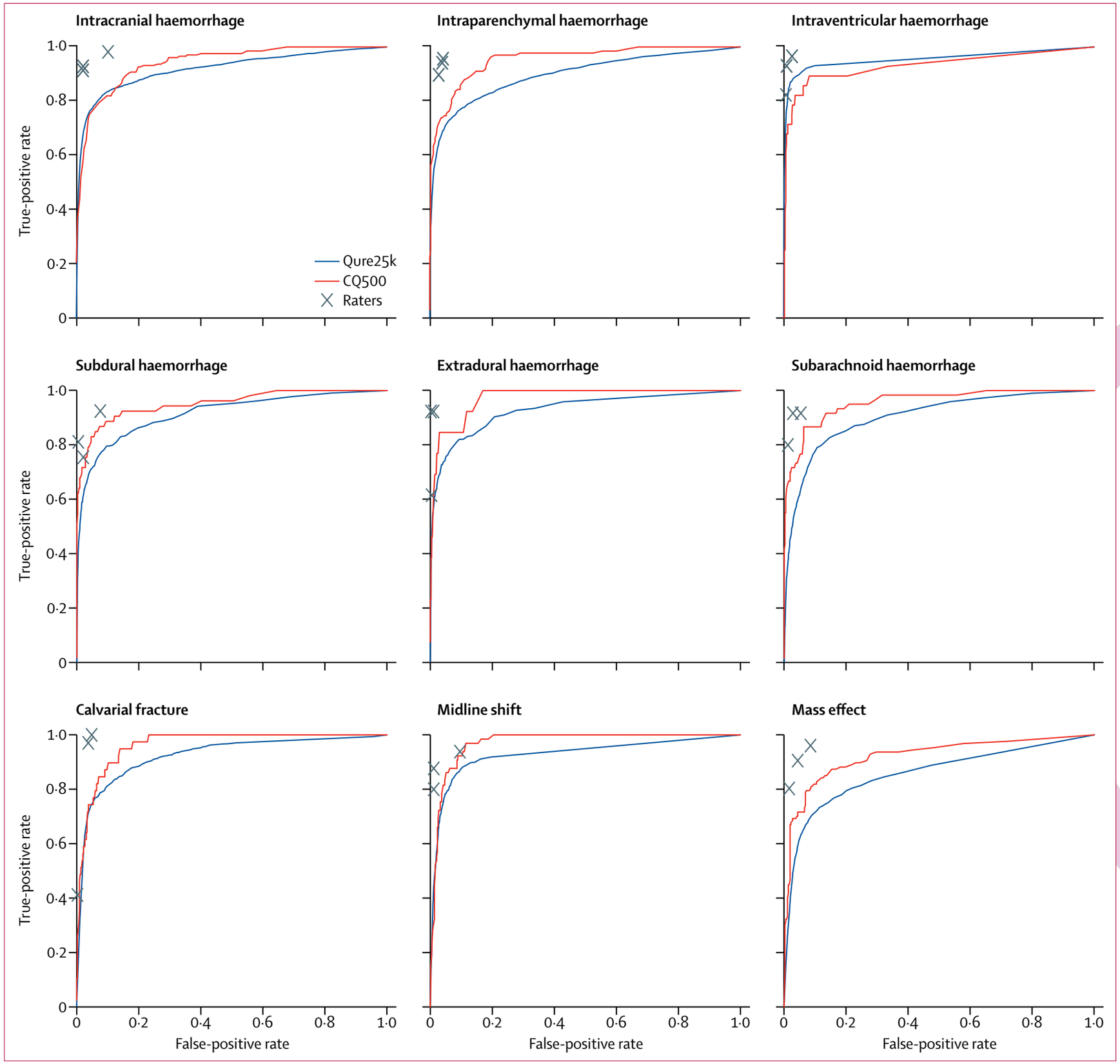

Figure 2: **ROC curves for the algorithms on Qure25k and CQ500 datasets**
Individual raters' true positive and false positive rates measured against their consensus on the CQ500 dataset are also plotted along with the ROCs for comparison. ROC=receiver operating characteristic.

Accurate predictions: true positives

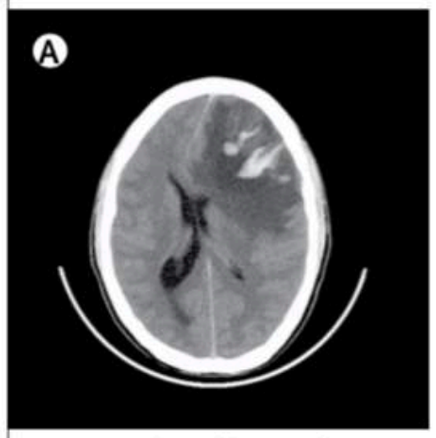

Intraparenchymal haemorrhage (in left frontal region)

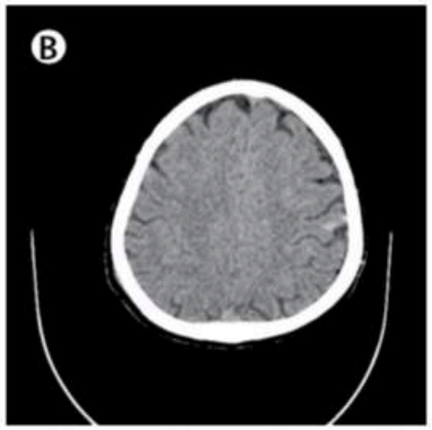

Subarachnoid haemorrhage (in left parietal region)

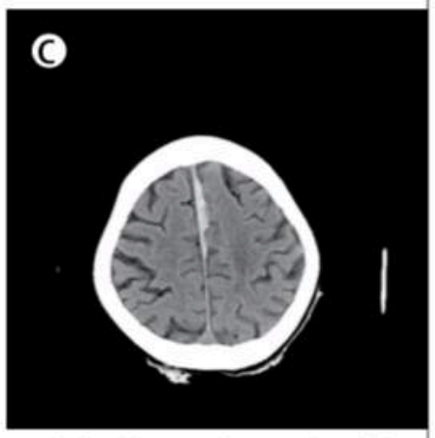

Subdural haemorrhage (along falx)

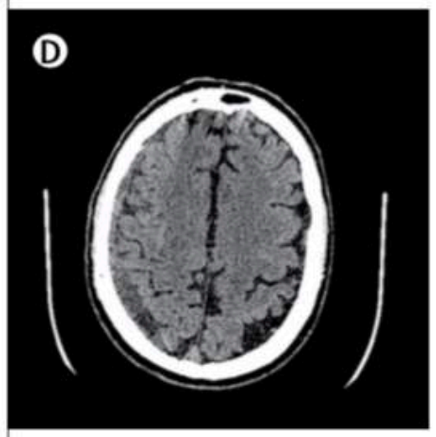

Subdural haemorrhage (chronic in right parietal convexity)

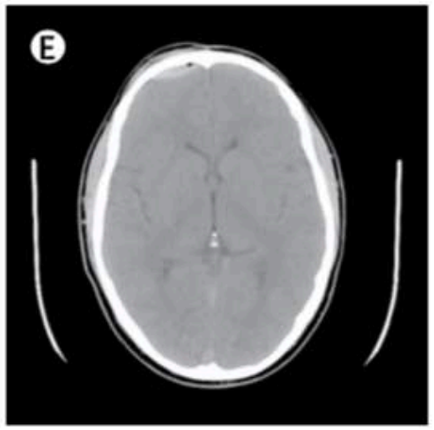

Extradural haemorrhage (in right frontal convexity)

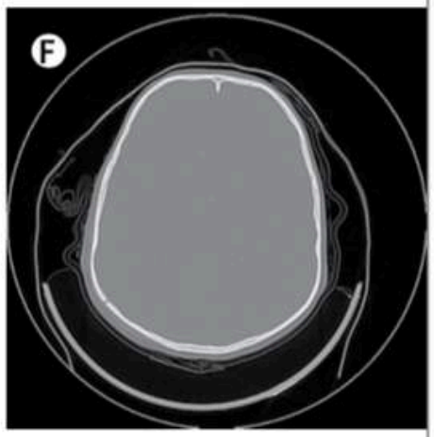

Calvarial fracture (in right parietal bone)

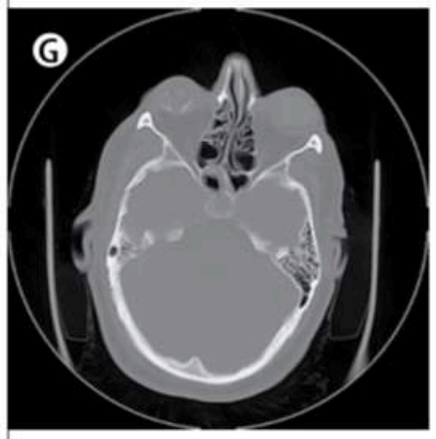

Calvarial fracture (in right temporal bone)

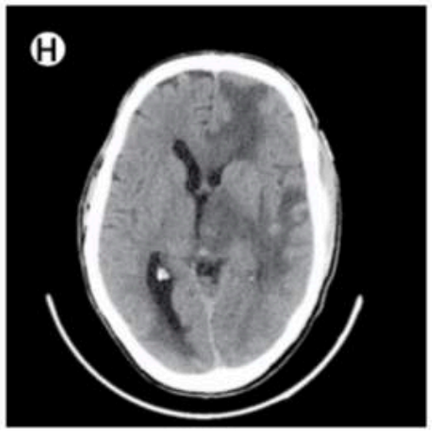

Midline shift

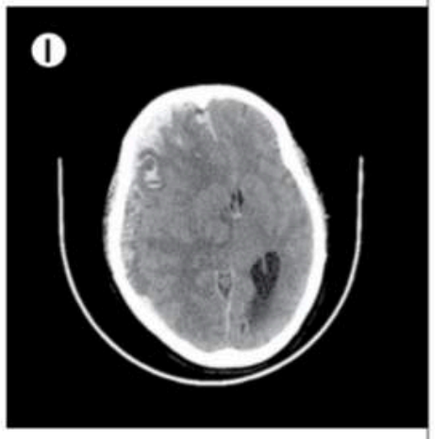

Midline shift

Erroneous predictions

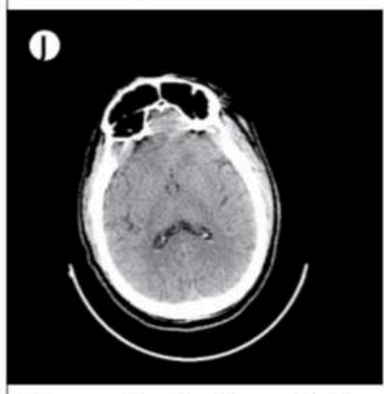

False negative: tiny intraventricalar haemorrhage

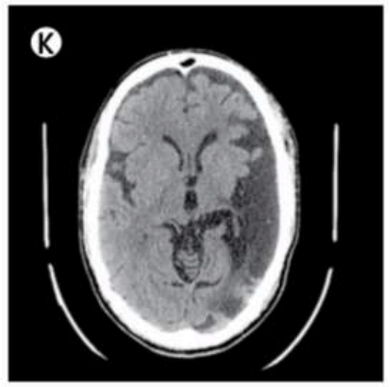

False positive: predicted as subdural haemorrhage

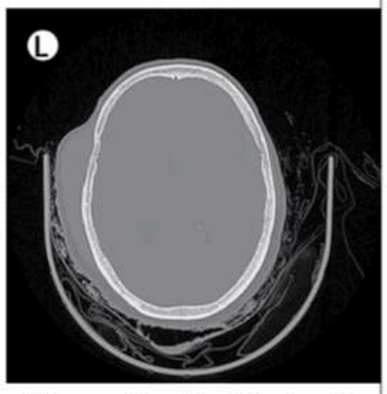

False negative: calvarial fracture (in right parietal bone)

Contents lists available at ScienceDirect

Medical Image Analysis

journal homepage: www.elsevier.com/locate/media

Robust whole-brain segmentation: Application to traumatic brain injury

Christian Ledig [a,*], Rolf A. Heckemann [e,b,c], Alexander Hammers [b,c,d], Juan Carlos Lopez [e], Virginia F.J. Newcombe [g], Antonios Makropoulos [a], Jyrki Lötjönen [f], David K. Menon [g], Daniel Rueckert [a]

[a] Biomedical Image Analysis Group, Department of Computing, Imperial College London, UK
[b] The Neurodis Foundation, CERMEP, Lyon, France
[c] Division of Brain Sciences, Faculty of Medicine, Imperial College London, UK
[d] The PET Centre, Division of Imaging Sciences and Biomedical Engineering Kings College London, St Thomas Hospital, London, UK
[e] MedTech West, Institute of Neuroscience and Physiology, University of Gothenburg, Sweden
[f] Knowledge Intensive Services, VTT Technical Research Centre of Finland, Tampere, Finland
[g] University Division of Anaesthesia, University of Cambridge, Addenbrooke's Hospital, Cambridge, UK

ARTICLE INFO

Article history:
Received 8 April 2014
Received in revised form 14 December 2014
Accepted 15 December 2014
Available online 24 December 2014

Keywords:
Traumatic brain injury
Magnetic resonance imaging
Multi-atlas segmentation
Brain image segmentation
Expectation–maximisation

ABSTRACT

We propose a framework for the robust and fully-automatic segmentation of magnetic resonance (MR) brain images called "Multi-Atlas Label Propagation with Expectation–Maximisation based refinement" (MALP-EM). The presented approach is based on a robust registration approach (MAPER), highly performant label fusion (joint label fusion) and intensity-based label refinement using EM. We further adapt this framework to be applicable for the segmentation of brain images with gross changes in anatomy. We propose to account for consistent registration errors by relaxing anatomical priors obtained by multi-atlas propagation and a weighting scheme to locally combine anatomical atlas priors and intensity-refined posterior probabilities. The method is evaluated on a benchmark dataset used in a recent MICCAI segmentation challenge. In this context we show that MALP-EM is competitive for the segmentation of MR brain scans of healthy adults when compared to state-of-the-art automatic labelling techniques. To demonstrate the versatility of the proposed approach, we employed MALP-EM to segment 125 MR brain images into 134 regions from subjects who had sustained traumatic brain injury (TBI). We employ a protocol to assess segmentation quality if no manual reference labels are available. Based on this protocol, three independent, blinded raters confirmed on 13 MR brain scans with pathology that MALP-EM is superior to established label fusion techniques. We visually confirm the robustness of our segmentation approach on the full cohort and investigate the potential of derived symmetry-based imaging biomarkers that correlate with and predict clinically relevant variables in TBI such as the Marshall Classification (MC) or Glasgow Outcome Score (GOS). Specifically, we show that we are able to stratify TBI patients with favourable outcomes from non-favourable outcomes with 64.7% accuracy using acute-phase MR images and 66.8% accuracy using follow-up MR images. Furthermore, we are able to differentiate subjects with the presence of a mass lesion or midline shift from those with diffuse brain injury with 76.0% accuracy. The thalamus, putamen, pallidum and hippocampus are particularly affected. Their involvement predicts TBI disease progression.

© 2014 The Authors. Published by Elsevier B.V. This is an open access article under the CC BY license (http://creativecommons.org/licenses/by/4.0/).

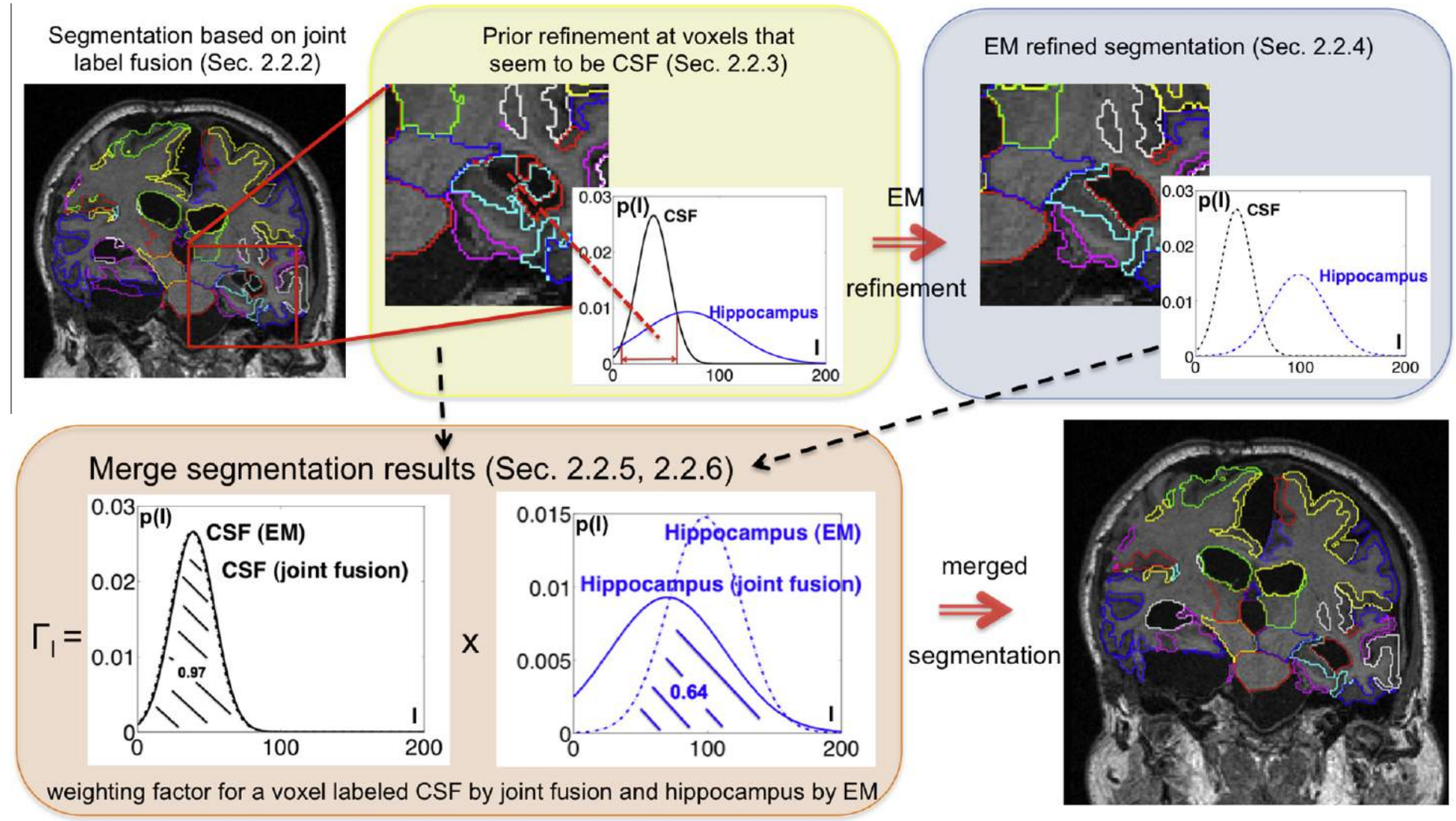

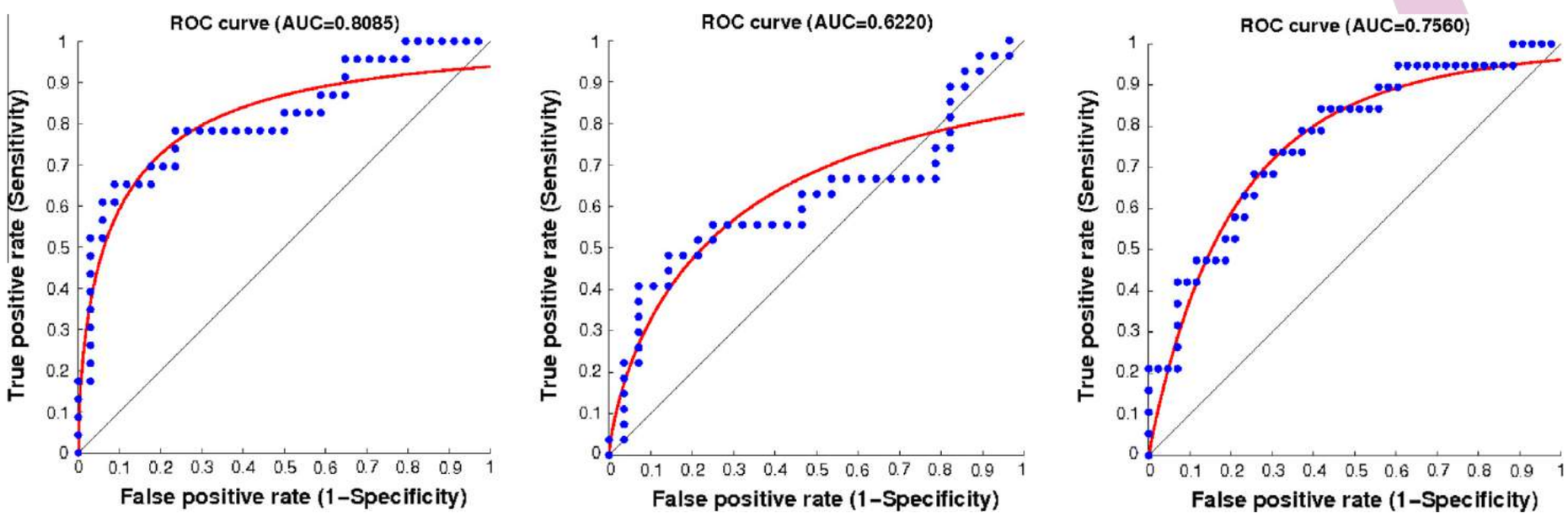

Fig. 11. Receiver operating characteristic curves for classifying subjects according to MC using the sum of cortical AAI (left), and according to GOS at baseline (middle) and follow up time point (right) using the accumulated non-cortical AAI.

CREACTIVE Imaging substudy

Obiettivo: valutare il ruolo biomarker basati su imaging TC di routine come tool prognostico

1. Raccolta di un dataset da centri GiViTI partecipanti al sottostudio imaging del progetto CREACTIVE. Raccolta delle CT disponibili da percorso clinico, senza richiesta di protocollo
2. Utilizzo di tecniche di analisi di immagine per l'estrazione di biomarker legati a dimensioni, forma, localizzazione di emorragie ed edema intraparenchimali, sia all'ammissione che nella loro evoluzione temporale

CREACTIVE Imaging substudy

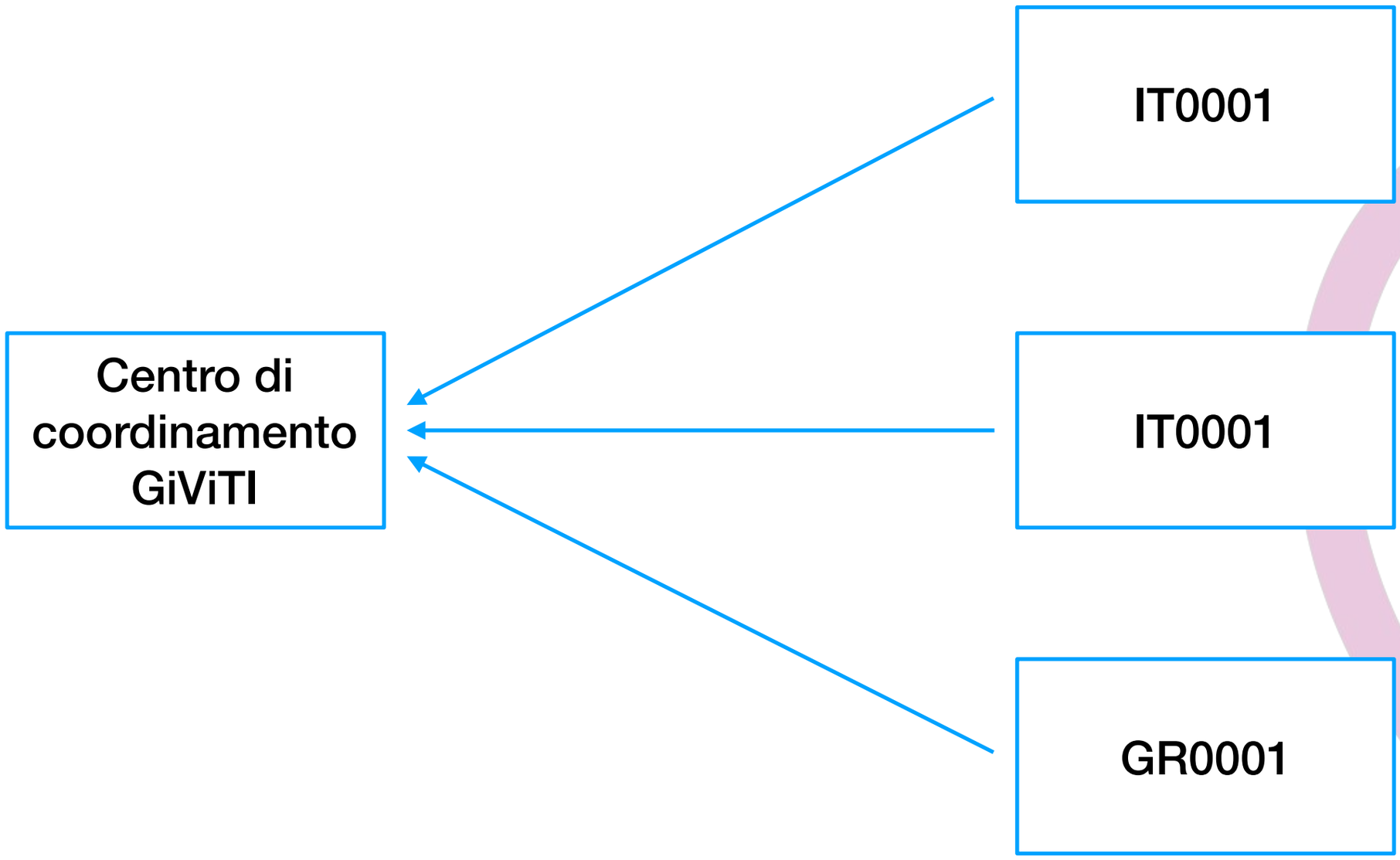

CREACTIVE Imaging substudy

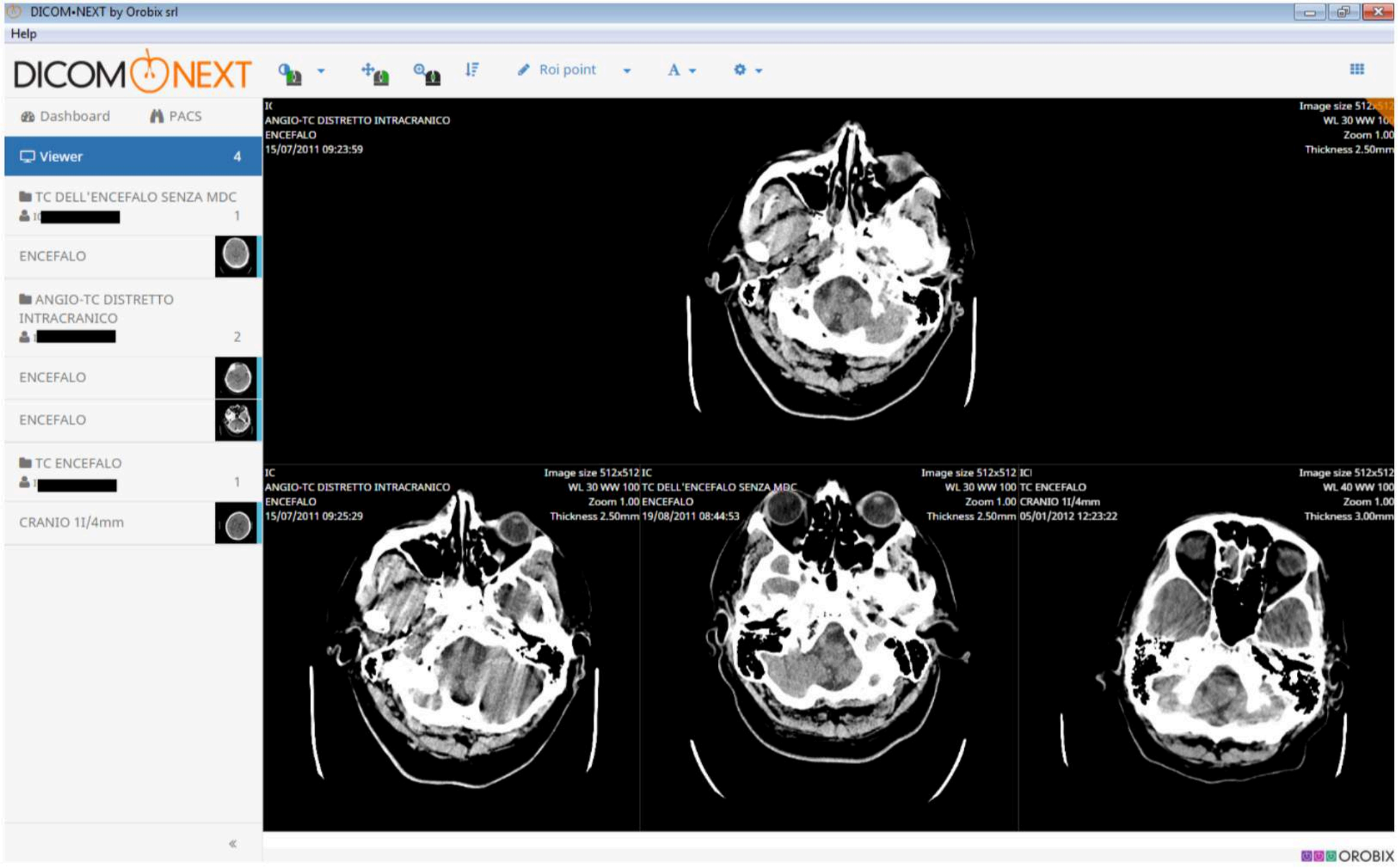

Imaging repository

8th February 2018

	Patients	Series
GR001	28	58
IL001	1	1
IT029	3	5
IT031	4	11
IT034	1	1
IT036	32	122
IT038	1	4
IT062	4	5
IT064	112	583
IT079	74	190
IT088	14	15
IT099	45	177
IT100	145	493
IT101	17	48
IT442	17	69
IT510	2	2
IT513	1	1
IT544	57	224
SI009	129	474

Patients: 687
Series: 2483

Imaging repository

8th February 2018

	Patients	Series
GR001	28	58
IL001	1	1
IT029	3	5
IT031	4	11
IT034	1	1
IT036	32	122
IT038	1	4
IT062	4	5
IT064	112	583
IT079	74	190
IT088	14	15
IT099	45	177
IT100	145	493
IT101	17	48
IT442	17	69
IT510	2	2
IT513	1	1
IT544	57	224
SI009	129	474

Patients: 687
Series: 2483

6th November 2018

	Patients	Series
GR001	42	81
IL001	1	1
IT029	3	5
IT031	4	11
IT034	1	1
IT036	32	123
IT038	1	4
IT062	4	5
IT064	135	657
IT079	205	608
IT088	14	15
IT099	45	177
IT100	207	720
IT101	17	48
IT438	10	39
IT442	17	69
IT510	2	2
IT513	1	1
IT544	57	224
SI009	206	758

Patients: 1004
Series: 3549

Automatic image processing system

Aim: evaluate the viability of imaging biomarkers based on routine CT imaging as a prognostic tool

- routine CT collected from participating centers, with fiducial-based annotations on hemorrhagic lesions
- scans anonymized and uploaded to CREACTIVE study center
- 1921 (6th February) quality-controlled follow-up series collected from 637 patients (data collection ongoing)
- target of 550 accurate manual segmentation of hemorrhagic lesions and edema

Current activities:

- development of automated lesion and edema segmentation
- follow-up evaluation of volumes
- evaluation of prognostic model augmented with imaging data

Dataset (in progress)

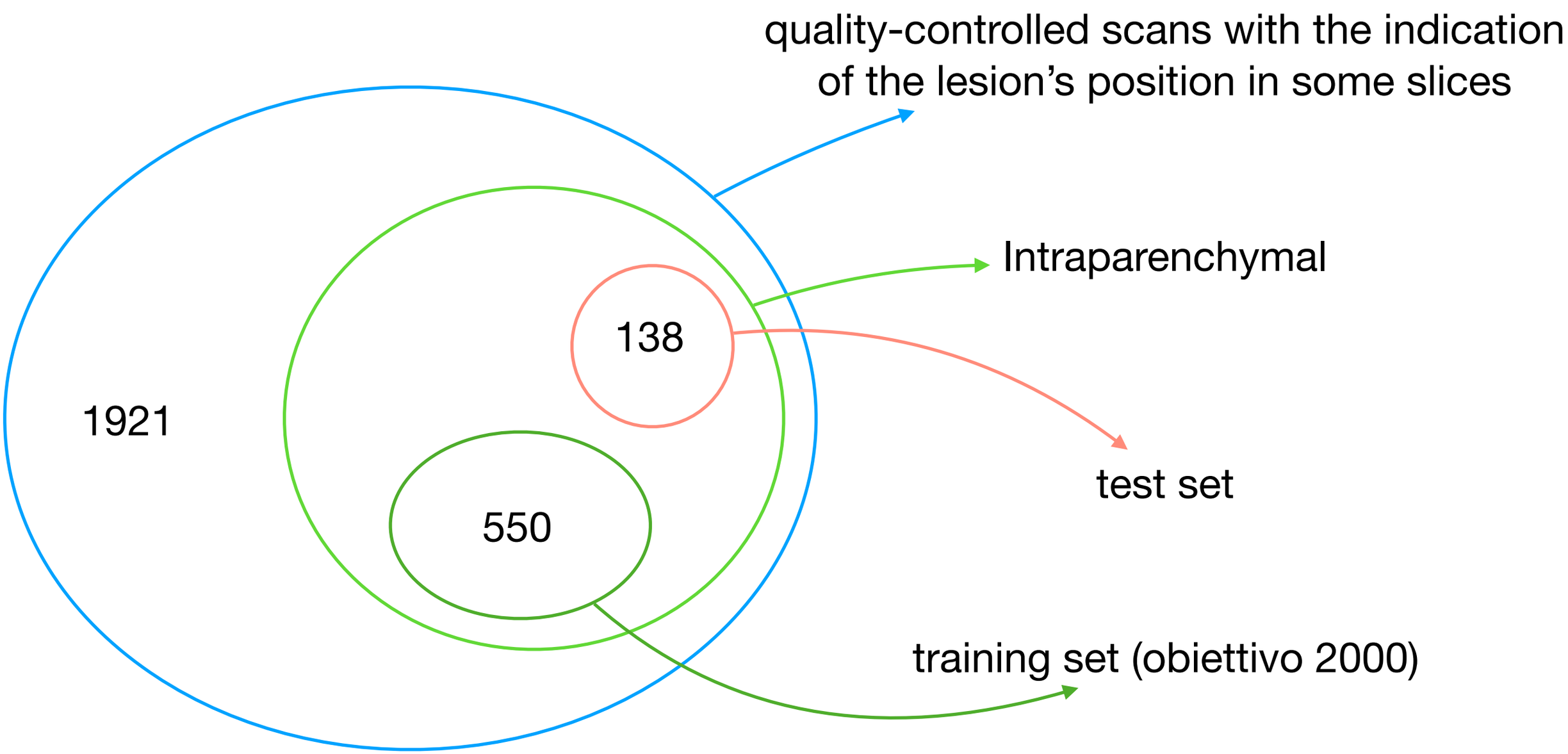

Dataset

Axial

Sagittal

Coronal

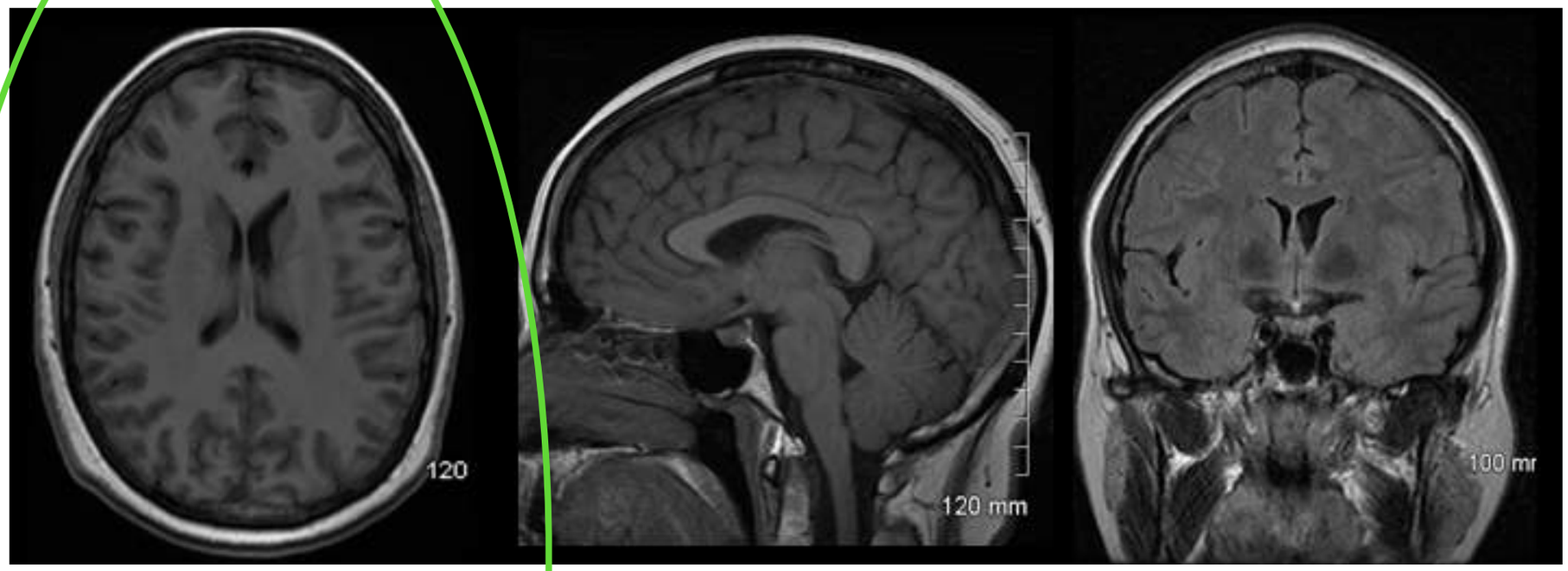

Intraparenchymal

Subdural

Subarachnoid

Original TC slice

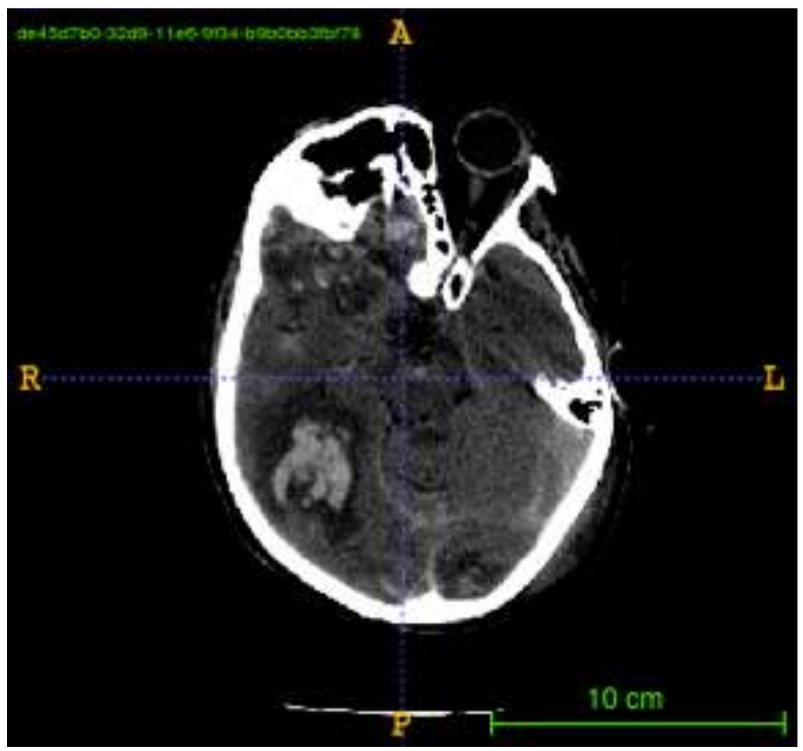

Manual segmentation

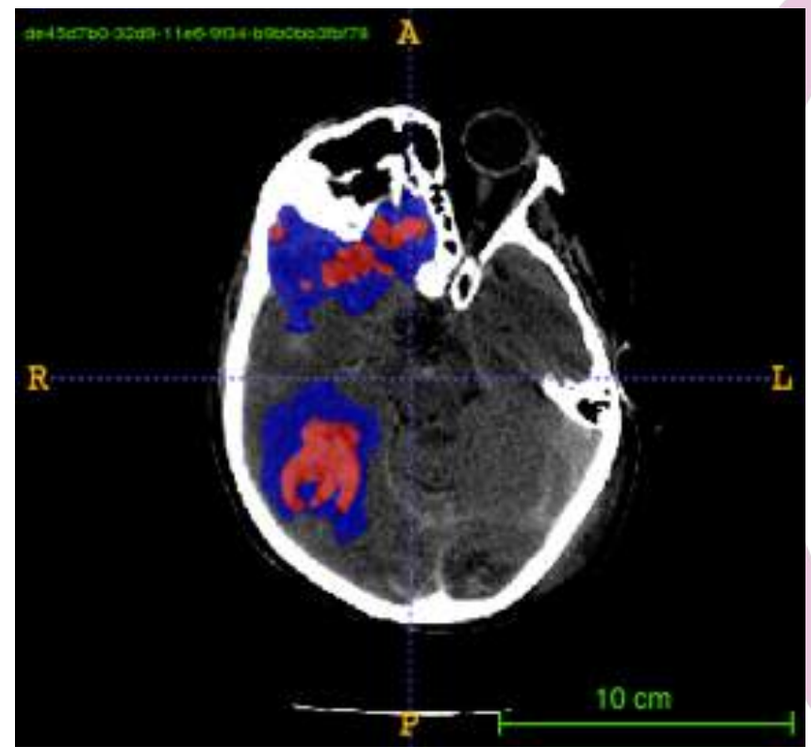

BLUE: edema
RED: hematoma

Automated segmentation model

A total of 1921 quality-controlled series were collected from 637 patients, after excluding series with strong artifacts (due to the presence of intracranial, radio-opaque devices in the scan).

Manual segmentation of **intraparenchymal hemorrhagic lesions** and **edema** was performed on an initial dataset of 504 series from 141 patients.

The dataset has been employed to train a **deep learning-based**, dense segmentation method (U-Net) for **automatic segmentation and sizing of lesion and edema**. Activity for manual segmentation of a batch of 550 series was started and is currently ongoing, with the aim of improving the performance of the automated segmentation method.

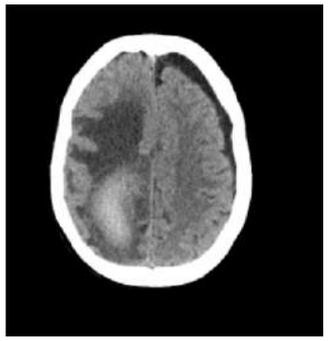

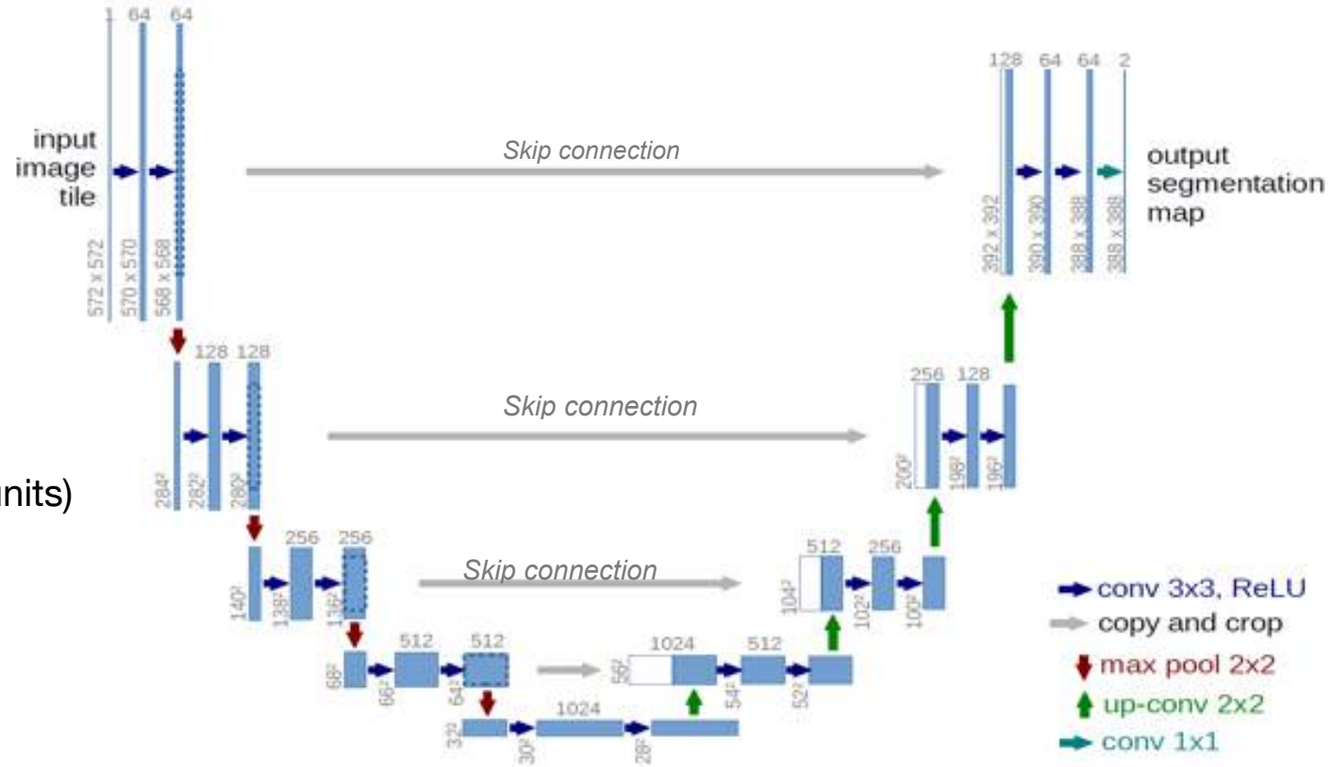

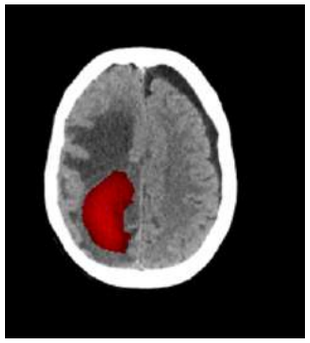

TC image PRE-PROCESSING:

- Clamp in interval 0-80 (Hounsfiled units)
- Resize to 256x256 pixels

Automated segmentation model

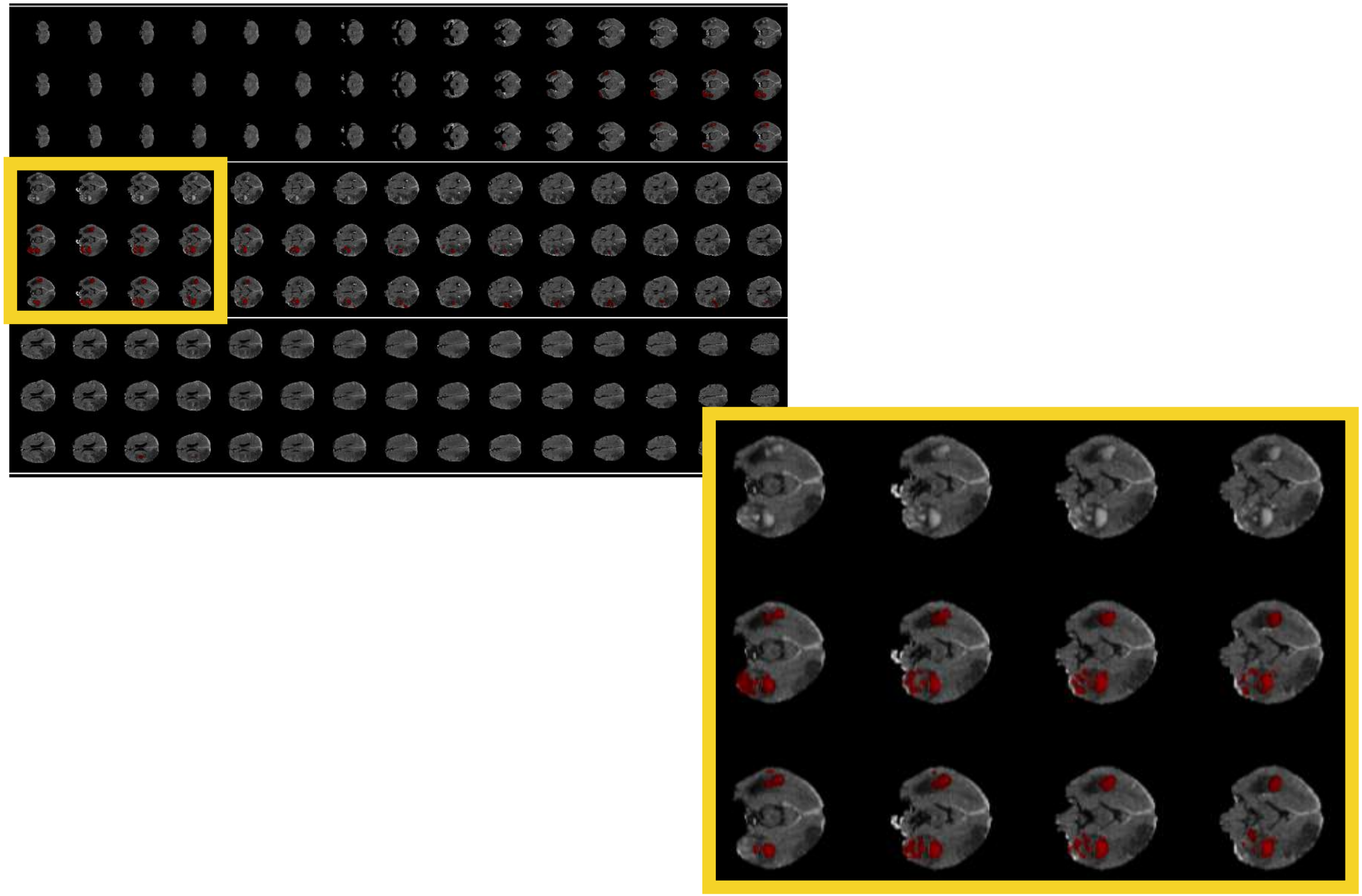

Hematoma segmentation

Dice coefficient:

- **Training** (159 scans): mean 0.61 std 0.24
- **Validation** (39 scans): mean 0.52 std 0.28

Dice coefficient:

- **Training** (368 scans): mean 0.67 std 0.23
- **Validation** (41 scans): mean 0.61 std 0.21
- **Test** (95 scans): mean 0.55 std 0.28

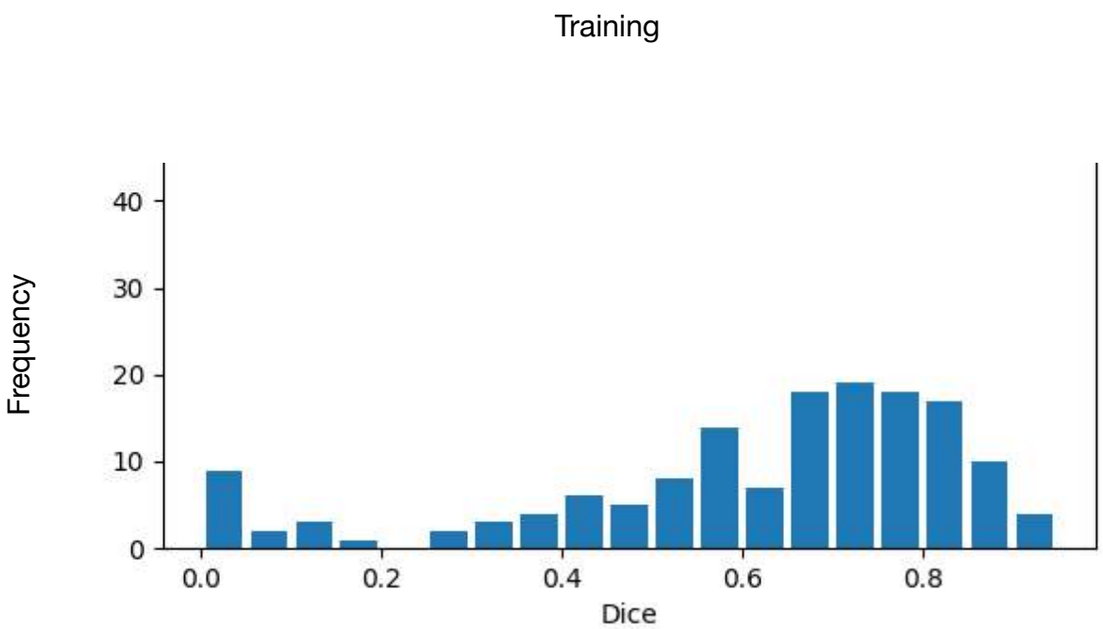

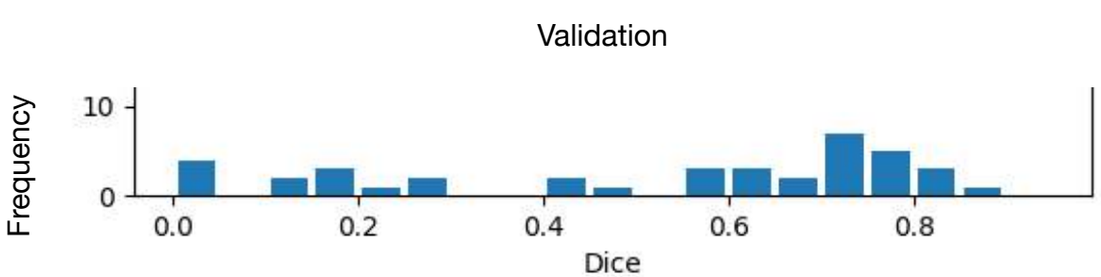

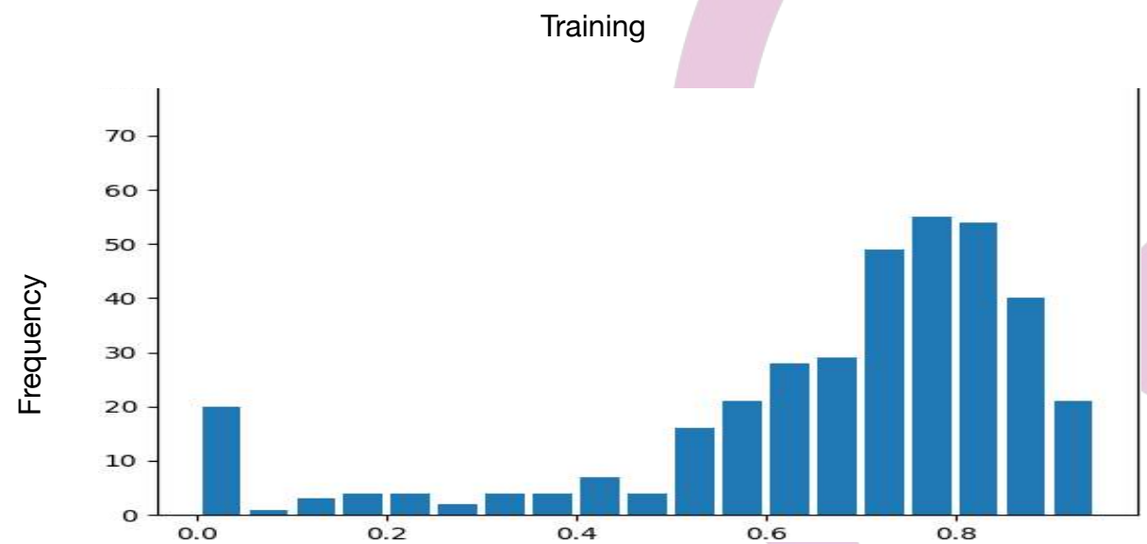

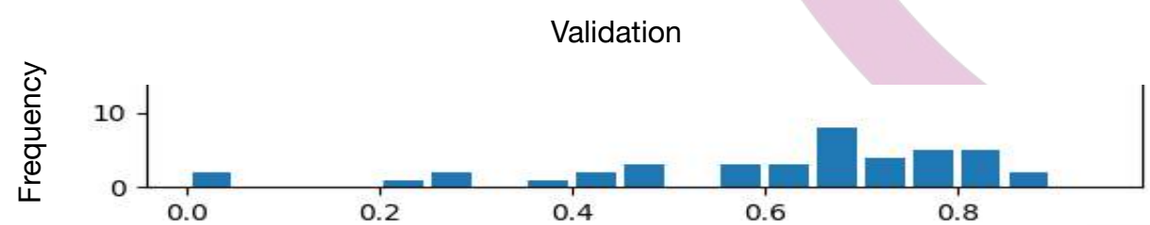

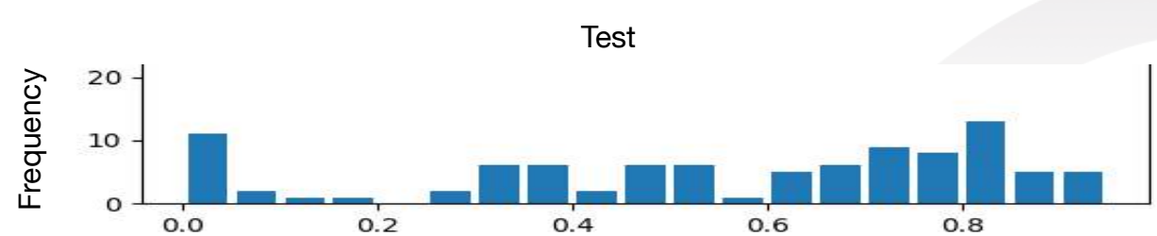

Hematoma segmentation

Dice coefficient:

- **Training** (159 scans): mean 0.61 std 0.24
- **Validation** (39 scans): mean 0.52 std 0.28

Dice coefficient:

- **Training** (368 scans): mean 0.67 std 0.23
- **Validation** (41 scans): mean 0.61 std 0.21
- **Test** (95 scans): mean 0.55 std 0.28

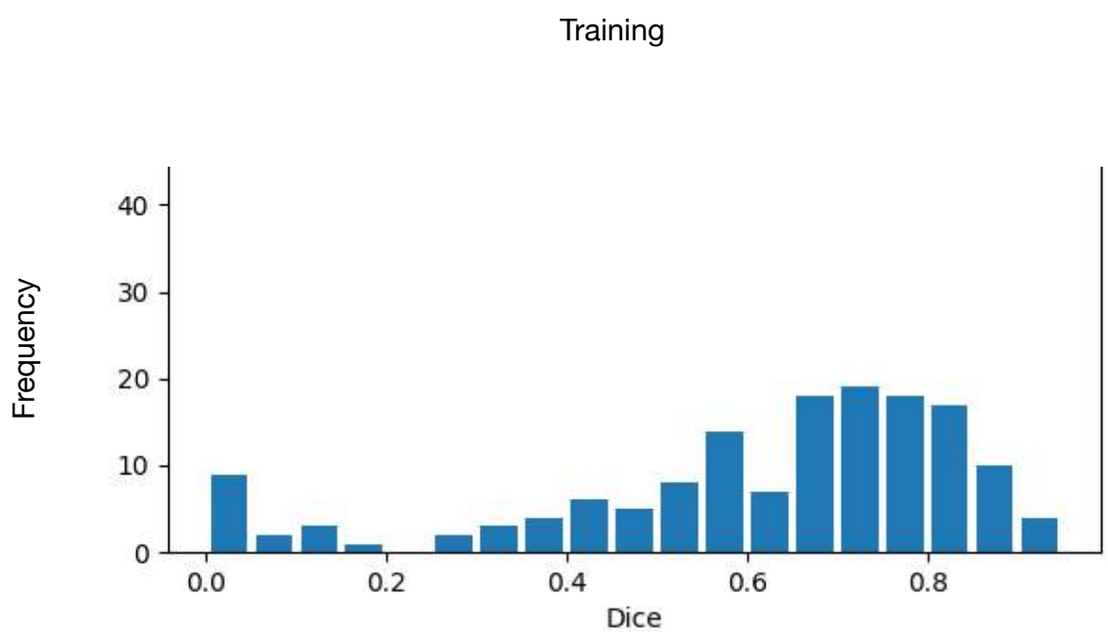

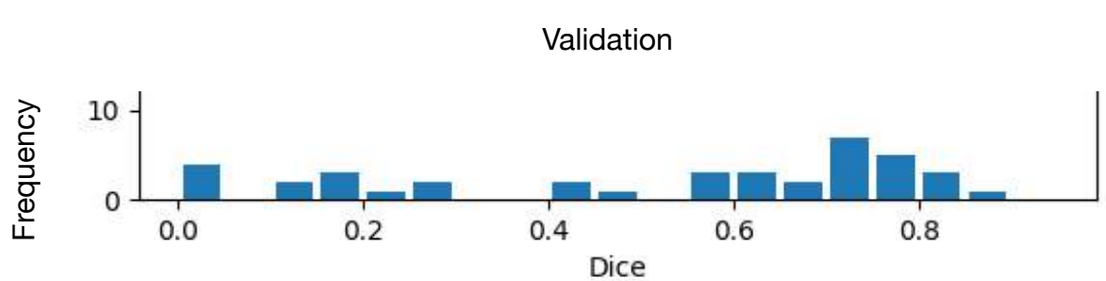

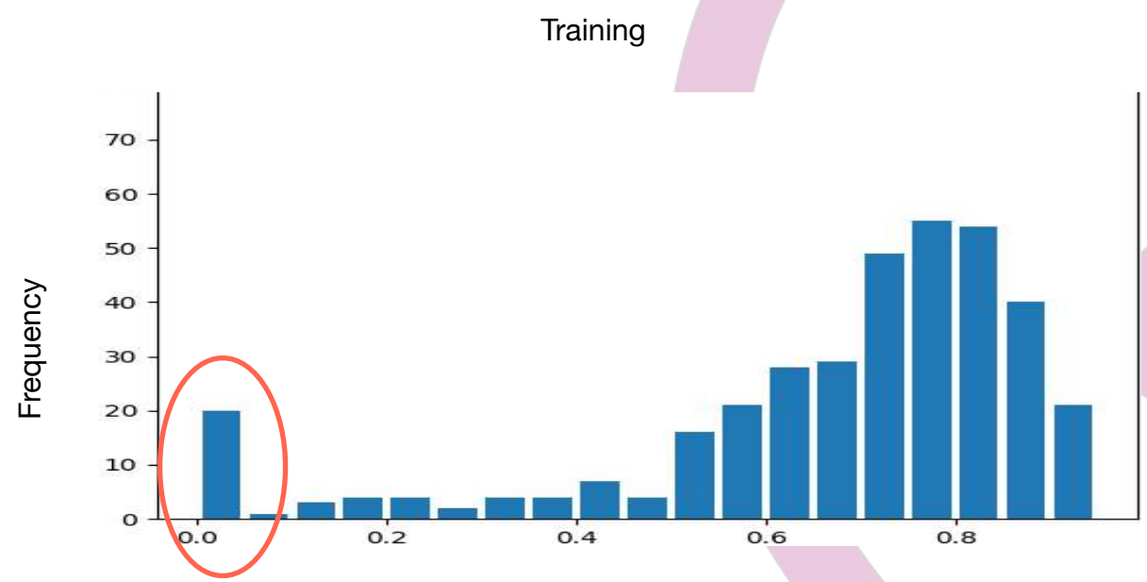

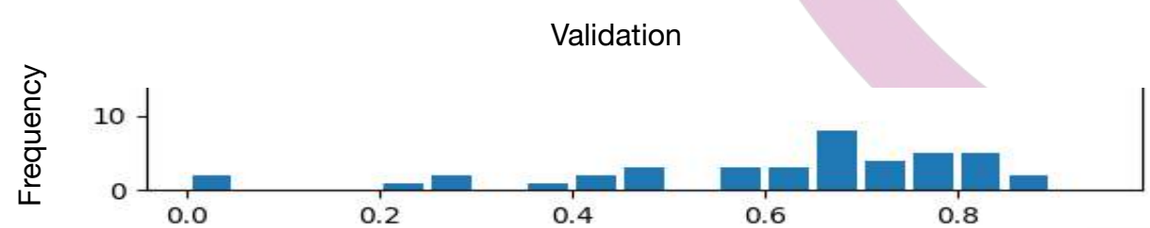

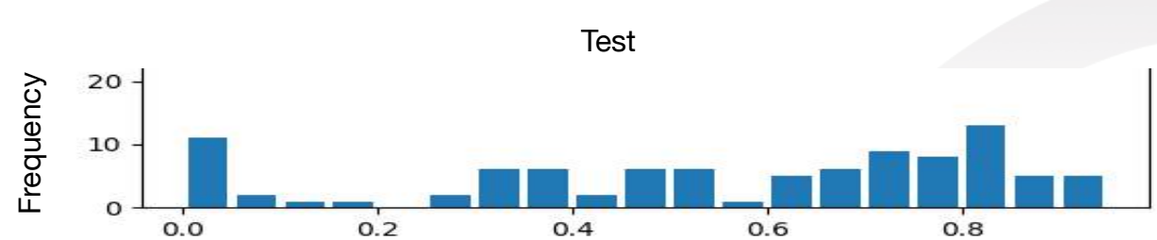

Hematoma segmentation

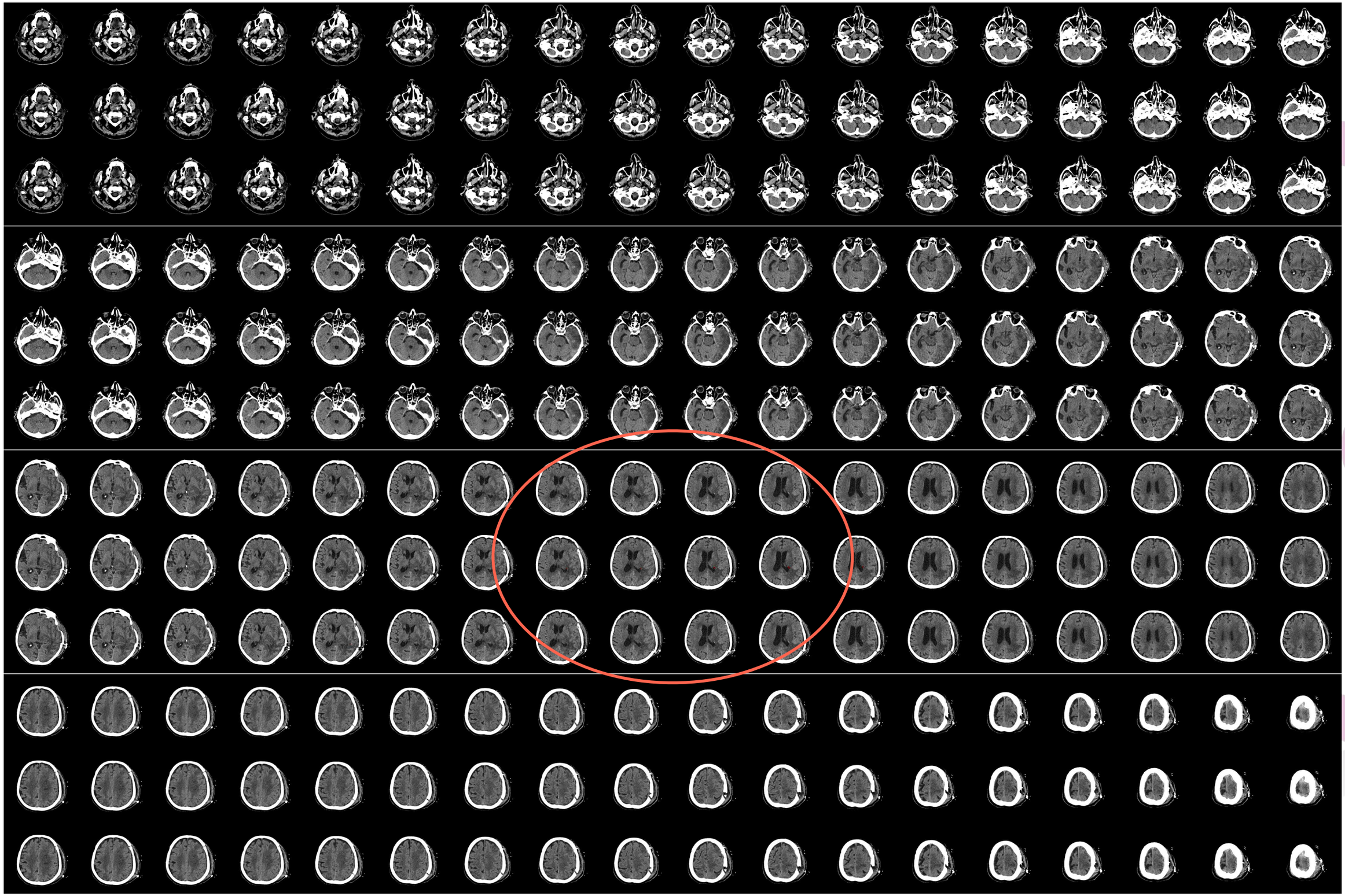

Hematoma segmentation

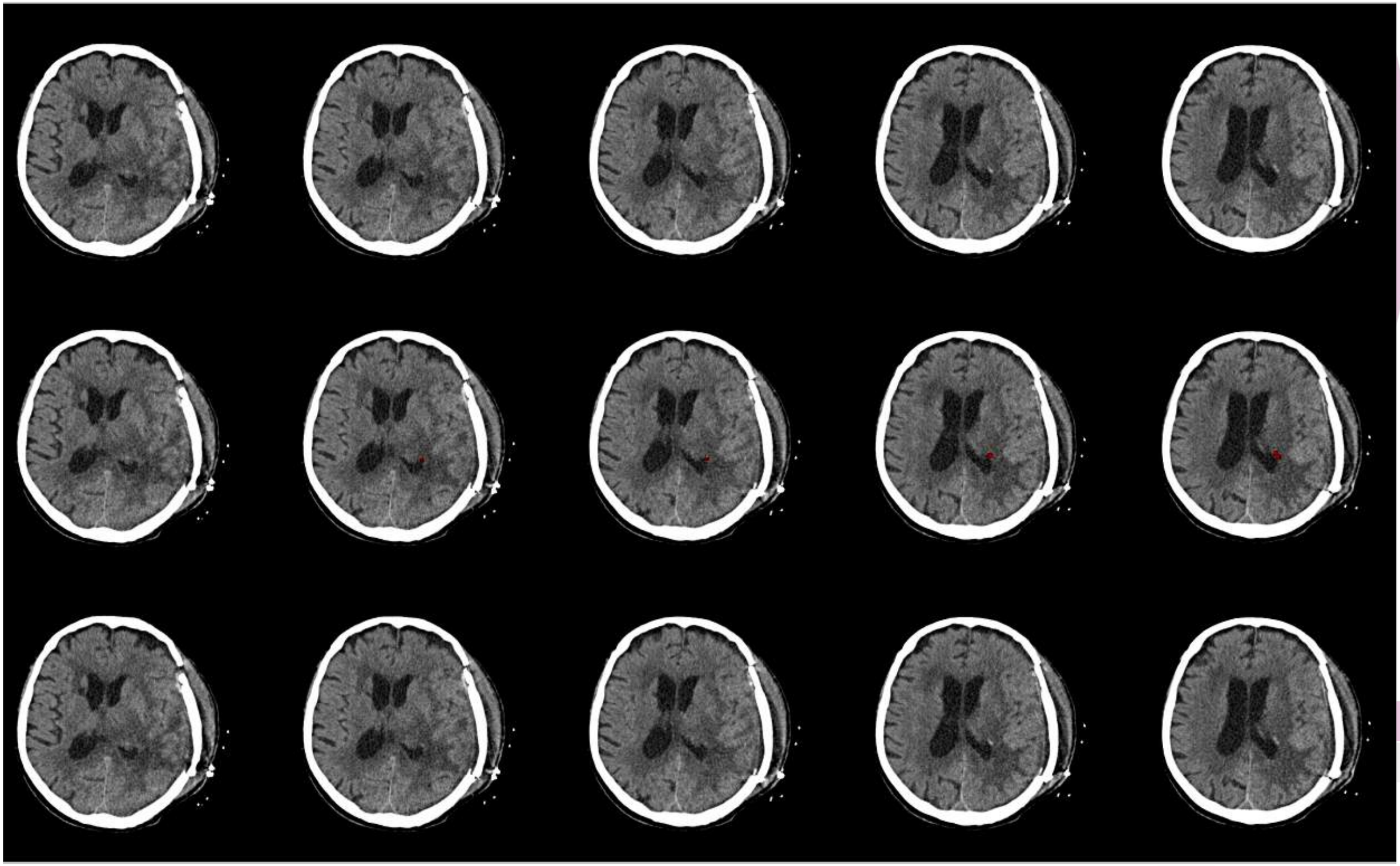

Hematoma segmentation

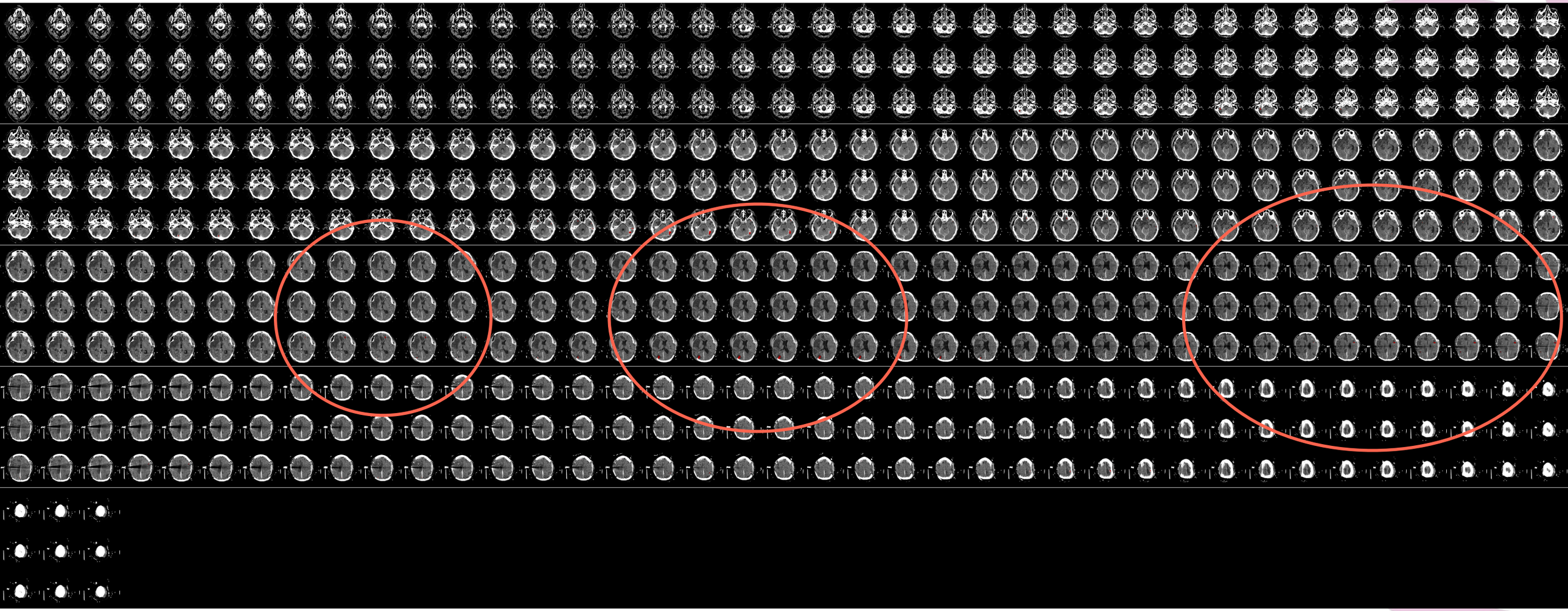

Hematoma segmentation

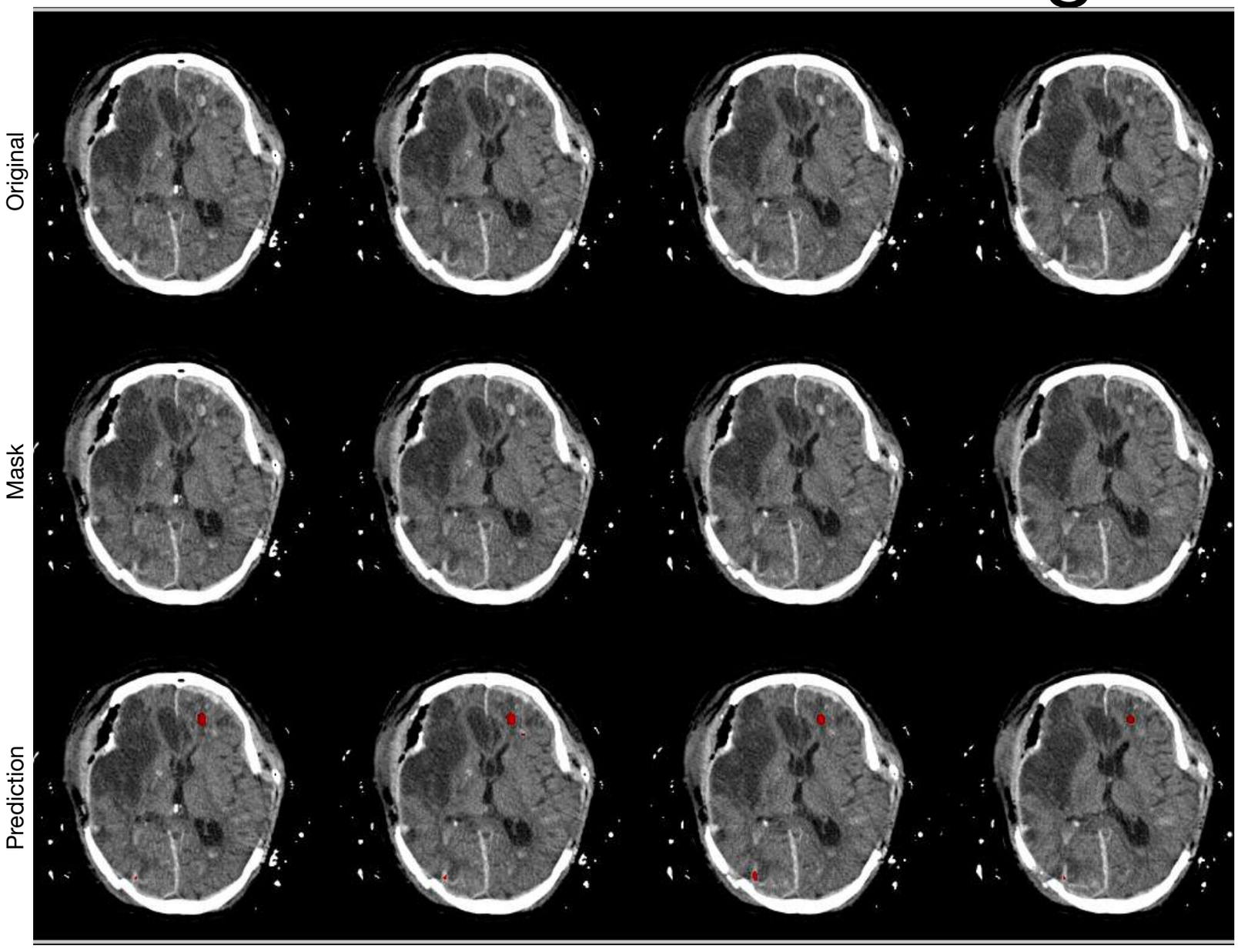

Hematoma segmentation

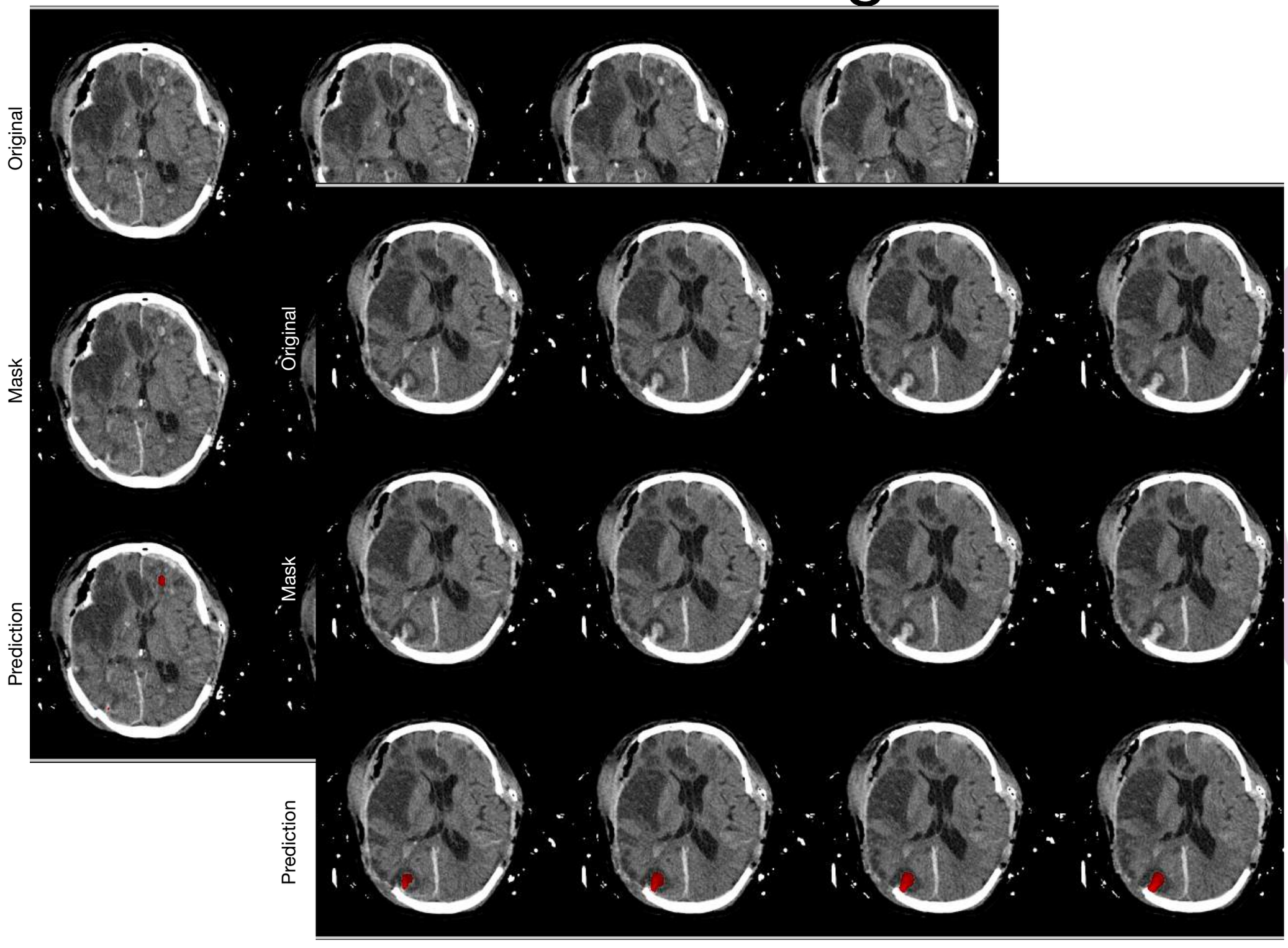

Hematoma segmentation

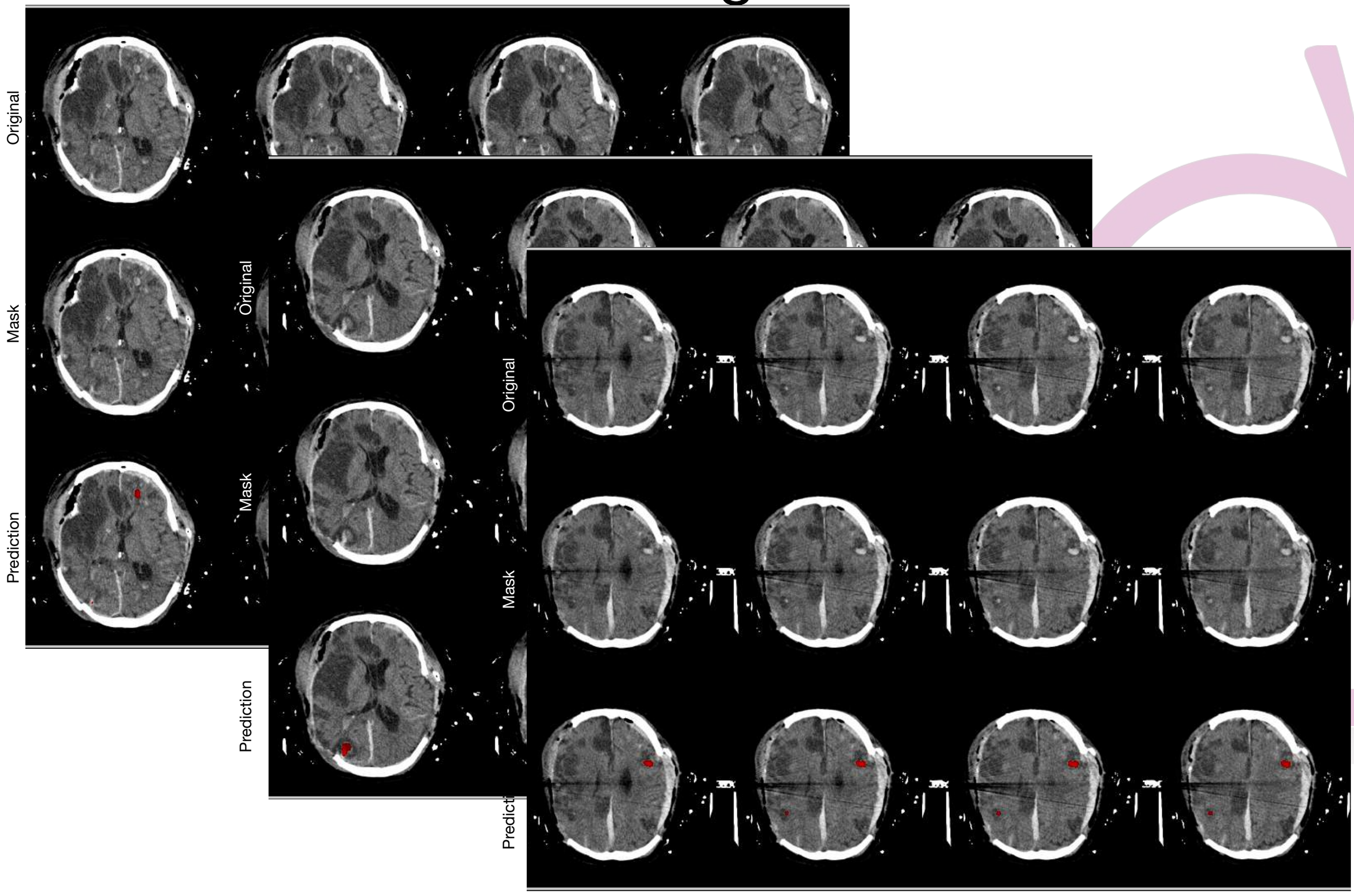

Hematoma segmentation

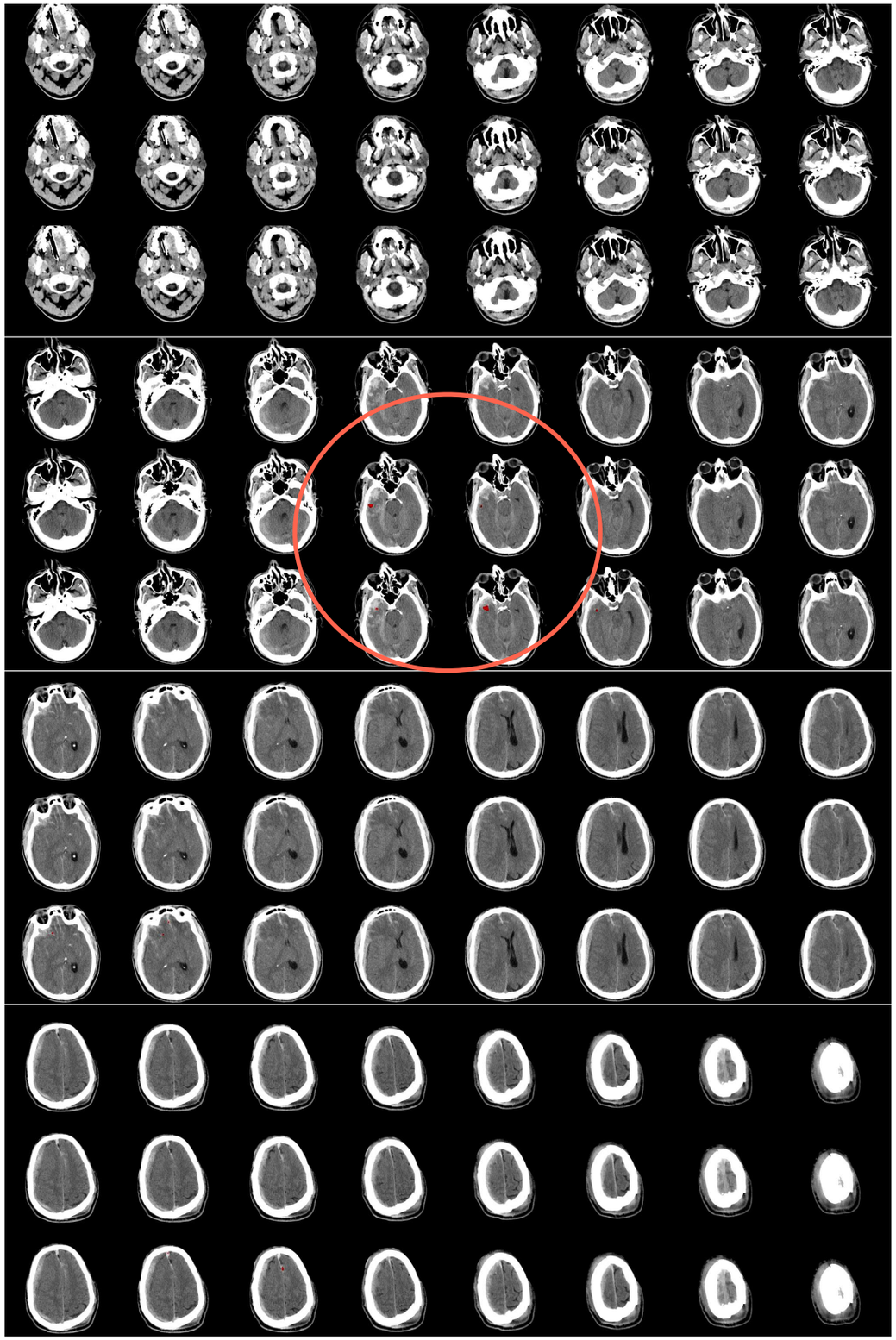

Hematoma segmentation

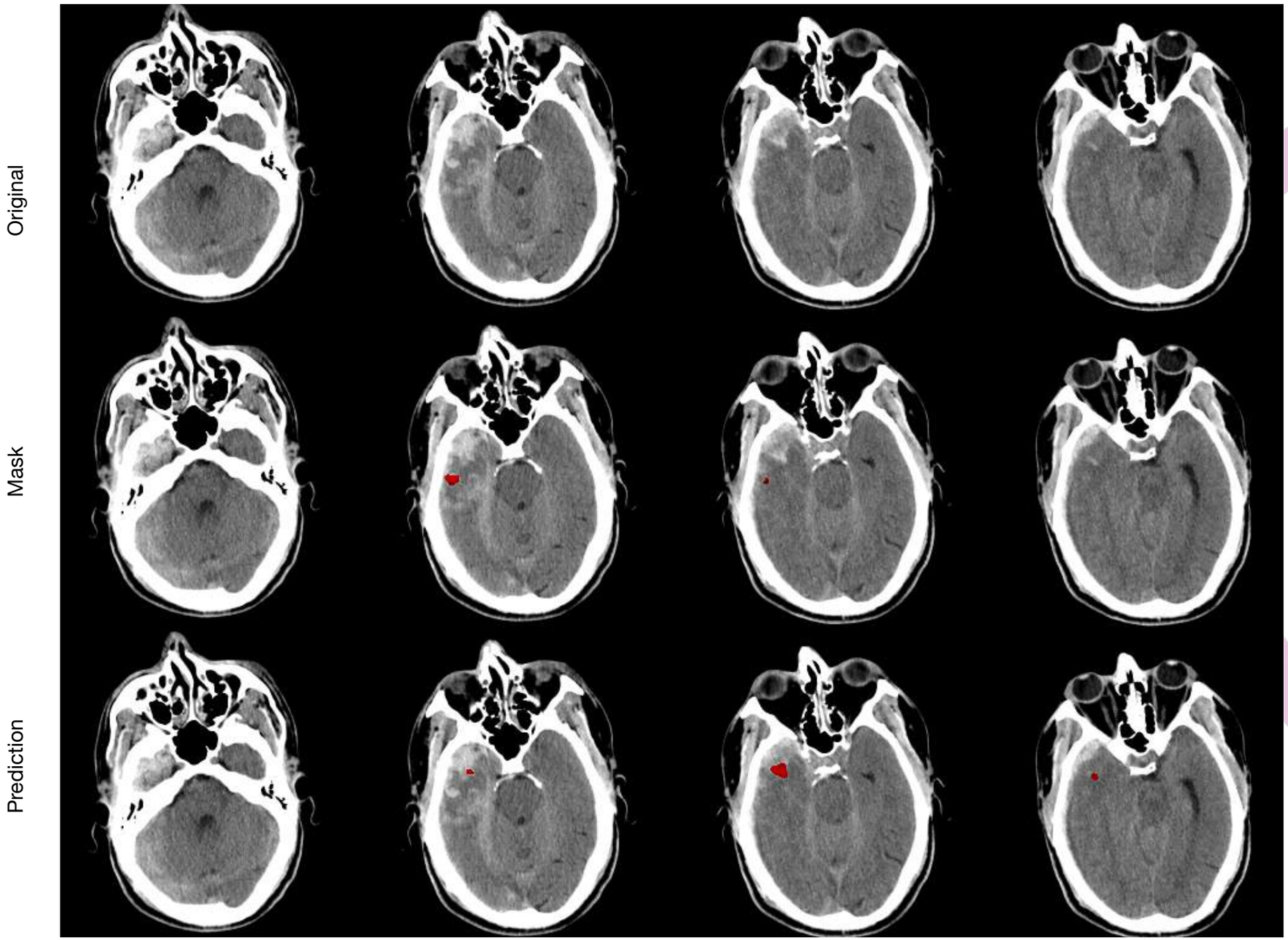

Hematoma segmentation

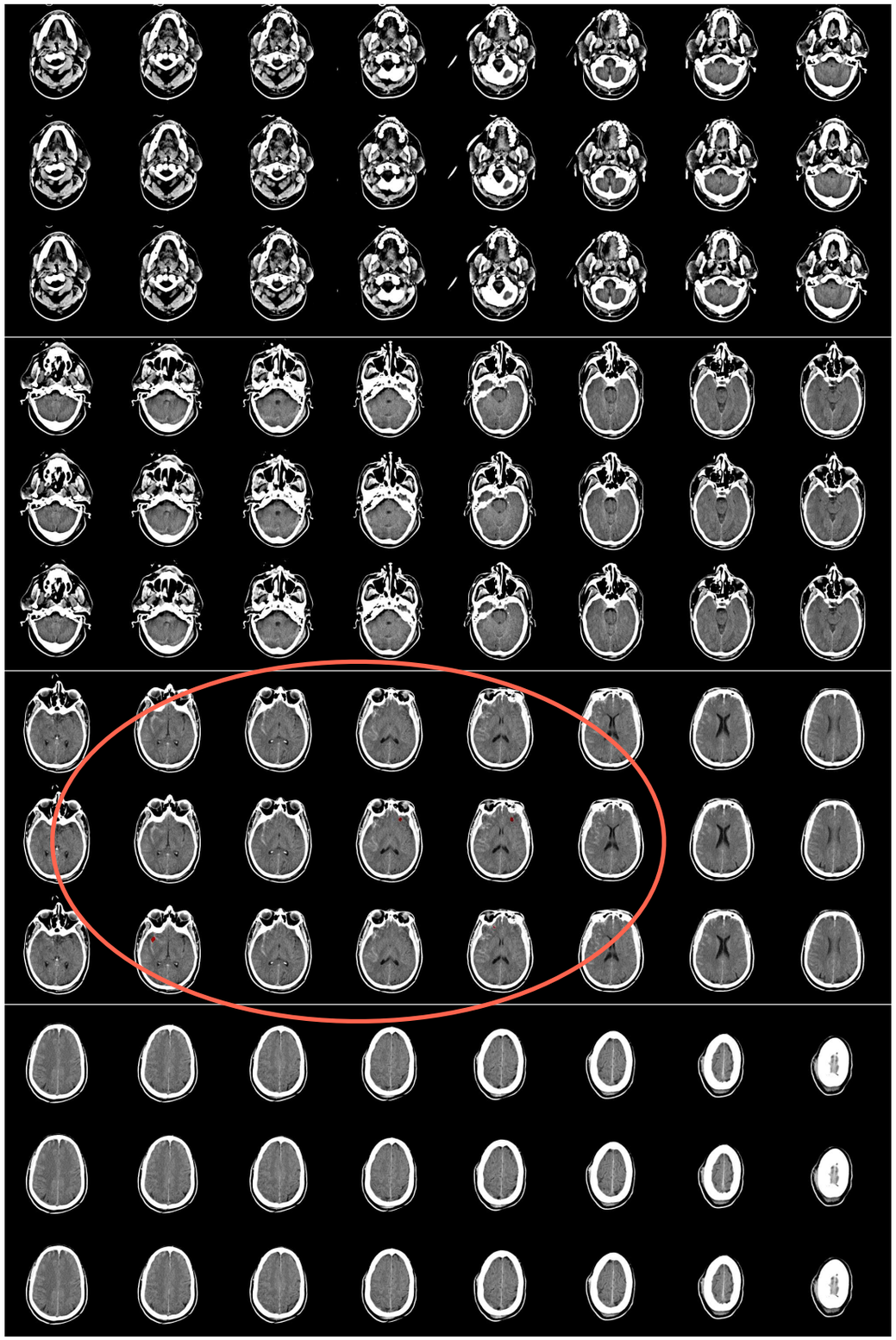

Hematoma segmentation

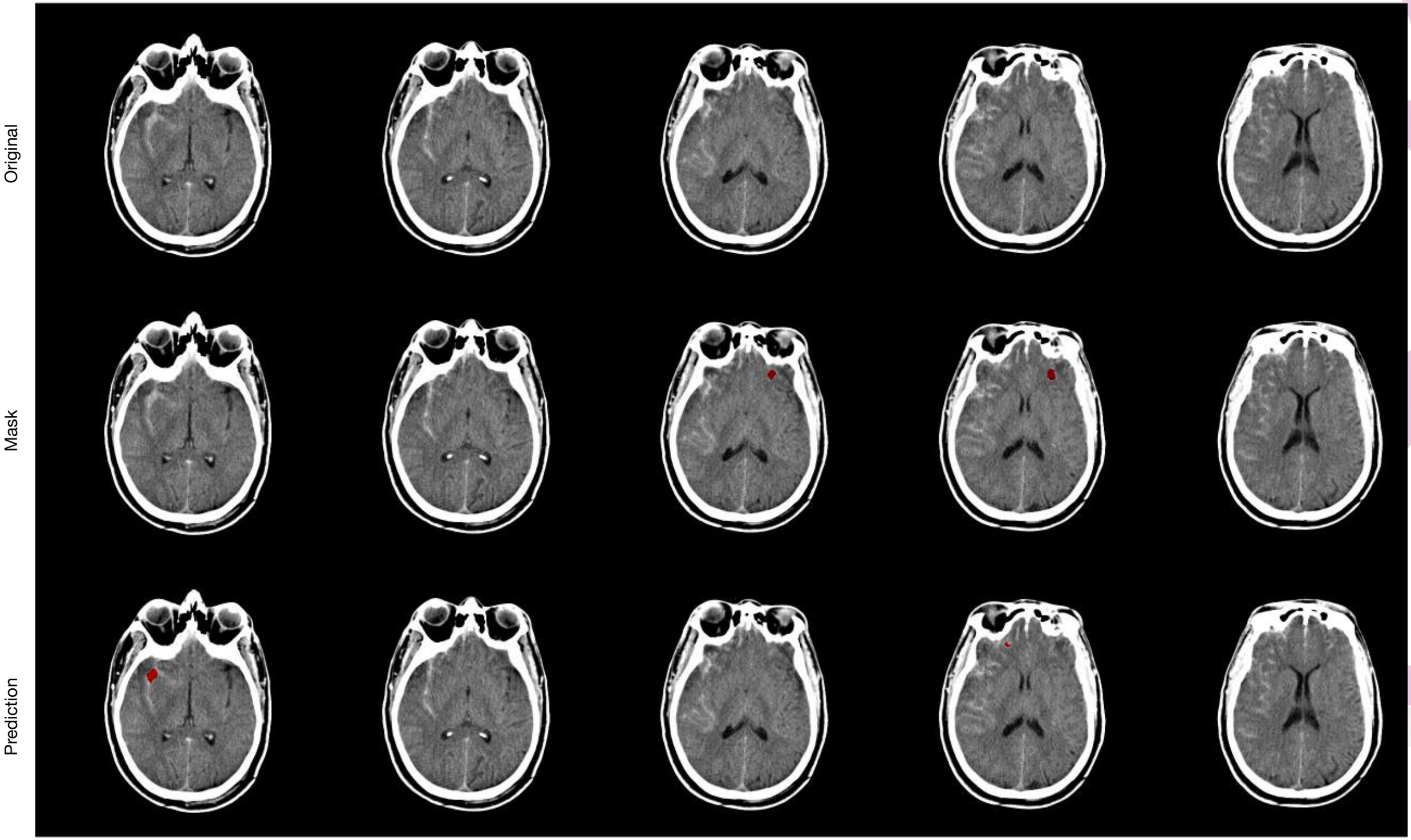

Hematoma segmentation

Dice coefficient:

- **Training** (368 scans): mean 0.67 std 0.23
- **Validation** (41 scans): mean 0.61 std 0.21
- **Test** (95 scans): mean 0.55 std 0.28

Dice coefficient:

- **Training** (349 scans): mean 0.71 std 0.16
- **Validation** (40 scans): mean 0.64 std 0.17
- **Test** (85 scans): mean 0.62 std 0.22

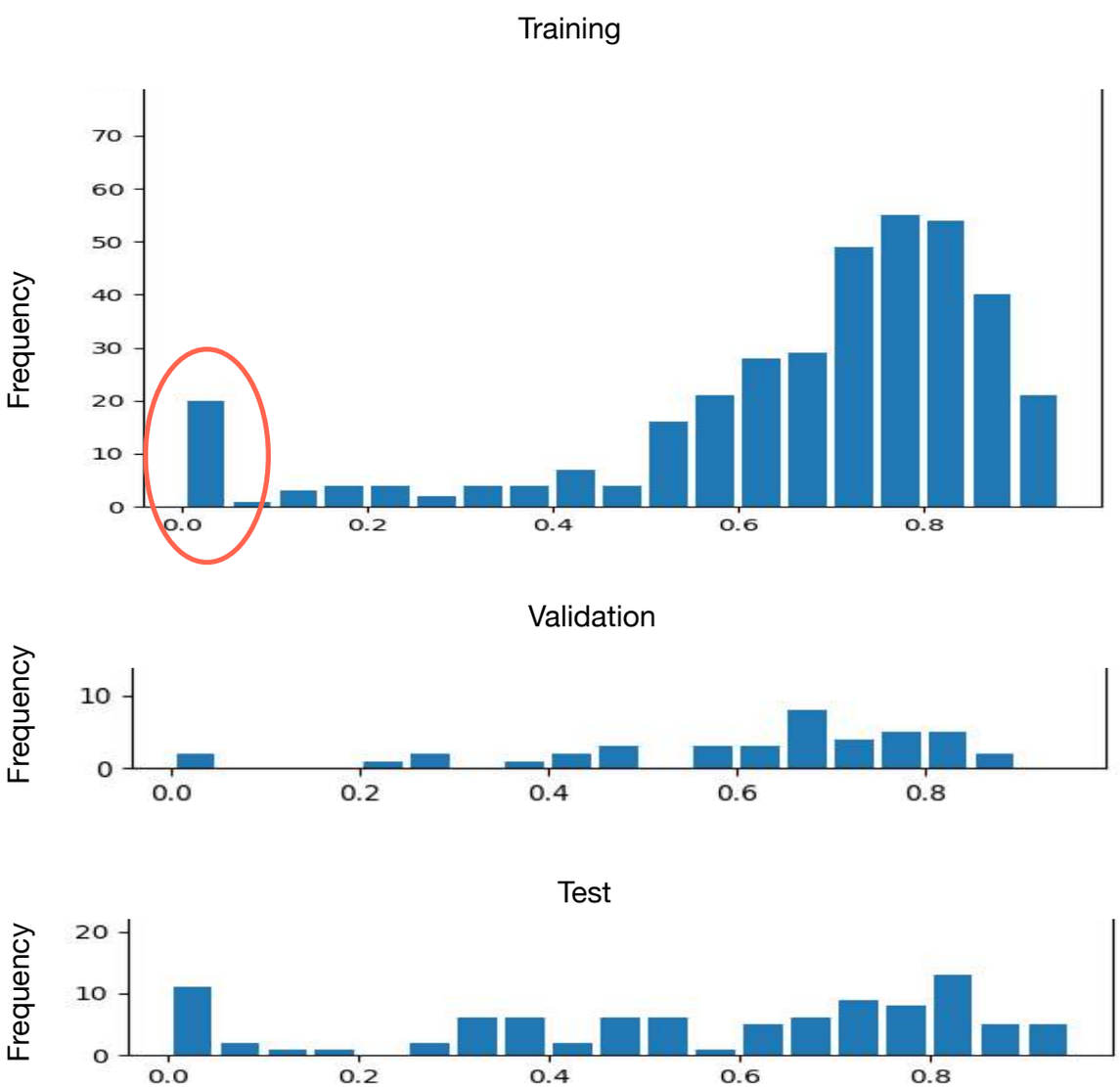

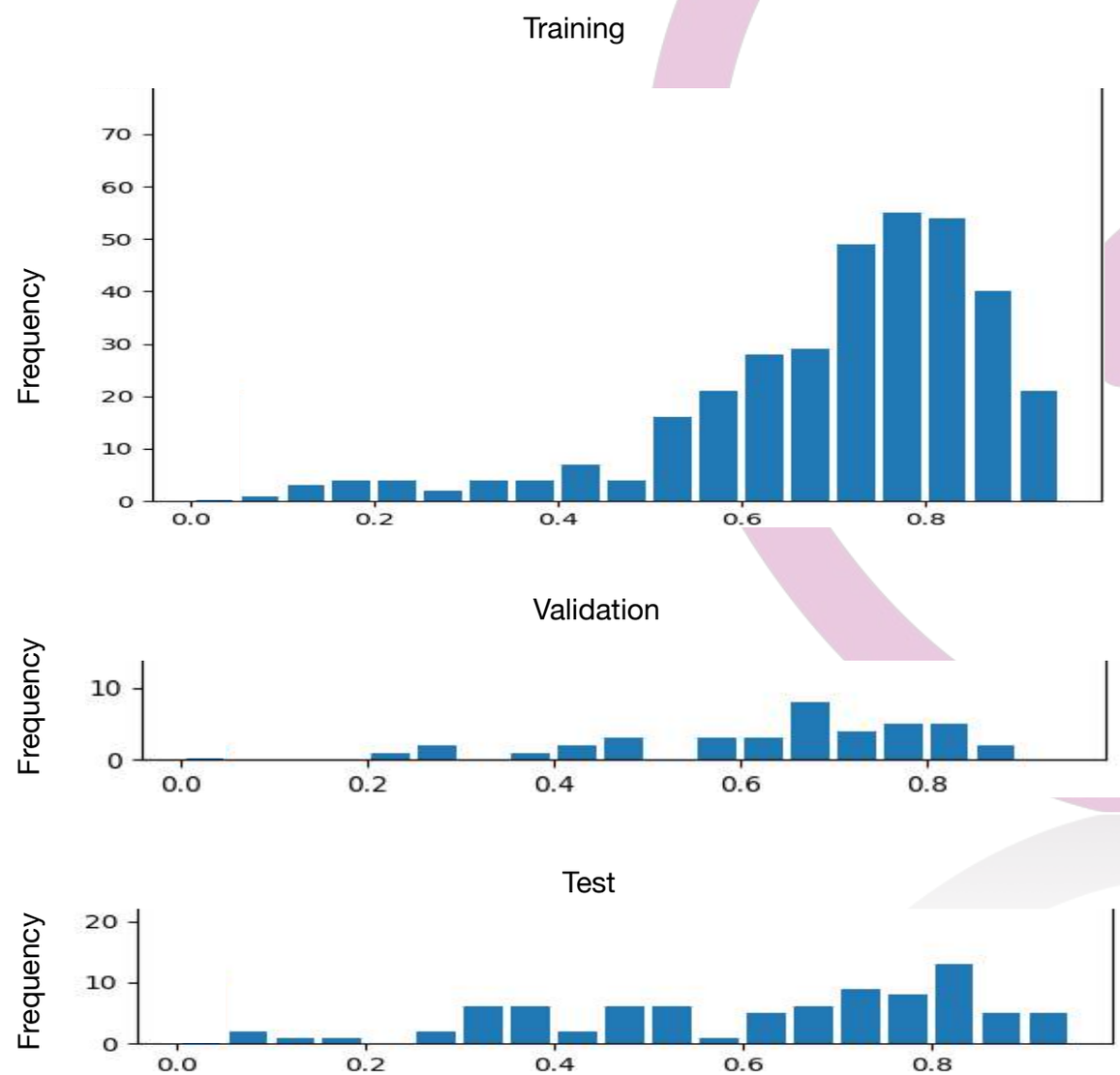

Hematoma segmentation

Dice coefficient:

- **Training** (159 scans): mean 0.61 std 0.24
- **Validation** (39 scans): mean 0.52 std 0.28

Dice coefficient:

- **Training** (368 scans): mean 0.67 std 0.23
- **Validation** (41 scans): mean 0.61 std 0.21
- **Test** (95 scans): mean 0.55 std 0.28

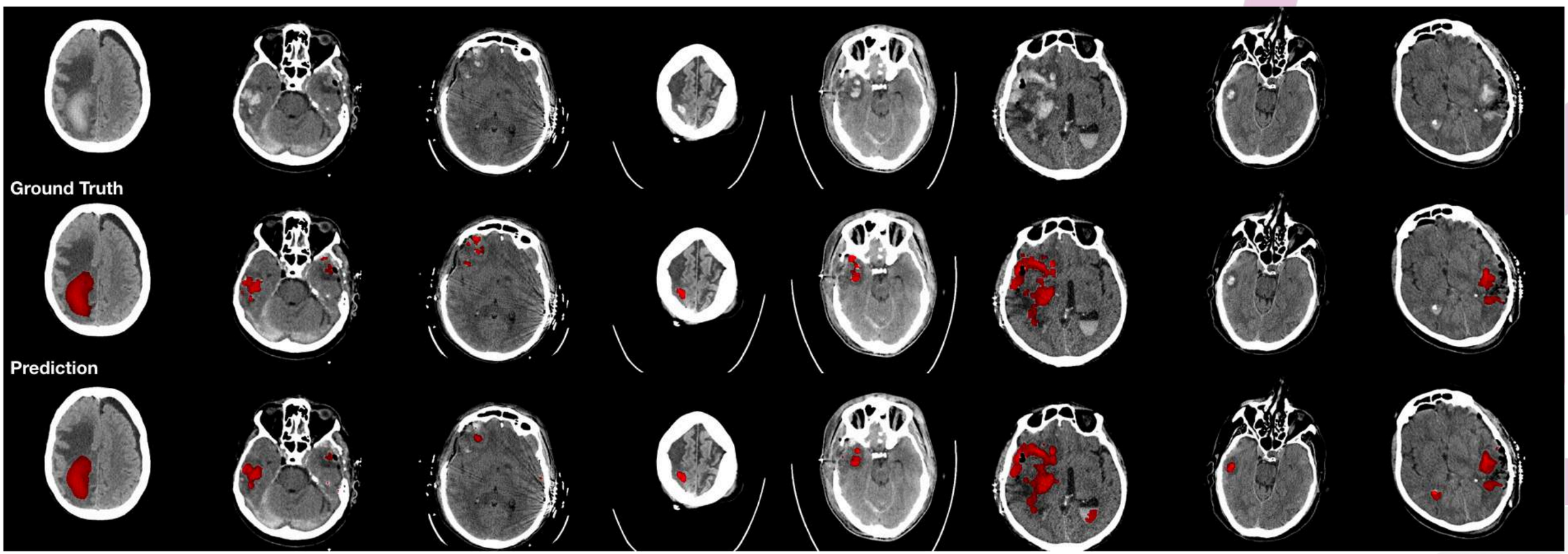

Hematoma volume estimation in follow-up scans

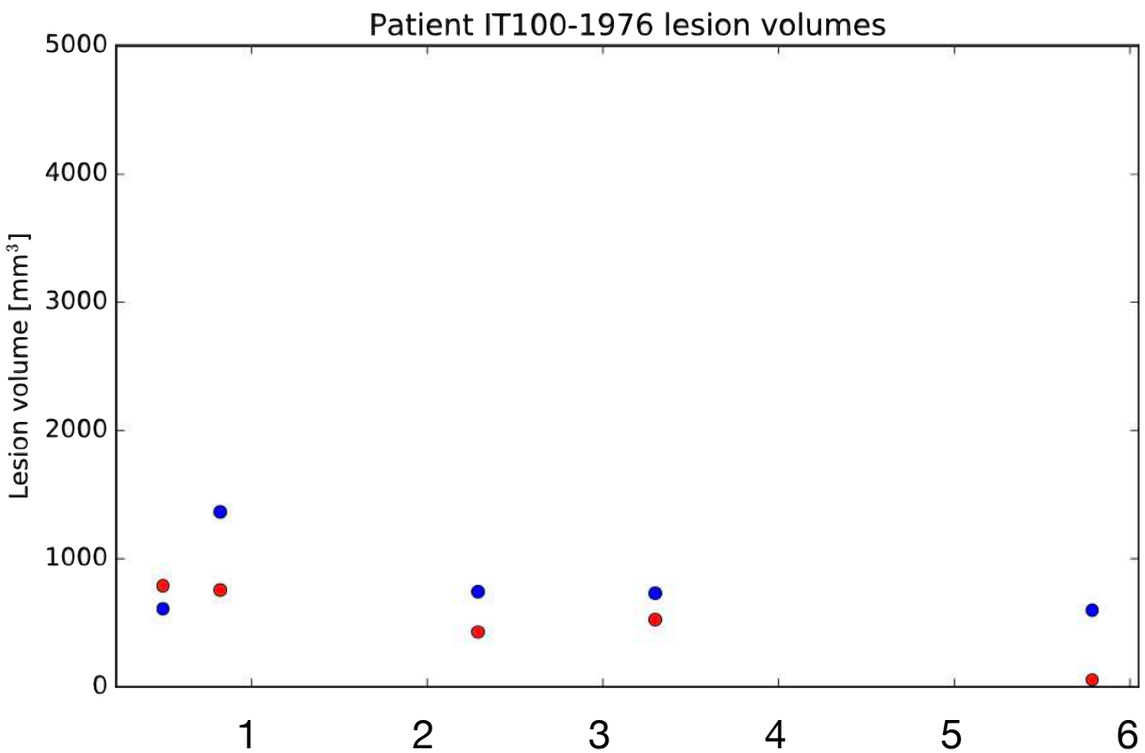

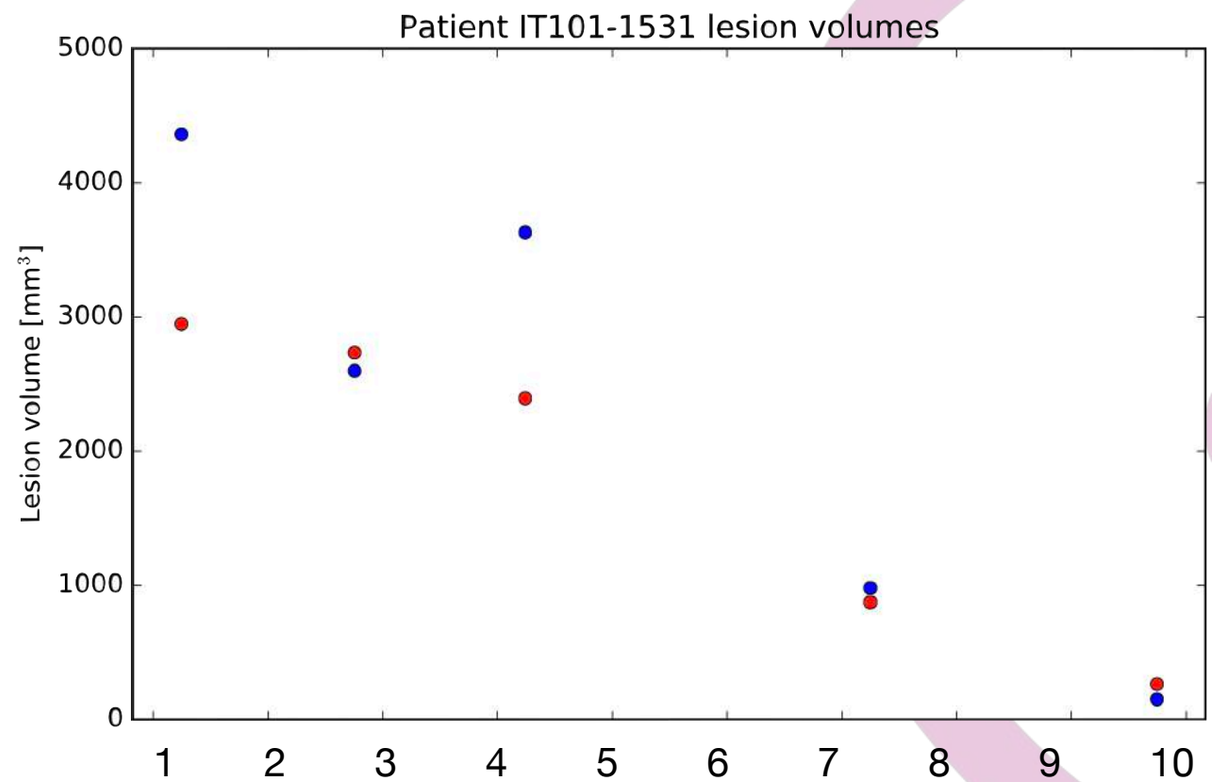

Blue: volume from ground truth.
Red: volume from automated segmentation.

Edema segmentation

Dice coefficient:

- **Training** (159 scans): mean 0.50 std 0.21
- **Validation** (39 scans): mean 0.46 std 0.19

Dice coefficient:

- **Training** (247 scans): mean 0.50 std 0.24
- **Validation** (39 scans): mean 0.50 std 0.21

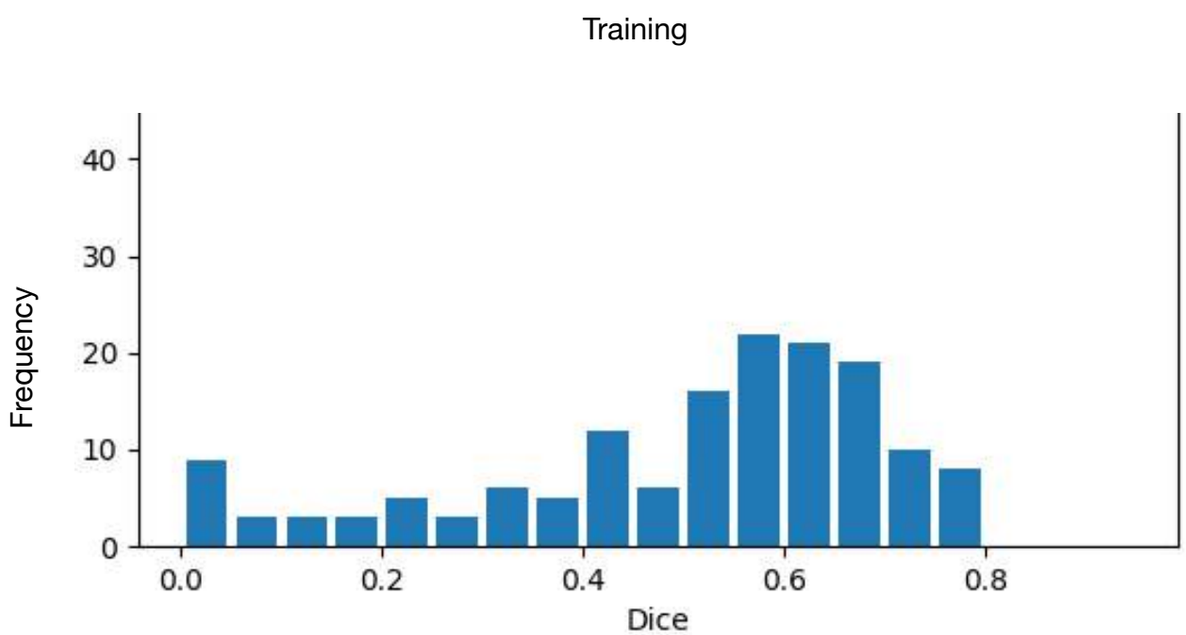

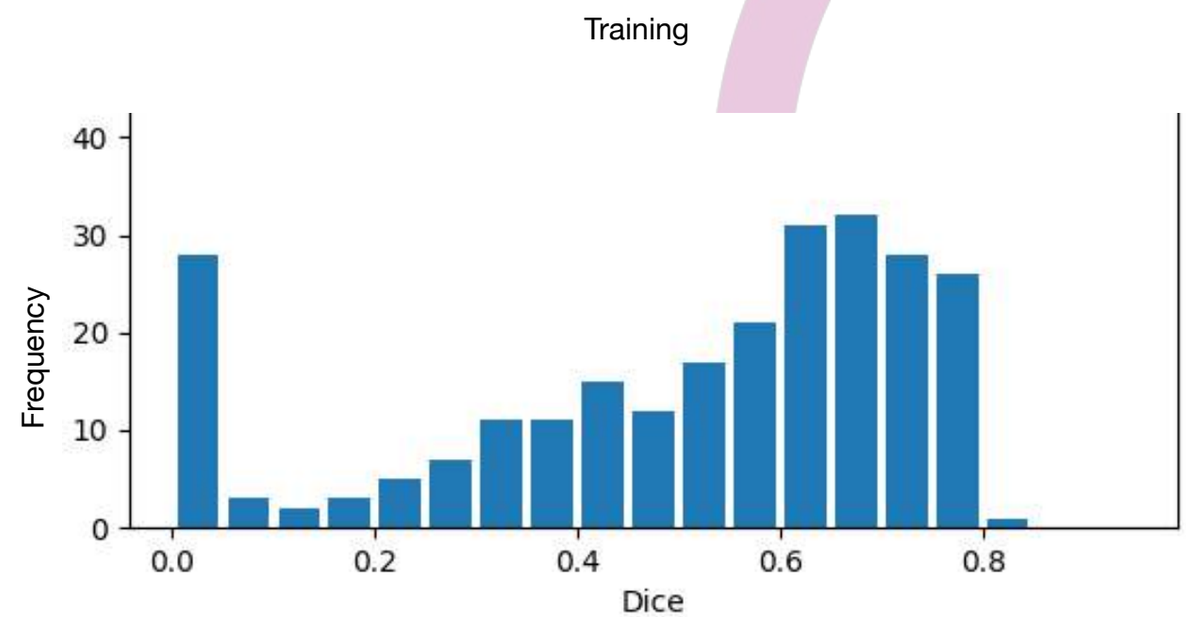

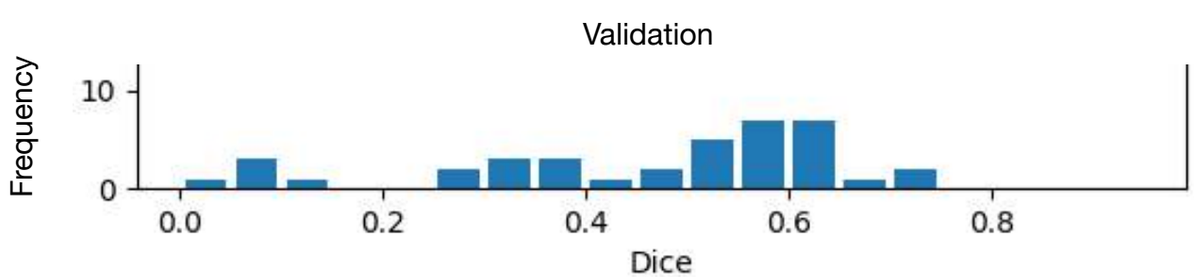

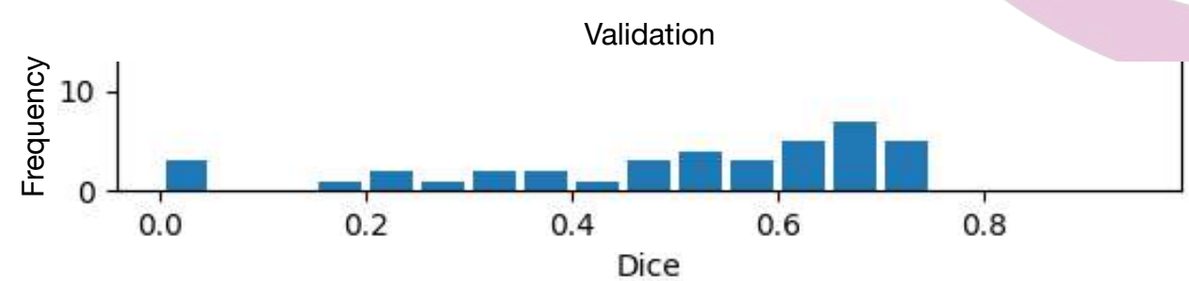

Edema segmentation

Dice coefficient:

- **Training** (159 scans): mean 0.50 std 0.21
- **Validation** (39 scans): mean 0.46 std 0.19

Dice coefficient:

- **Training** (247 scans): mean 0.50 std 0.24
- **Validation** (39 scans): mean 0.50 std 0.21

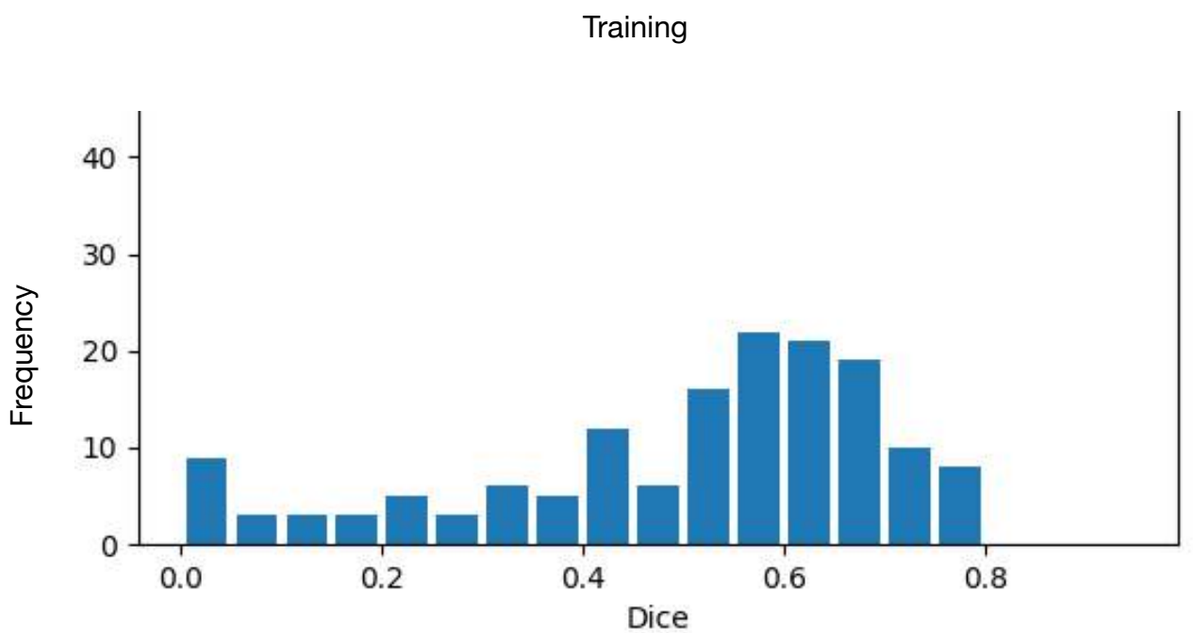

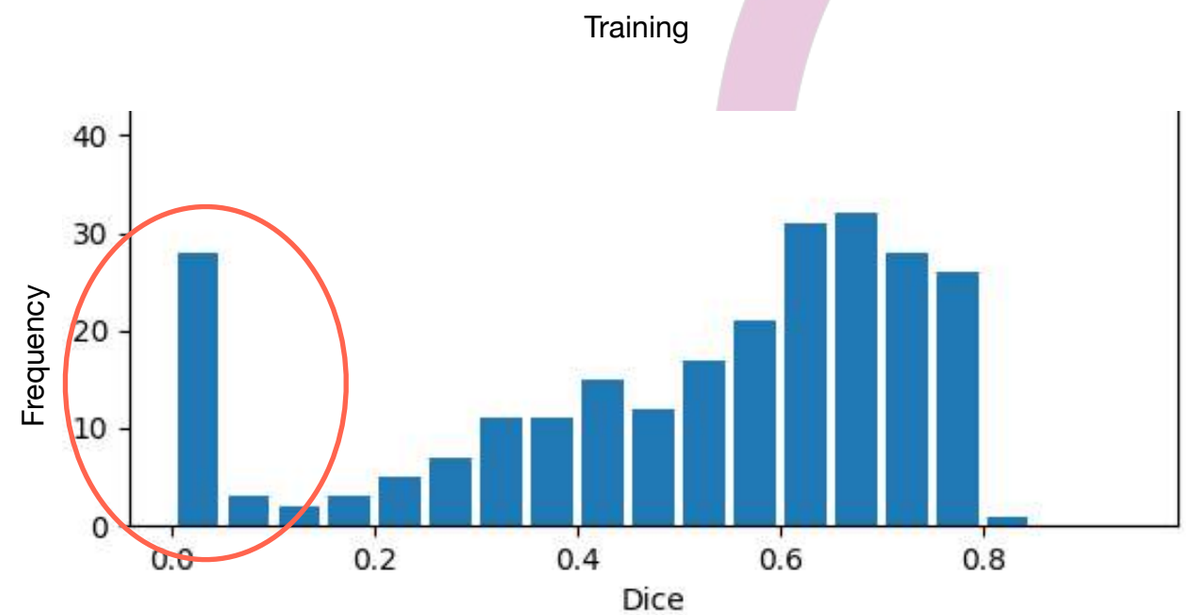

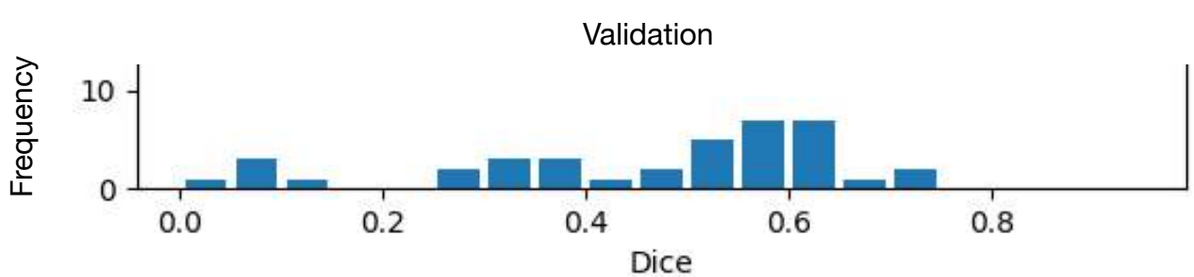

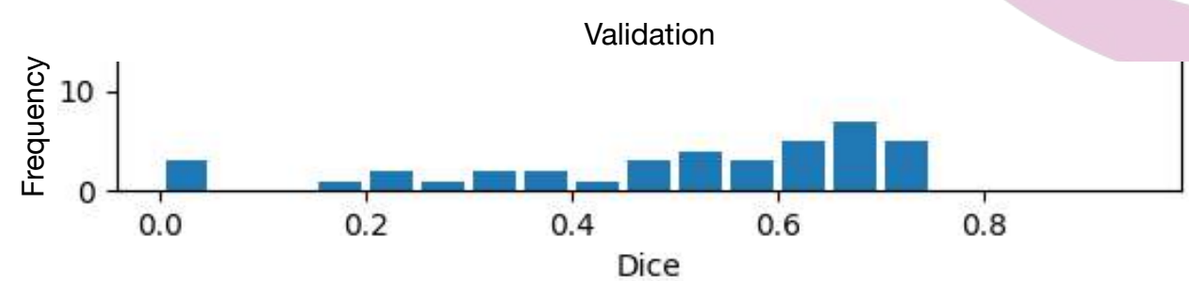

Edema segmentation

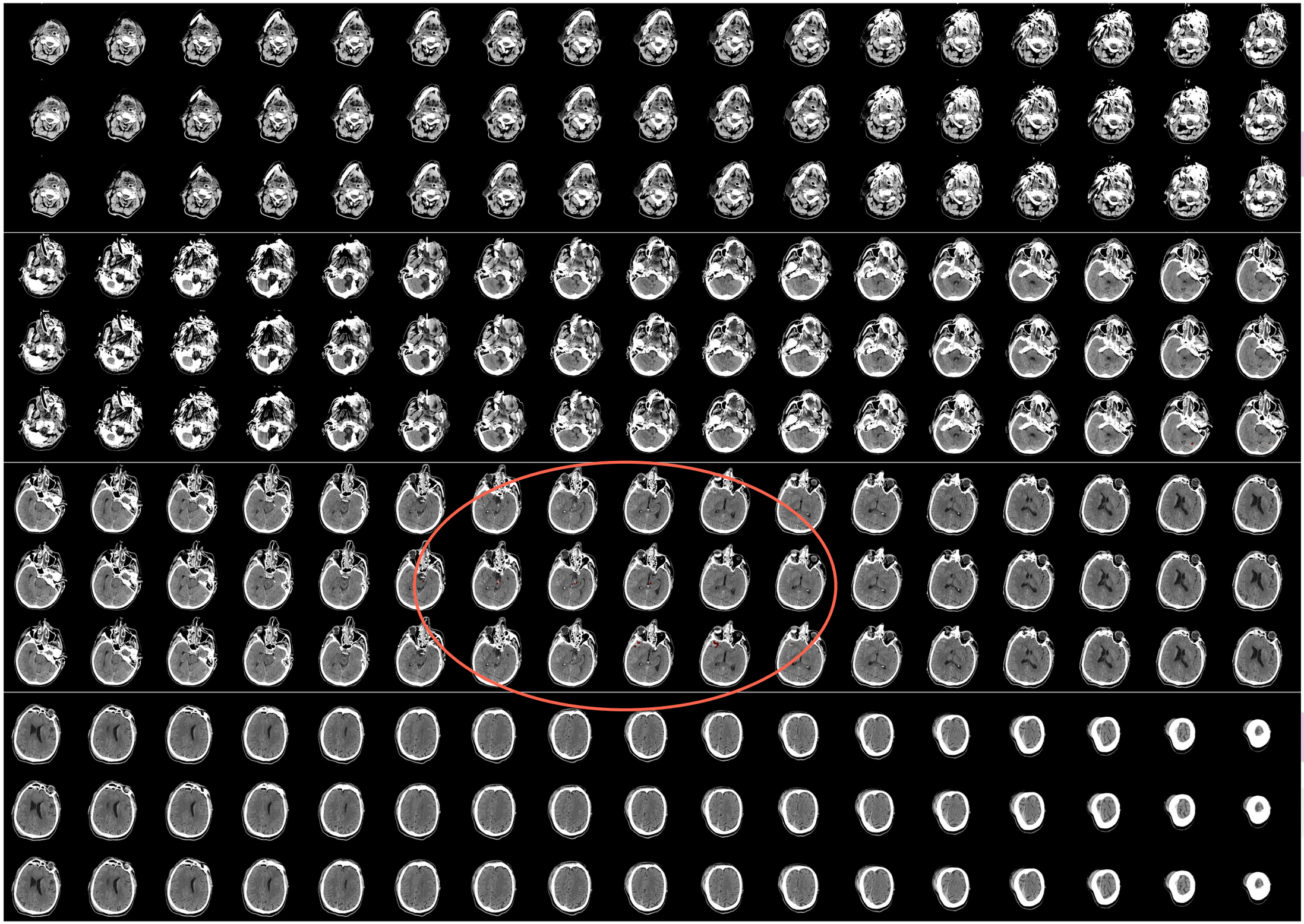

Edema segmentation

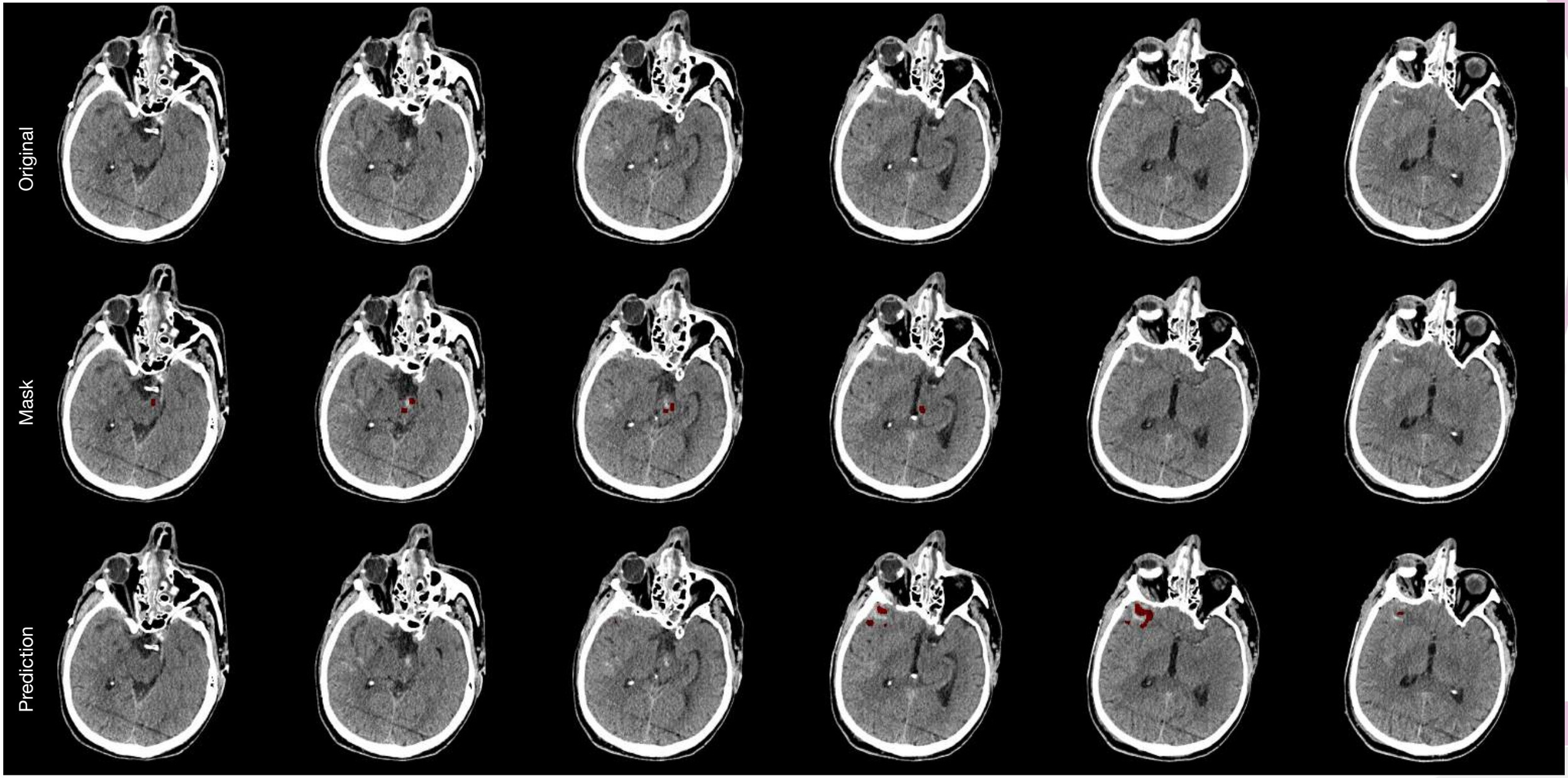

Edema segmentation

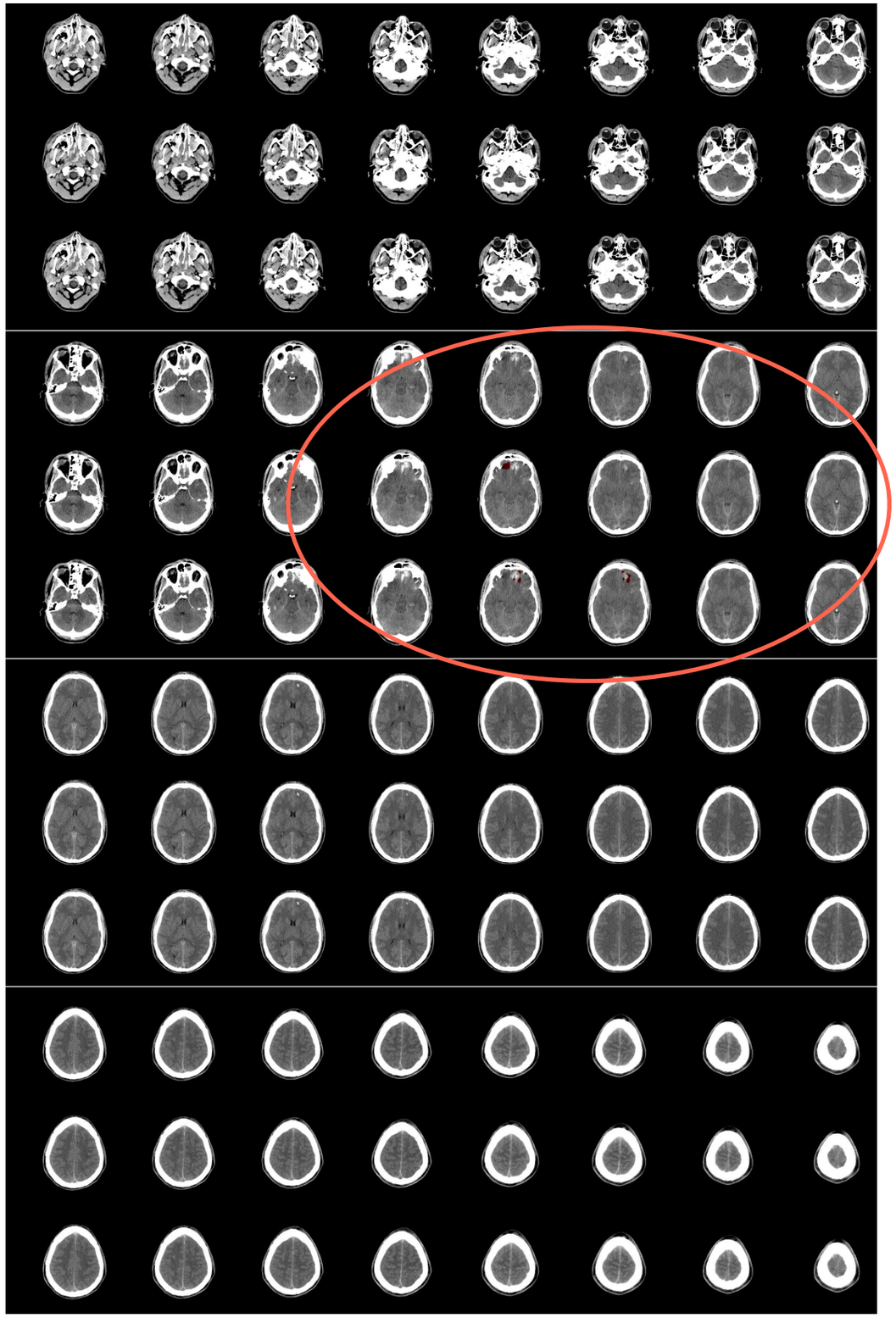

Edema segmentation

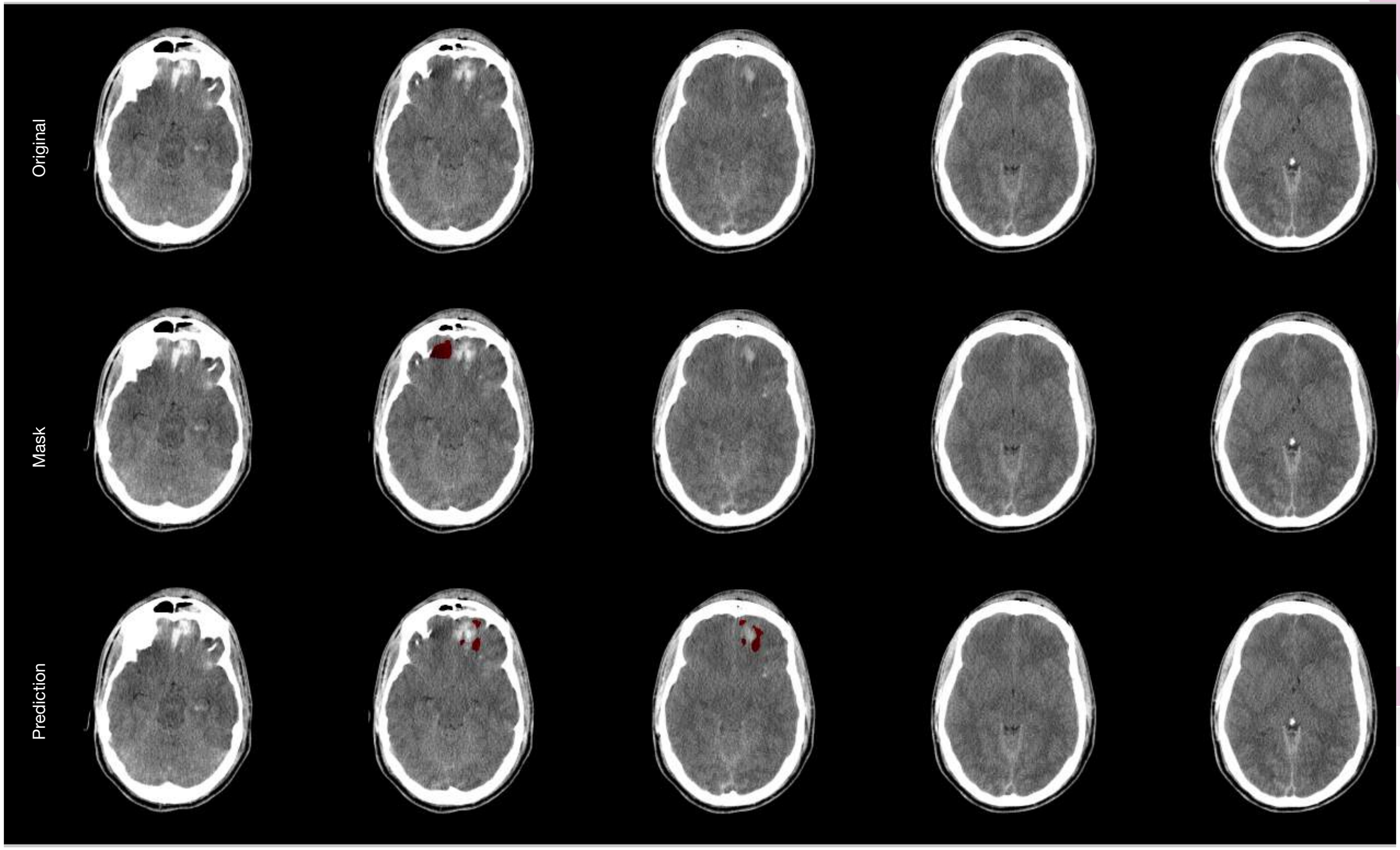

Edema segmentation

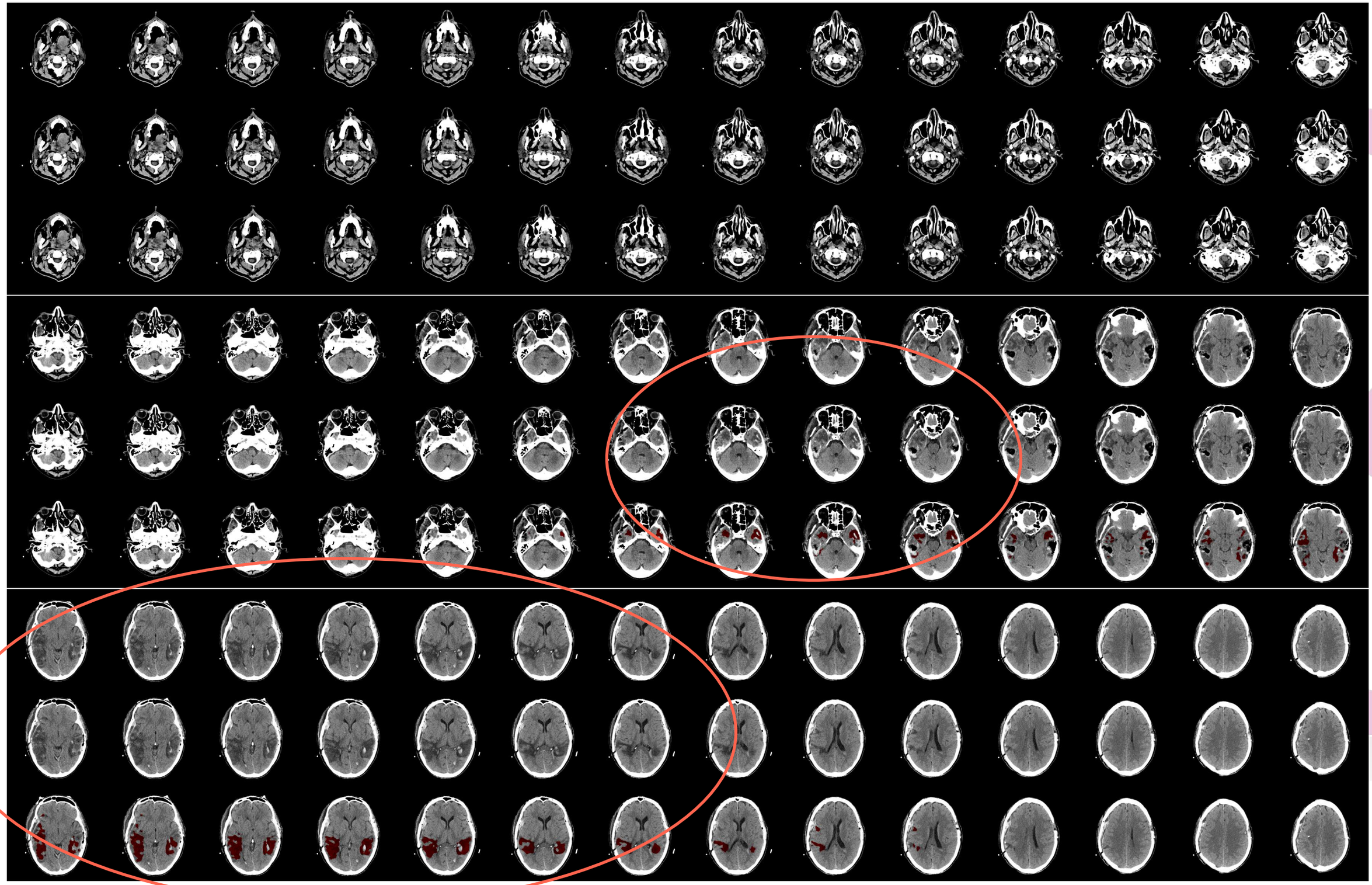

Edema segmentation

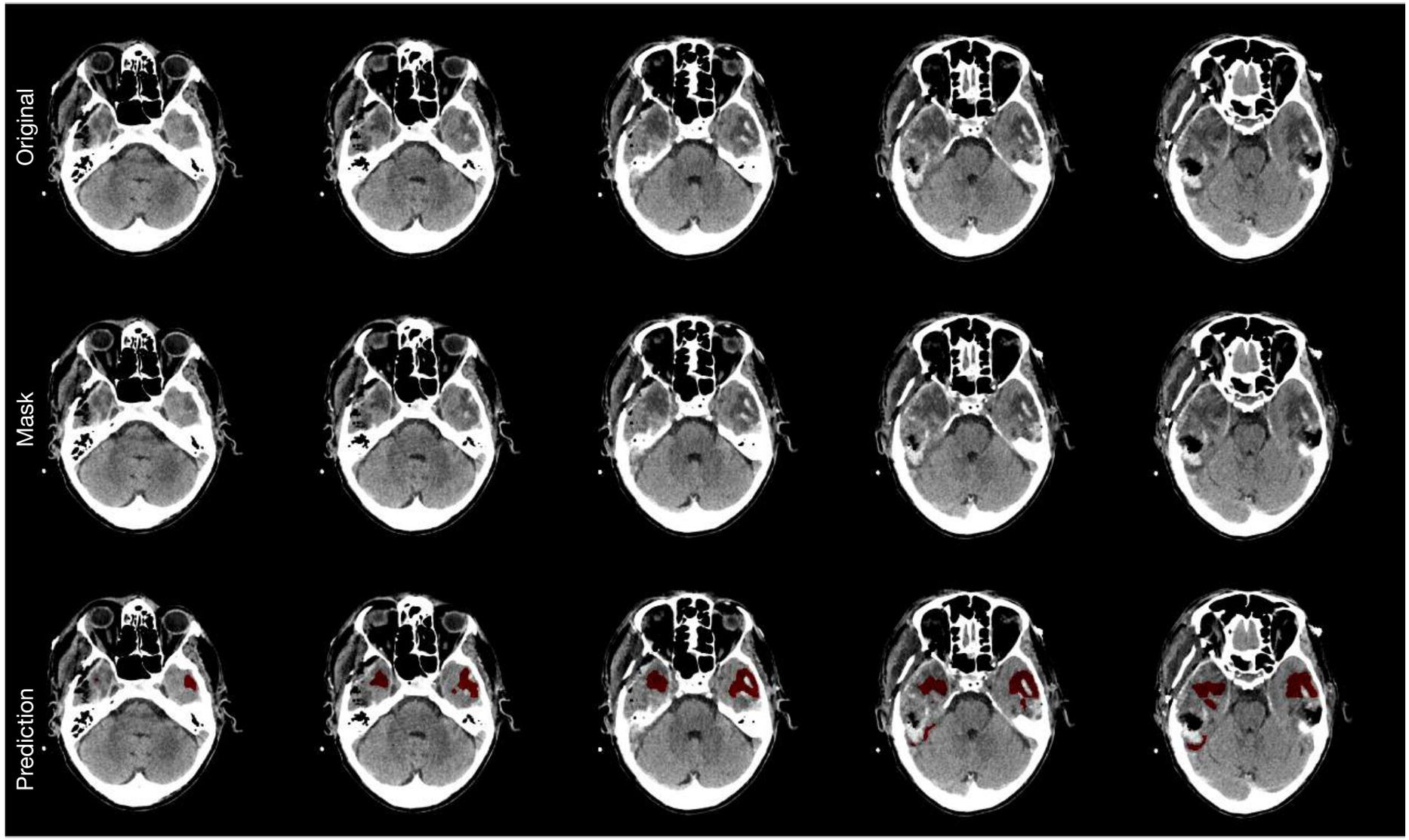

Edema segmentation

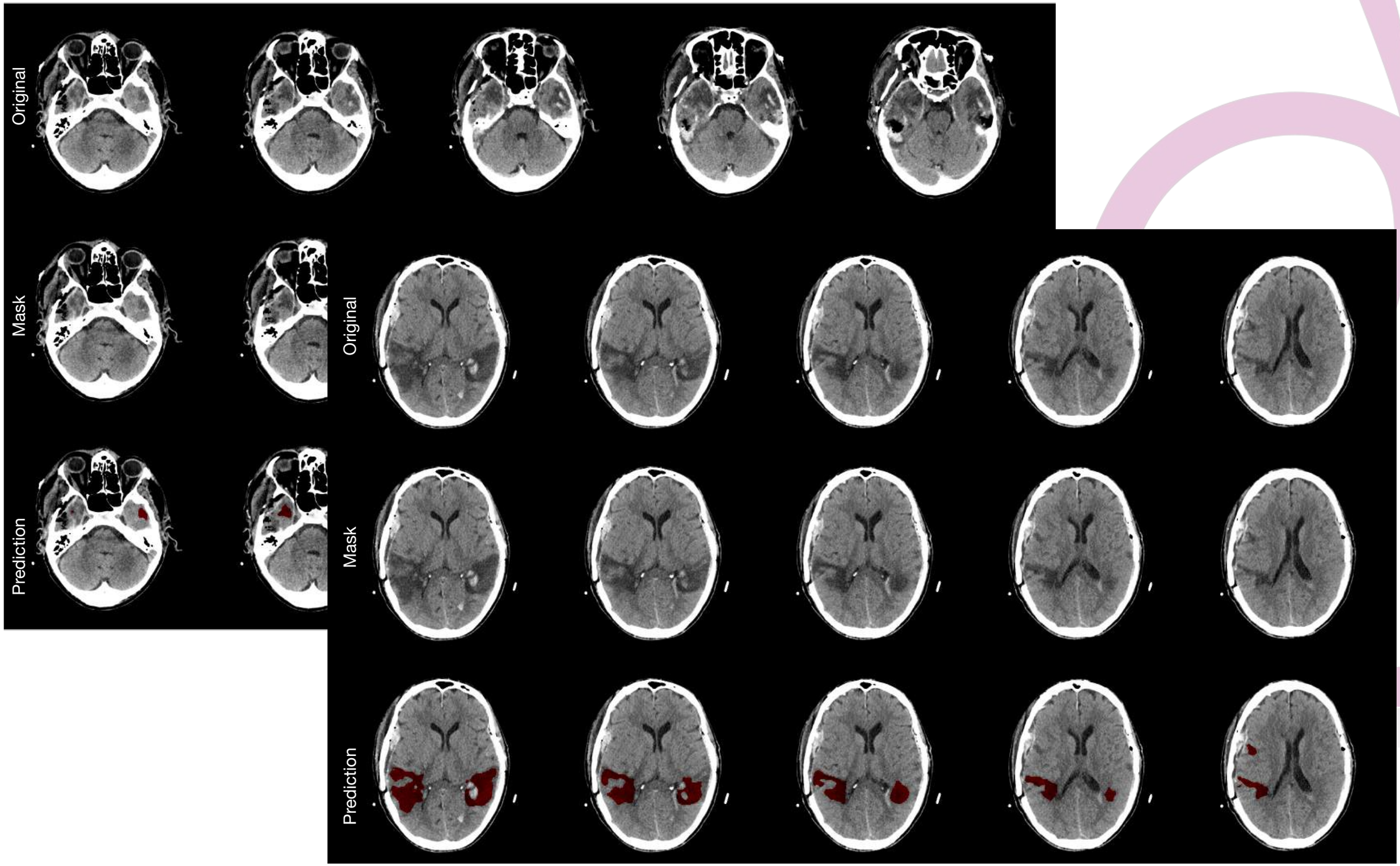

Edema segmentation

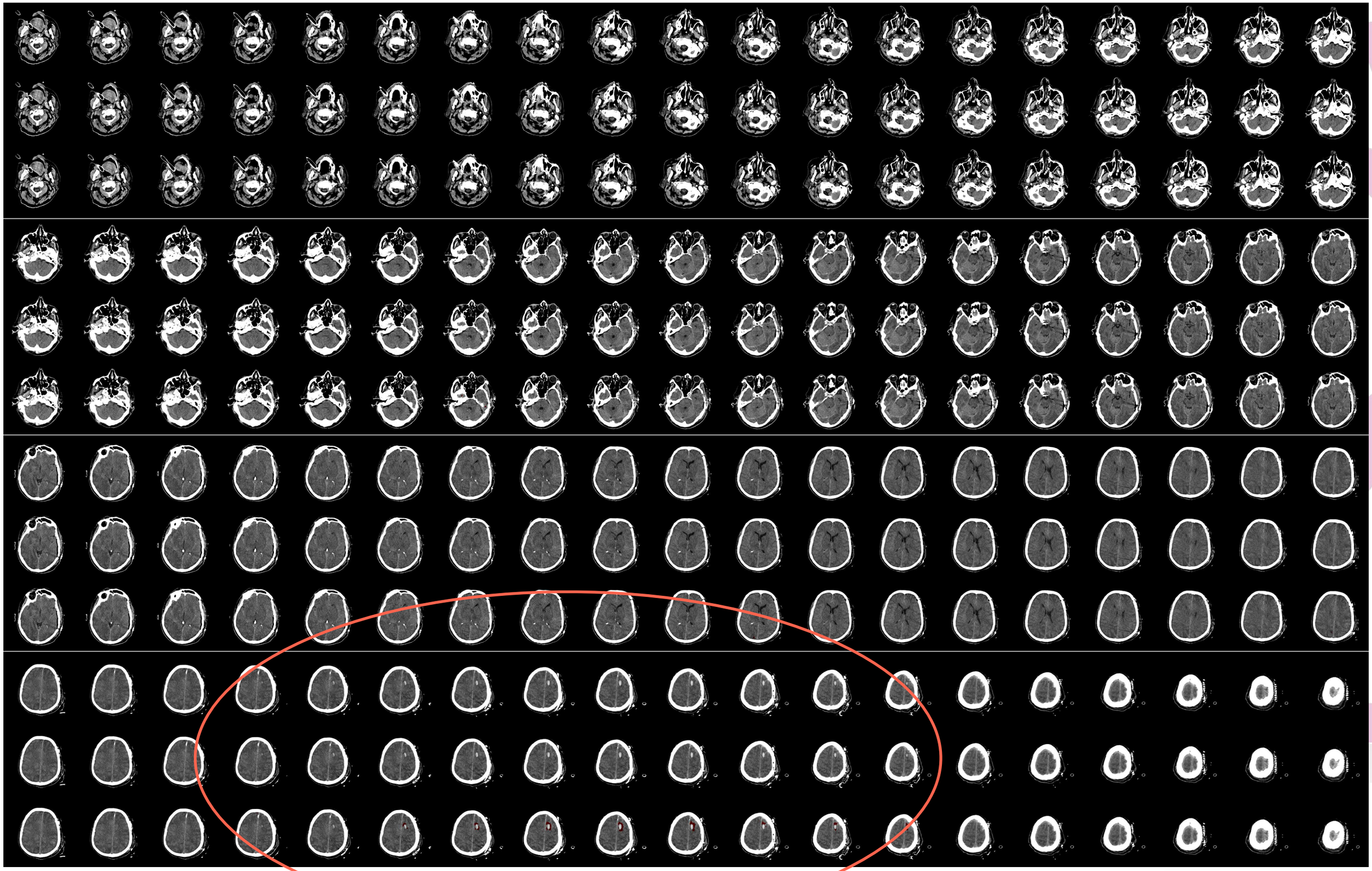

Edema segmentation

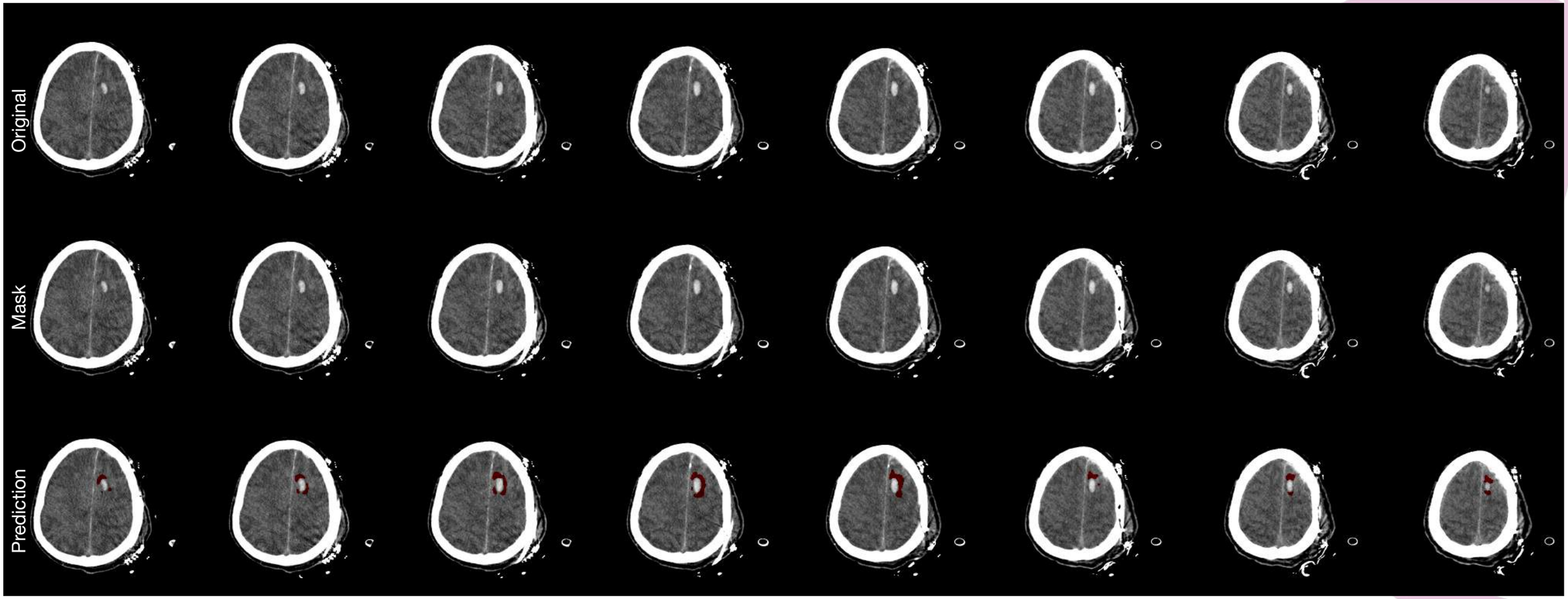

Edema segmentation

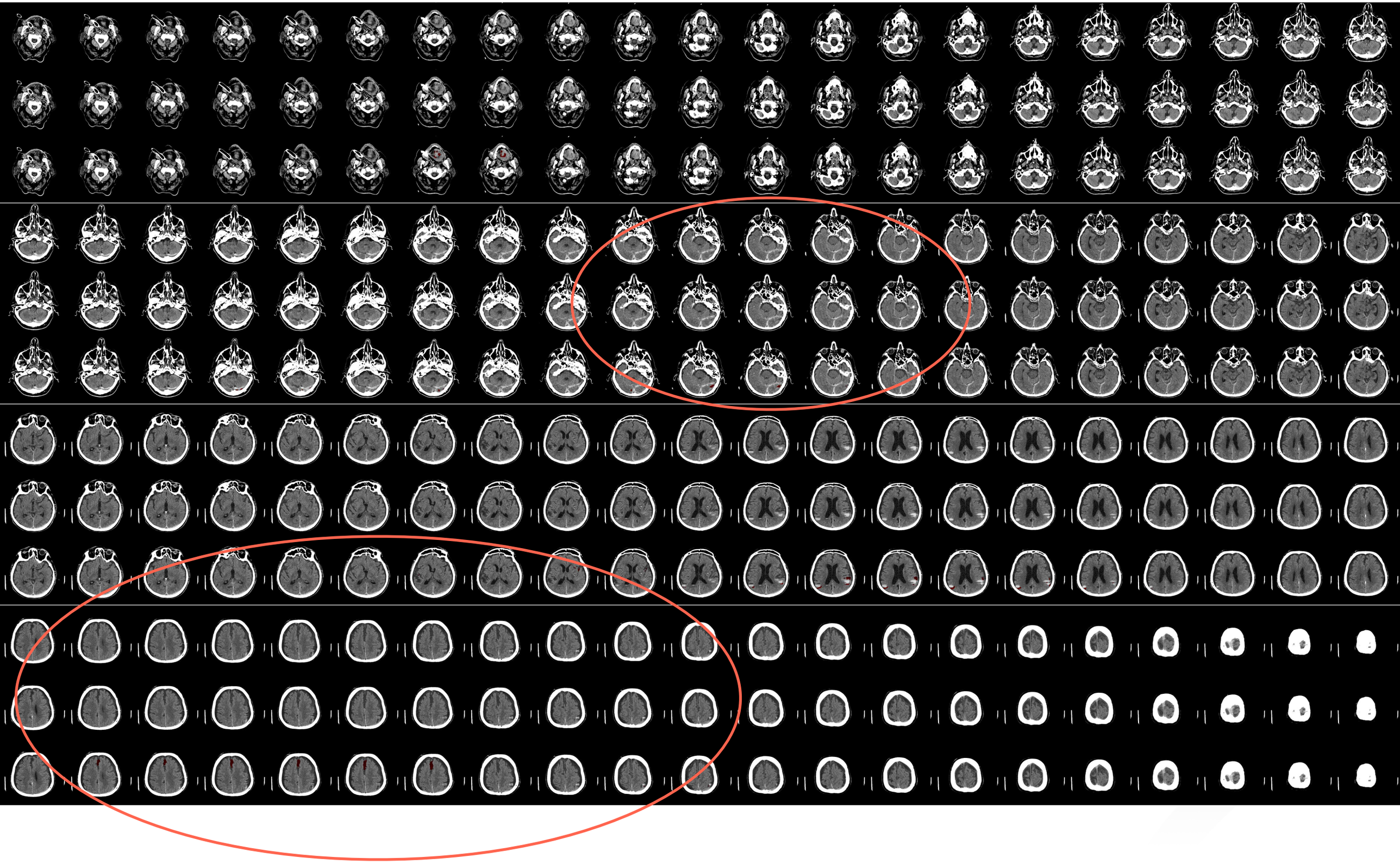

Edema segmentation

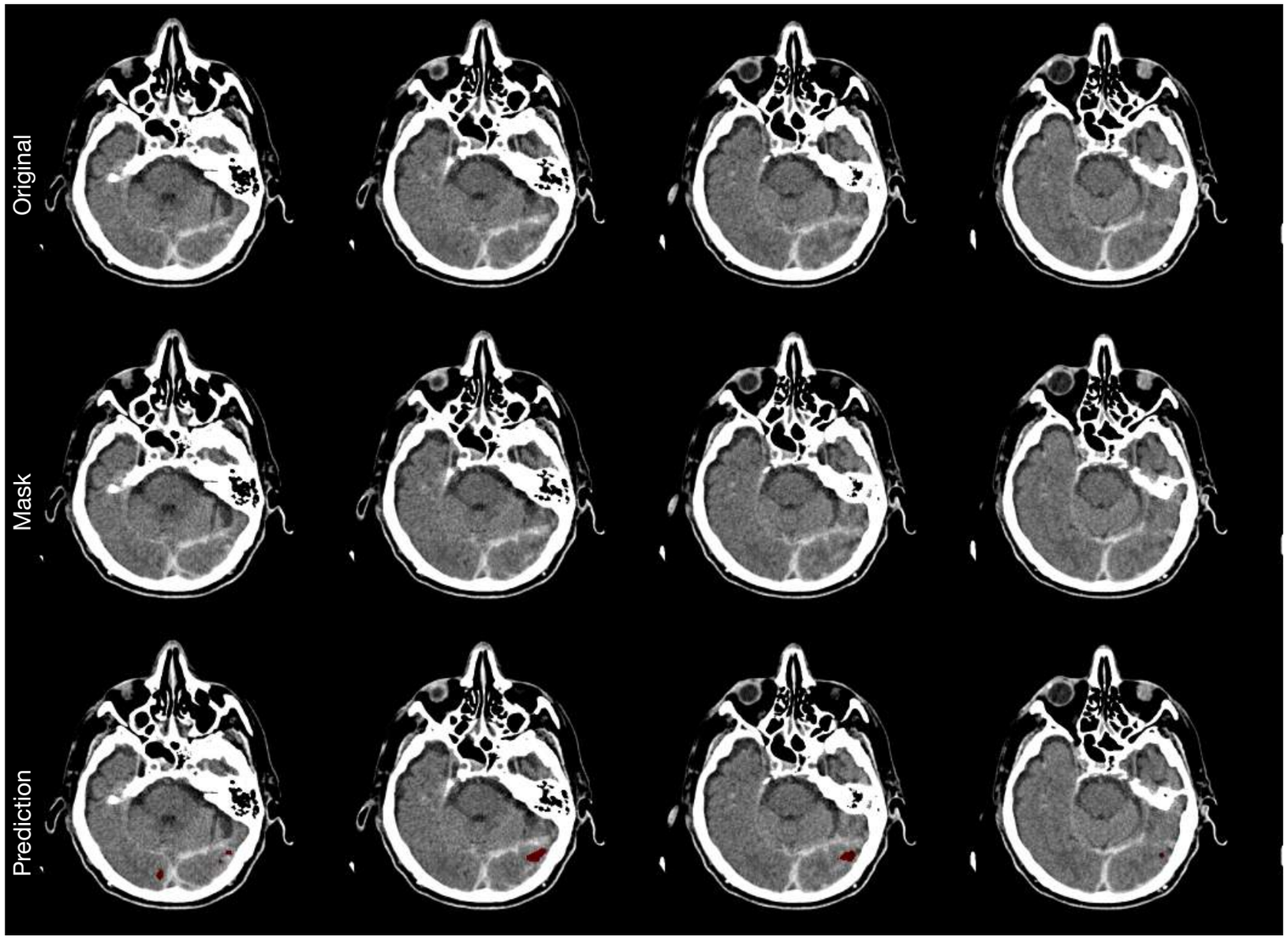

Edema segmentation

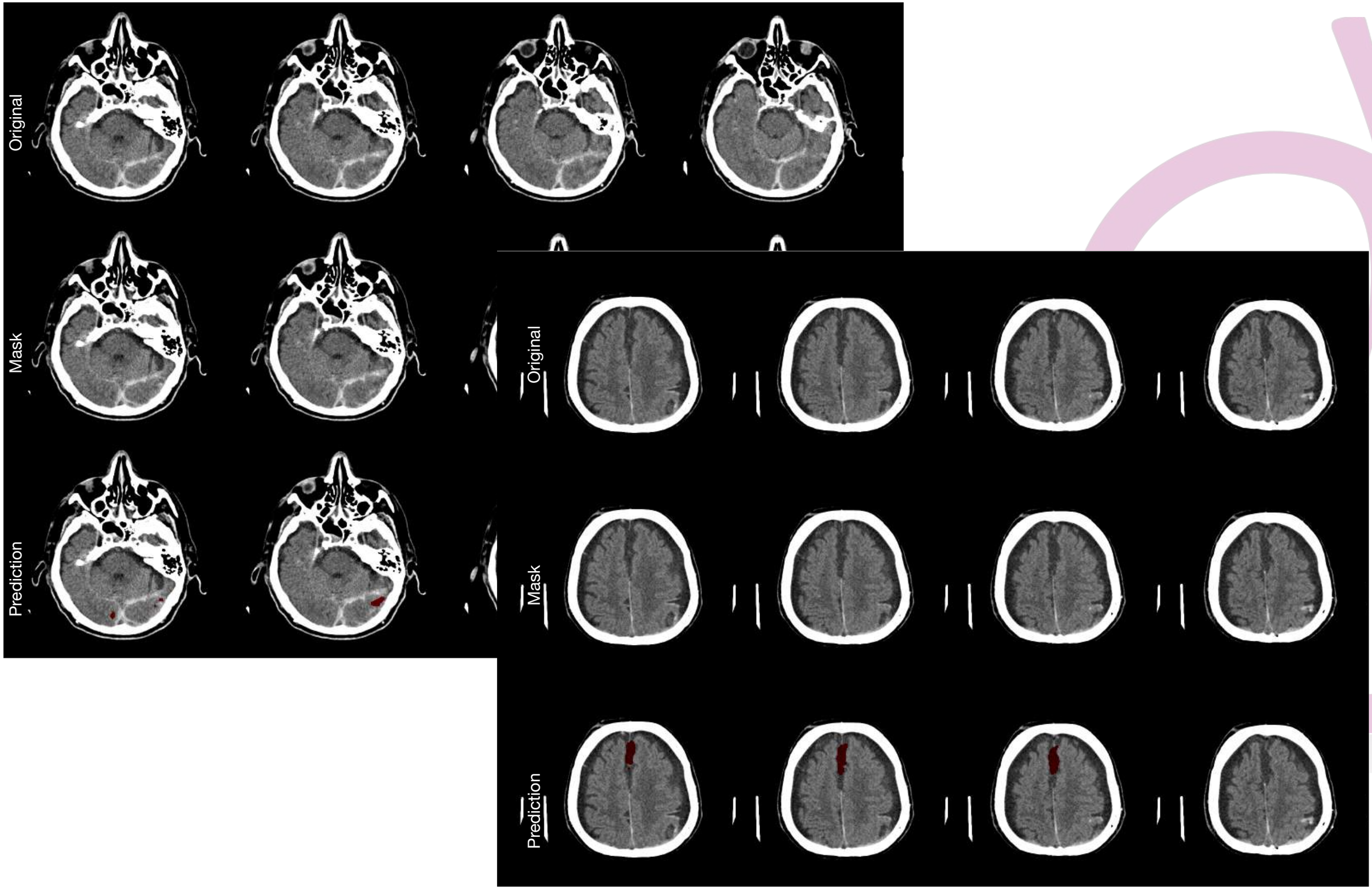

Edema segmentation

Dice coefficient:

- **Training** (159 scans): mean 0.50 std 0.21
- **Validation** (39 scans): mean 0.46 std 0.19

Dice coefficient:

- **Training** (247 scans): mean 0.50 std 0.24
- **Validation** (39 scans): mean 0.50 std 0.21

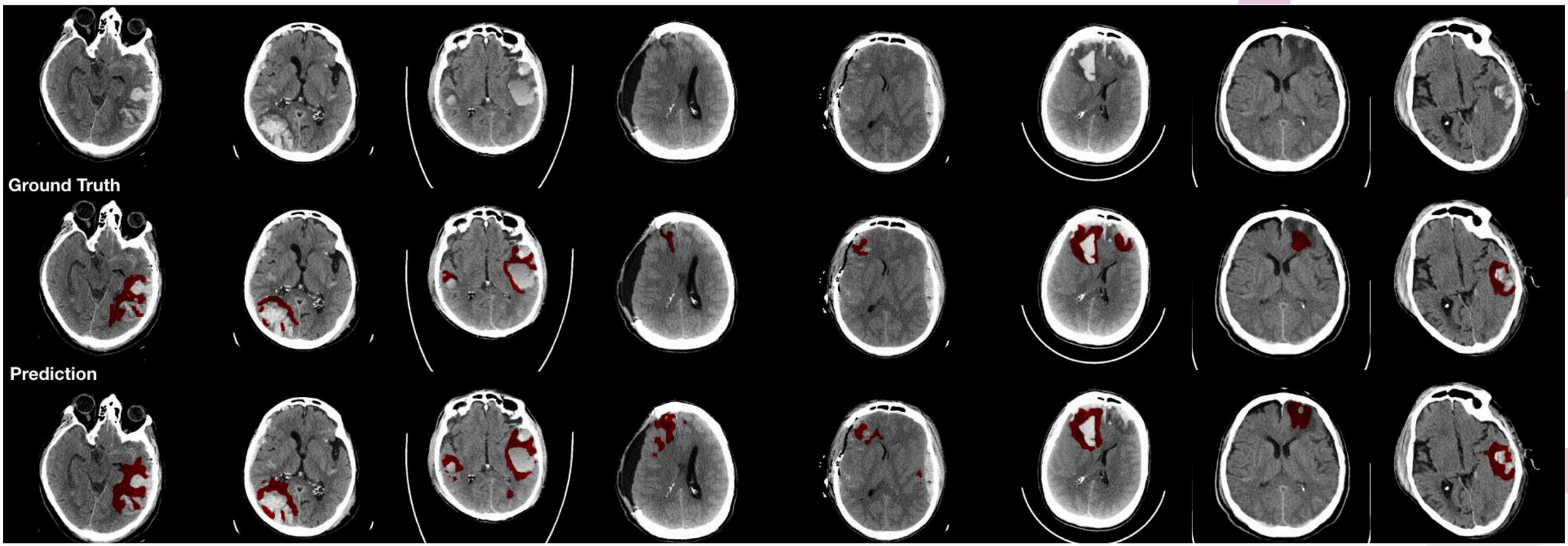

Edema segmentation

Dice coefficient:

- **Training** (247 scans): mean 0.50 std 0.24
- **Validation** (39 scans): mean 0.50 std 0.21

Dice coefficient:

- **Training** (247 scans): mean 0.57 std 0.17
- **Validation** (39 scans): mean 0.54 std 0.17

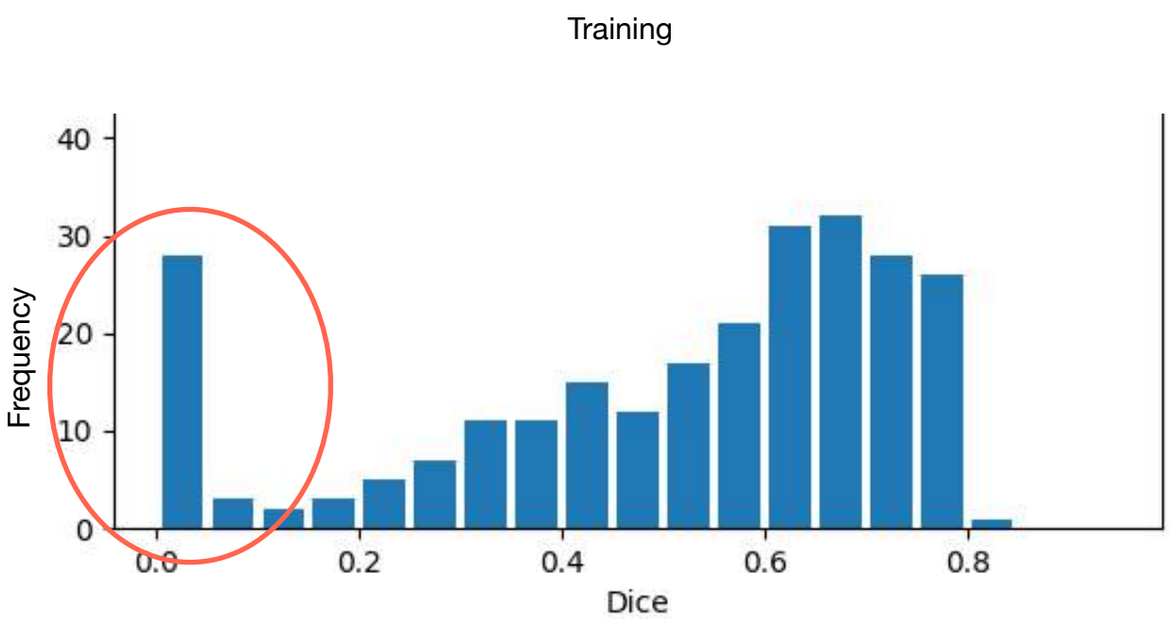

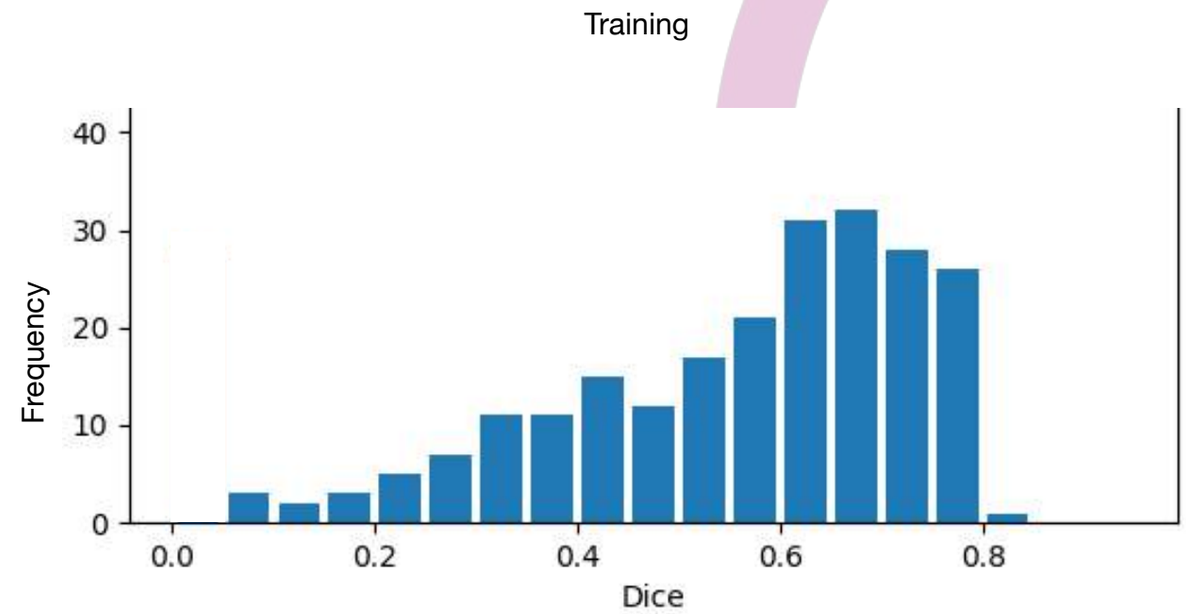

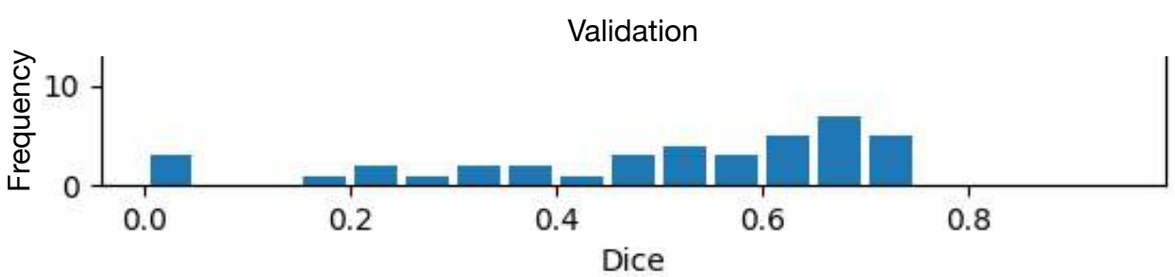

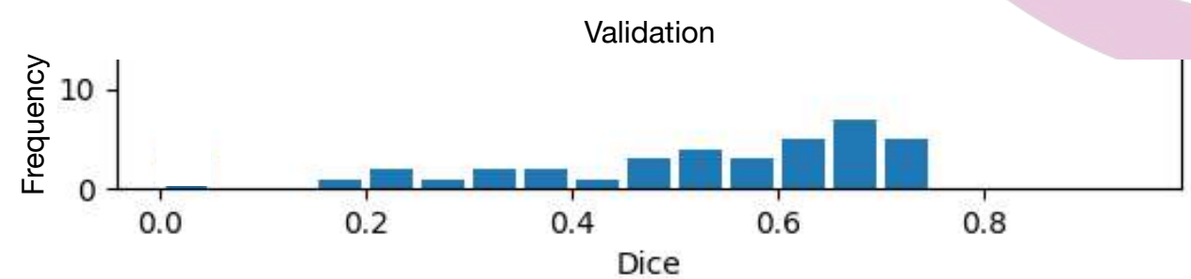

CT biomarkers

Aim: automatically extract imaging biomarkers from CT and from the related segmentation. Use them as further input of a prognostic model based on clinical markers.

The main biomarkers are:

- volume of the lesion
- volume of the edema
- number of lesions
- position of the lesion

This biomarkers will be more specific of the standard biomarkers like the Marshall classification. This should lead to a more precise determination of the clinical outcome.

Available data: Actually clinical data for 387 out of 567 patients who had an annotated lesion are available, for a total of 1204 series.
Of those, 64 patients had recovered, 92 survived with disability and 238 deceased.

DICOM.Next + Imaging biomarker

Modello finale per quantificazione biomarker distribuito a centri (inizio 2019) tramite DICOM.Next

OROBIX

TOOLS WITH A MIND

luca.antiga@orobix.com